IEEE Std C95.3™-2002
(Revision of
IEEE Std C95.3-1991)

IEEE Recommended Practice for Measurements and Computations of Radio Frequency Electromagnetic Fields With Respect to Human Exposure to Such Fields, 100 kHz–300 GHz

Sponsor

IEEE International Committee on Electromagnetic Safety
(Standards Coordinating Committee 28 on Non-Ionizing Radiation)

Approved 11 December 2002

IEEE-SA Standards Board

Abstract: Techniques and instrumentation for the measurement and computation of potentially hazardous electromagnetic (EM) fields both in the near field and the far field of the electromagnetic source are specified. The specifications previously set forth in IEEE Std C95.3™-1991 are extended and combined. Leakage and near-field measurements and a description of the concepts, techniques, and instruments that can be applied to the measurement of specific absorption rate (SAR) or the electric field strength in organisms (including humans) and phantoms exposed to electromagnetic fields are included. Below 100 MHz, the current flowing through the body to ground is measurable and can be used to determine the SAR and, therefore, a brief treatment of low-frequency body current measurement is included.
Keywords: electromagnetic field computation, electromagnetic field measurements, exposure assessment, non-ionizing radiation, RF/microwave hazard assessment, RF/microwave survey instruments, RF/microwave surveys, specific absorption rate (SAR) assessment

---

The Institute of Electrical and Electronics Engineers, Inc.
3 Park Avenue, New York, NY 10016-5997, USA

Print: ISBN 0-7381-3519-4 SH95077
PDF: ISBN 0-7381-3520-8 SS95077

IEEE Standards documents are developed within the IEEE Societies and the Standards Coordinating Committees of the IEEE Standards Association (IEEE-SA) Standards Board. The IEEE develops its standards through a consensus development process, approved by the American National Standards Institute, which brings together volunteers representing varied viewpoints and interests to achieve the final product. Volunteers are not necessarily members of the Institute and serve without compensation. While the IEEE administers the process and establishes rules to promote fairness in the consensus development process, the IEEE does not independently evaluate, test, or verify the accuracy of any of the information contained in its standards.

Use of an IEEE Standard is wholly voluntary. The IEEE disclaims liability for any personal injury, property or other damage, of any nature whatsoever, whether special, indirect, consequential, or compensatory, directly or indirectly resulting from the publication, use of, or reliance upon this, or any other IEEE Standard document.

The IEEE does not warrant or represent the accuracy or content of the material contained herein, and expressly disclaims any express or implied warranty, including any implied warranty of merchantability or fitness for a specific purpose, or that the use of the material contained herein is free from patent infringement. IEEE Standards documents are supplied "**AS IS**."

The existence of an IEEE Standard does not imply that there are no other ways to produce, test, measure, purchase, market, or provide other goods and services related to the scope of the IEEE Standard. Furthermore, the viewpoint expressed at the time a standard is approved and issued is subject to change brought about through developments in the state of the art and comments received from users of the standard. Every IEEE Standard is subjected to review at least every five years for revision or reaffirmation. When a document is more than five years old and has not been reaffirmed, it is reasonable to conclude that its contents, although still of some value, do not wholly reflect the present state of the art. Users are cautioned to check to determine that they have the latest edition of any IEEE Standard.

In publishing and making this document available, the IEEE is not suggesting or rendering professional or other services for, or on behalf of, any person or entity. Nor is the IEEE undertaking to perform any duty owed by any other person or entity to another. Any person utilizing this, and any other IEEE Standards document, should rely upon the advice of a competent professional in determining the exercise of reasonable care in any given circumstances.

Interpretations: Occasionally questions may arise regarding the meaning of portions of standards as they relate to specific applications. When the need for interpretations is brought to the attention of IEEE, the Institute will initiate action to prepare appropriate responses. Since IEEE Standards represent a consensus of concerned interests, it is important to ensure that any interpretation has also received the concurrence of a balance of interests. For this reason, IEEE and the members of its societies and Standards Coordinating Committees are not able to provide an instant response to interpretation requests except in those cases where the matter has previously received formal consideration.

Comments for revision of IEEE Standards are welcome from any interested party, regardless of membership affiliation with IEEE. Suggestions for changes in documents should be in the form of a proposed change of text, together with appropriate supporting comments. Comments on standards and requests for interpretations should be addressed to:

Secretary, IEEE-SA Standards Board
445 Hoes Lane
P.O. Box 1331
Piscataway, NJ 08855-1331
USA

Note: Attention is called to the possibility that implementation of this standard may require use of subject matter covered by patent rights. By publication of this standard, no position is taken with respect to the existence or validity of any patent rights in connection therewith. The IEEE shall not be responsible for identifying patents for which a license may be required by an IEEE standard or for conducting inquiries into the legal validity or scope of those patents that are brought to its attention.

Introduction

(This introduction is not part of IEEE Std C95.3-2002, IEEE Recommended Practice for Measurements and Computations of Radio Frequency Electromagnetic Fields with Respect to Human Exposure, 100 kHz–300 GHz.)

In 1960, the American Standards Association approved the initiation of the Radiation Hazards Standards project under the co-sponsorship of the Department of the Navy and the Institute of Electrical and Electronics Engineers.

Prior to 1988, C95 standards were developed by accredited standards committee C95, and submitted to ANSI for approval and issuance as ANSI C95 standards. Between 1988 and 1990, the committee was converted to Standards Coordinating Committee 28 under the sponsorship of the IEEE Standards Board, and in 2001,became also known as the International Committee on Electromagnetic Safety (ICES). In accordance with policies of the IEEE, C95 standards will be issued and developed as IEEE standards, as well as being submitted to ANSI for recognition.

The present scope of ICES is:

"Development of standards for the safe use of electromagnetic energy in the range of 0 Hz–300 GHz relative to the potential hazards of exposure of man, volatile materials, and explosive devices to such energy. The committee does not address infrared, visible, ultraviolet, or ionizing radiation. The committee will coordinate with other committees whose scopes are contiguous with ICES."

IEEE International Committee on Electromagnetic Safety is responsible for this recommended practice. There are five subcommittees concerned with the following:

— I Techniques, Procedures, Instrumentation, and Computation
— II Terminology, Units of Measurements and Hazard Communication
— III Safety Levels with Respect to Human Exposure, 0–3 kHz
— IV Safety Levels with Respect to Human Exposure, 3 kHz–300 GHz
— V Safety Levels with Respect to Electro-Explosive Devices

Three standards, two recommended practices, and one guide have been issued. Current versions are as follows:

IEEE Std C95.1™, 1999 edition, IEEE Standard for Safety Levels with Respect to Human Exposure to Radio Frequency Electromagnetic Fields, 3 kHz–300 GHz.

IEEE Std C95.2™-1999 IEEE Standard for Radio Frequency Energy and Current Flow Symbols. (Supersedes ANSI C95.2-1982)

IEEE Std C95.3-2002, IEEE Recommended Practice for Measurements and Computations of Radio Frequency Electromagnetic Fields with Respect to Human Exposure to such Fields, 100 kHz–300 GHz. (Supersedes IEEE Std C95.3-1991.)

IEEE Std C95.4-2002, IEEE Recommended Practice for Determining Safe Distances from Radio Frequency Transmitting Antennas When Using Electric Blasting Caps During Explosive Operations.

IEEE Std 1460™-1996, IEEE Guide for the Measurement of Quasi-Static Magnetic and Electric Fields.

This recommended practice extends the specifications previously set forth in IEEE Std C95.3-1991. This document includes leakage and near-field measurements. Further, many contemporary RF exposure guidelines and standards, including IEEE Std C95.1-1991, recommend limits for specific absorption rate (SAR) in biological tissues and limits for induced current and contact current associated with exposure to electromagnetic fields. Therefore, this recommended practice includes a description of the concepts,

computational techniques, and measurement techniques and instrumentation that can be applied to the determination of SAR in organisms and phantoms exposed to electromagnetic fields, and a description of the instrumentation and techniques for measuring induced and contact currents. This document also discusses several methods that can be used to calibrate field-measuring instruments, instruments for measuring SAR, and instruments used for measuring induced and contact current.

This document is intended primarily for use by engineers, biophysicists, and other specialists who are familiar with basic electromagnetic (EM) field theory and practice, and the potential hazards associated with EM fields. It will be most useful to bioeffects researchers, instrument developers, and manufacturers, those developing calibration systems and standards, and individuals involved in critical hazard assessments or surveys.

Subcommittee 1 on Techniques, Procedures, Instrumentation and computation was originally organized on 7 April 1960, to establish specifications for techniques and instrumentation used in evaluating potentially hazardous radio frequency (RF) radiation. In June 1985 the scope was clarified and the purpose was extended to establish specifications for techniques and instrumentation to be used in evaluating potential RF hazards to mankind from exposure to manmade sources of EM radiation or from the exposure of volatile materials and explosive devices to such radiation. The subcommittee does not address infrared, visible, ultraviolet, or ionizing radiation

The following is a list of participants in Subcommittee I on Techniques, Procedures, Instrumentation, and Computation of IEEE International Committee on Electromagnetic Safety (ICES—Standards Coordinating Committee 28).

Howard Bassen, *Chair*

Ronald C. Petersen, *Secretary*

Eleanor R. Adair
Edward Aslan
Tadeusz M. Babij
Quirino Balzano
David Baron
John A. Bergeron
Aviva Brecher
C. K. Chou
Robert F. Cleveland
Jules Cohen
David L. Conover
Alice Fahy-Elwood
Om P. Gandhi
Arthur W. Guy
Wayne C. Hammer
James B. Hatfield
William D. Hurt
Veronica Ivans
Motohisa Kanda*
Werner Kumbier
Niels Kuster
John A. Leonowich
Raymond Luebbers
Ed Mantiply
Stewart Maurer
Martin Misakian
Michael R. Moore
Richard G. Olsen
John M. Osepchuk
Brad J. Roberts
Veli Santomaa
Richard A. Tell
Donald J. Umbdenstock
Louis A. Williams, Jr.

*Deceased

The following members of the balloting committee voted on this standard. Balloters may have voted for approval, disapproval, or abstention.

J. Robert Ashley
William Bailey
David Baron
Aviva Brecher
C. K. Chou
Jules Cohen
Robert Curtis
Thahn Dovan
Kenneth Gettman
Gregory Gorsuch
Sheila Johnston
Shaiela Kandel
Joseph L. Koepfinger
John Leonowich
James Lin
Arthur Light
Patrick Mason
Daleep Mohla
Abdul Mousa
Michael Newman
John M. Osepchuk
Ronald C. Petersen
Steve Pittman
Vikram Punj
Markus Riederer
Ervin Root
Mays Swicord
Arthur Varanelli
Louis A. Williams, Jr.
Richard Woods
Donald W. Zipse
Marvin Ziskin

When the IEEE-SA Standards Board approved this standard on 11 December 2002, it had the following membership:

James T. Carlo, *Chair*
James H. Gurney, *Vice Chair*
Judith Gorman, *Secretary*

Sid Bennett
H. Stephen Berger
Clyde R. Camp
Richard DeBlasio
Harold E. Epstein
Julian Forster*
Howard M. Frazier
Toshio Fukuda
Arnold M. Greenspan
Raymond Hapeman
Donald M. Heirman
Richard H. Hulett
Lowell G. Johnson
Joseph L. Koepfinger*
Peter H. Lips
Nader Mehravari
Daleep C. Mohla
William J. Moylan
Malcolm V. Thaden
Geoffrey O. Thompson
Howard L. Wolfman
Don Wright

*Member Emeritus

Also included is the following nonvoting IEEE-SA Standards Board liaison:

Alan Cookson, *NIST Representative*
Satish K. Aggarwal, *NRC Representative*

Noelle D. Humenick
IEEE Standards Project Editor

Contents

IEEE Recommended Practice for Measurements and Computations of Radio Frequency Electromagnetic Fields With Respect to Human Exposure to Such Fields, 100 kHz–300 GHz

1. Overview

1.1 Scope

The scope of this recommended practice is to revise and develop specifications for preferred methods for measuring and computing external radio frequency electromagnetic fields to which persons may be exposed. In addition, the document will specify preferred methods for the measurement and computation of the resulting fields and currents that are induced in bodies of humans exposed to these fields over the frequency range of 100 kHz–300 GHz.

Although the scope of ICES (formerly SCC28) includes potential hazards resulting from exposure of flammable volatile materials and explosive devices to EM radiation, this document is devoted exclusively to the measurement and calculation of human exposure to electromagnetic fields. This is because the necessary specifications and definitions pertaining to fuels and explosive devices are still being developed, and there are implications that the instrumentation requirements may be substantially different from those addressed here. Nevertheless, the measurement techniques and instruments described here are applicable to the measurement of fields in the vicinity of flammable materials and explosive devices, even though exposure standards for these situations have not been established.

1.2 Purpose

The purpose of this recommended practice is to specify techniques and instrumentation for the measurement and computation of potentially hazardous electromagnetic (EM) fields both in the near field and the far field of the electromagnetic source.[1] In doing so, this document incorporates and extends the specifications previously set forth in IEEE Std C95.3™-1991 [B136].[2] This recommended practice includes leakage and

[1]It is beyond the scope of this recommended practice to define what constitutes a hazardous radio frequency electromagnetic field. Maximum permissible exposure guides can be found, for example, in IEEE Std C95.1-1991 or the recommendations of the International Commission on Non-Ionizing Radiation Protection [B132]. It should be kept in mind that the limits given in such documents are continually under review and are subject to change as new information becomes available.

[2]The numbers in brackets correspond to those in the Bibliography in Annex G.

near-field measurements. Further, IEEE Std C95.1™-1991 and other contemporary standards and guidelines for personnel exposure include specific absorption rate (SAR) in biological tissues as a parameter to be determined. Accordingly, this document contains a description of the concepts, techniques, and instruments that can be applied to the measurement and computation of SAR or the electric field strength in organisms (including humans) and phantoms exposed to electromagnetic fields. Below approximately 100 MHz, the current flowing through the body to ground is measurable and can be used to determine the SAR, and therefore, a brief treatment of low-frequency body current measurement is also included.

This document is intended primarily for use by engineers, biophysicists, and other specialists who are familiar with basic electromagnetic (EM) field theory and practice, and the potential hazards associated with exposure to EM fields. It will probably be most useful to bioeffects researchers, instrument developers and manufacturers, those developing calibration systems and standards, and individuals involved in critical hazard assessments or surveys. Interested parties seeking a less technical document describing how to measure potentially hazardous fields may refer to NCRP Report 119 [B196]. However, the material in Clause 3, Clause 4, and Clause 5 of this document, which treats measurement problems, desirable instrument characteristics, and procedures for measuring external fields should be of value to anyone concerned with potential EM hazards.

Subcommittee 1 on Techniques, Procedures, Instrumentation, and Computation was originally organized on 7 April 1960, to establish specifications for techniques and instrumentation used in evaluating potentially hazardous radio frequency (RF) radiation. In June 1985, the scope was clarified and the purpose was extended to establish specifications for techniques and instrumentation to be used in evaluating potential RF hazards to mankind from exposure to manmade sources of EM radiation or from exposure of volatile materials and explosive devices to such radiation. It is not intended to include infrared, visible, ultraviolet, or ionizing radiation.

Although the scope of SCC-28 includes potential hazards resulting from exposure of flammable volatile materials and explosive devices to EM radiation, this document is devoted exclusively to potential hazards to personnel. This is because the necessary specifications and definitions pertaining to fuels and explosive devices are still being developed, and there are implications that the instrumentation requirements may be substantially different from those addressed here. However, the measurement techniques and instruments described here are applicable to the measurement of fields in the vicinity of flammable materials and explosive devices, even though exposure standards for these situations have not been established.

1.3 Frequency range

The techniques and instrumentation specified herein are useful for field measurements over the frequency range of approximately 100 kHz to about 100 GHz.[3] No single measurement technique or instrumentation arrangement is valid over the wide frequency range covered by this recommended practice. In general, techniques and instrumentation developed for use in the frequency range below about 900 MHz apply to the measurement of both the electric and magnetic field strengths. To evaluate potentially hazardous near-field situations at frequencies below a few hundred MHz, measurement of both the electric and the magnetic field strength is required. A series of commercially available instruments has been developed for this purpose. For body currents, measurements can be made with simple, portable laboratory instruments over the frequency range of 0 to about 100 MHz. SAR can be measured using RF-transparent temperature sensors over the frequency range of 100 kHz to about 6 GHz and can be measured in phantoms using E-field probes over the frequency range of 300 MHz to about 3 GHz. Above about 6 GHz, absorption is confined to the surface of a biological system and thermographic cameras can be used to measure the surface SAR up to about 300 GHz.

[3]These frequency limits should not be considered rigid, but are given as a general guide. Normally, a given instrument does not abruptly become invalid at a specific frequency; rather its accuracy, sensitivity, or both, deteriorate over some frequency range until finally it is no longer usable. For example, an instrument designed for the lower frequencies may cover the entire broadcast band down to 0.5 MHz. When using a given instrument, one should be aware of its frequency limitations.

1.4 Quantities and parameters to be measured

For frequencies above 300 MHz, and for measurements performed at distances from the source greater than a a^2/λ (a is the largest dimension of the effective aperture of the source, and λ is the wavelength) with a probe whose dimensions are much less than a, power density S is usually a meaningful quantity that has been widely adopted as a hazard indicator. However, power density is difficult to determine, except in cases of stationary, single-component, plane-wave fields of known polarization. In fact, no existing instrument actually measures power density directly; all measure one or more components of the electric field strength (E), or the magnetic field strength (H), or both, and then infer an equivalent power density from the far-field, plane-wave relationship $S = |E|^2/(120\pi)$ or $120\pi|H|^2$, where E is the rms electric field strength in volts per meter, H is the rms magnetic field strength in amperes per meter, and S is the power density in watts per meter squared. In the near field, and where scattering, reflections, or multiple sources are present, the field configuration can be extremely complex and one must measure both E and H separately.[4] In many instances, measurements will be required in the reactive or radiating near-field regions where reactive fields or standing waves exist.[5] Under these more general conditions, the time-averaged power density is not a reliable hazard indicator, even if practical probes could be developed for its measurement. Under these complex conditions, induced current (for frequencies below about 100 MHz) and SAR (for frequencies between about 100 kHz and about 6 GHz) are the more meaningful quantities.

Because for plane waves all of the preceding parameters are simply related to power density, no loss of generality would occur with the use of these parameters for far-field measurements. As stated previously, some commercially available meters actually measure $|E|^2$ or $|H|^2$, while indicating equivalent plane-wave power density. Therefore, they do provide a valid indication of the exposure level and, hence, the potential hazard, even though they may not indicate the actual power density at the point of measurement. Because RF-hazard measurement instrumentation is currently not available to measure absolute peak values, except for pulses of RF energy of duration greater than a few milliseconds, rms values will be considered unless otherwise stated. As the state-of-the-art advances, recommendations will be extended to include absolute peak quantities. For internal dosimetry (within body tissues), the quantities used are SAR (W/kg), internal rms, and peak electric field strength (V/m), internal current (A), and current density (A/m^2).

1.5 Types of situations covered

This recommended practice is intended for use in situations typified by the following.

1.5.1 External fields

a) Leakage fields
b) Radiation fields
c) Reactive fields

Leakage fields are generally interpreted as those resulting from the unintentional emission of RF energy, whereas radiation fields are generally interpreted as those resulting from equipment designed to intentionally radiate EM energy. Reactive fields are present in the immediate vicinity of sources of both leakage and radiation fields and tend to be stronger near radiators of small dimensions with respect to wavelength. Multipath interference due to the scattering and reflection of energy from objects or conducting surfaces is an additional complicating factor and is present to some degree in most situations. Accurate measurements should include procedures for estimating or avoiding multipath effects and near-field measurement errors. Some useful techniques for measurements in multipath environments are given in Clause 6 (see 6.3.2 and 6.3.3).

[4]For well-defined sources where analysis indicates that only one field component is sufficient to show compliance with a particular maximum permissible exposure (MPE) level or radio frequency protection guide (RFPG), only that component need be measured.

[5]See definitions in Clause 3.

1.5.2 Specific absorption rate (SAR)

The need for SAR measurements within models of exposed personnel is twofold. First, over the frequency range where SAR is meaningful (approximately 100 kHz–6 GHz), it is the underlying basis for the maximum permissible exposure (MPE) values found in many contemporary RF safety standards and guidelines, including those of IEEE Std C95.1-1991. That is, the MPEs in terms of the external fields, induced current, and induced current density are derived from the basic dosimetric quantity SAR over its meaningful frequency range [B55]. The external field strength MPEs in many RF exposure guidelines and standards, e.g., IEEE Std C95.1-1991, ICNIRP [B132], limit the whole-body-averaged SAR to 0.4 and 0.08 W/kg for the controlled and uncontrolled environments, respectively. Compliance with such standards and guidelines is assured if the whole-body-averaged SAR and specific local (or spatial-peak) SAR criteria, e.g., 8 W/kg and 1.6 W/kg in any gram of tissue in the shape of a cube, are met, even if the field strength MPEs are exceeded. Generally, accepted SAR measurement methods [B55], [B195] include the measurement of the rate of temperature rise within the exposed object or the measurement of the internal electric field strength. The temperature rise may be characterized by a whole-body-averaged (calorimetric) measurement, a point measurement (via a thermometer implanted in the object being exposed), or thermographic camera analyses of bisected phantom models and animal carcasses that have been exposed to large RF fields. The internal electric field strength may be measured with an implantable E-field probe or may be computed using sophisticated numerical methods.[6]

The second need for determining SAR is that even under far-field plane-wave exposure conditions, the SAR varies widely with frequency, polarization, and spatial location within an object. The determination of the SAR provides a much-needed insight into the spatial distribution of absorbed energy, particularly with respect to different organs of the exposed subject.

1.5.3 Induced and contact current

Internal currents are induced in humans when partial or whole-body exposures to RF fields occur. The issue of induced body currents generally becomes a consideration at lower frequencies, typically below 100 MHz, and especially below 30 MHz. Most often, the evaluation of excessive induced body current occurs in the near-field region of the RF source. For greatest accuracy in predicting the magnitude of these induced currents in humans, use of a full size model is required. The model is placed in the near-field region of the source in question, simulating the position, posture, and size of the potentially exposed individual. Then, special measurement techniques are used to evaluate the RF-induced currents. A complication associated with evaluating the magnitude of induced RF current relates to pathways through which these currents flow in the body. For example, when the exposure is such that the electric field is parallel to the axis of the body, the induced currents flow through the body, or parts of the body, commonly through the legs and the feet to the ground or floor (whichever is the lowest potential surface in contact with the body). The use of instrumentation, which is in effect placed in series with the body and ground, can provide a measure of these electric field induced currents. In the case of magnetic field exposure, however, the currents that are induced in the body, called eddy currents, most commonly circulate about the cross sections of the anatomy, with the greater magnitudes being at the outer periphery of the body, near the surface. These circulating currents tend not to exit the body in the same fashion as electric field induced currents and, consequently, represent a major measurement challenge. Assessments of induced currents should, however, give consideration to both electric and magnetic field contributions.

2. References

This recommended practice shall be used in conjunction with the following publication. When the following specification is superseded by an approved revision, the revision shall apply.[7]

---

[6]Protocols for determining the peak spatial-average SAR induced by specific products, e.g., hand-held radio transceivers used for personal wireless communications, are developed by IEEE Standards Coordinating Committee 34.

IEEE Std C95.1™, 1999 edition, IEEE Standard for Safety Levels with Respect to Human Exposure to Radio Frequency Electromagnetic Fields, 3 kHz–300 GHz. [8]

3. Definitions

For the purposes of this recommended practice, the following terms and definitions apply.

3.1 amplitude modulated average power output: The radio frequency power delivered to the transmitter output terminals averaged over a modulation cycle.

3.2 anechoic chamber: A room or enclosure in which reflections of electromagnetic waves from the boundary surfaces have relatively small values.

3.3 antenna: A device designed for radiating (or receiving) electromagnetic energy.

3.4 antenna aperture: A surface, near or on an antenna, on which it is convenient to make assumptions regarding field values for the purpose of computing fields at external points.

NOTE—The aperture is often taken as that portion of a plane surface near the antenna, perpendicular to the direction of maximum radiation, through which the major part of the radiation passes.

3.5 antenna array: A system of antennas coupled together for the purpose of enhancing radiation in one or more directions and reducing radiation in other directions.

3.6 antenna directivity: The ratio of the transmitted radio frequency radiation intensity in a specified direction to the radiation intensity averaged over all directions.

NOTE—The average radiation intensity is equal to the power radiated by the antenna divided by 4π.

3.7 antenna effective aperture or effective area: In a given direction, the ratio of the power available at the terminals of a receiving antenna to the power density of a plane wave incident on the antenna from that direction; the wave being polarization-matched to the antenna.

NOTES

1—A plane wave of given power density and from a given direction is polarization-matched to an antenna if its polarization is that which results in maximum power at the antenna terminals.

2—The (total) effective aperture of an antenna may be decomposed into the sum of two partial effective apertures referred to two specified, orthogonal polarizations, respectively.

3—For a lossless and perfectly matched antenna, effective area in a given direction is equal to the square of the operating wavelength, times the gain in that direction, divided by 4π.

3.8 antenna field regions: Classification of the important spatial subdivisions of an antenna's electromagnetic field. The subdivisions, at non-uniquely defined distances from the antenna, include the reactive near-field region adjacent to the antenna, the radiating near-field region (for large antennas commonly referred to as the Fresnel region), a transition zone, and furthermost, the far-field region, also known as the Fraunhofer region. *See also:* **near-field region and far-field region.**

---

[7]The IEEE standards or products referred to in Clause 2 are trademarks owned by the Institute of Electrical and Electronics Engineers, Incorporated.

[8]IEEE publications are available from the Institute of Electrical and Electronics Engineers, 445 Hoes Lane, P.O. Box 1331, Piscataway, NJ 08855-1331, USA (http://standards.ieee.org/).

3.9 antenna gain (absolute gain in a given direction): The ratio of the radiation intensity, in a given direction, to the radiation intensity that would be obtained if the power accepted by the antenna was radiated isotropically.

NOTES

1—Gain does not include losses arising from impedance and polarization mismatches.

2—The radiation intensity corresponding to the isotropically radiated power is equal to the power accepted by the antenna divided by 4π.

3—If an antenna is without dissipative loss, then in any given direction, its gain is equal to its directivity.

4—If the direction is not specified, the direction of maximum radiation intensity is implied.

5—The term "absolute gain" is used in those instances where added emphasis is required to distinguish gain from relative gain, for example, absolute gain measurements.

3.10 antenna gain, partial (for a given polarization): In a given direction, that part of the radiation intensity corresponding to a given polarization, divided by the radiation intensity that would be obtained if the power accepted by the antenna were radiated isotropically.

NOTES

1—The (total) gain of an antenna, in a specified direction, is the sum of the partial gains for any two orthogonal polarizations.

2—The gain of aperture antennas, e.g., parabolic reflectors, is usually referenced to an isotropic radiator; The gain of linear antennas, dipoles, and colinear arrays is usually referenced to a half-wave dipole.

3.11 antenna lobe: A part of the antenna radiation pattern between adjacent minima.

3.12 antenna pattern: The spatial distribution of a quantity that characterizes the electromagnetic fields radiated by an antenna.

NOTES

1—The distribution can be expressed as a mathematical function or as a graphic representation.

2—The quantities that are most often used to characterize the radiation from an antenna are proportional to, or equal to, power density, radiation intensity, directivity, phase, polarization, and field strength.

3—The spatial distribution of the EM field characteristics over any surface is also an antenna pattern.

4—When the amplitude or relative amplitude of a specified component of the electric field vector is plotted graphically, it is called the amplitude pattern, field pattern, or voltage pattern. When the square of the amplitude or relative amplitude is plotted, it is called a power pattern.

3.13 antenna terminal impedance or driving-point impedance: The ratio of complex voltage to complex current at the terminals of a transmitting antenna, or the ratio of the open-circuit voltage to the short-circuit current at the terminals of a receiving antenna.

3.14 athermal effect (nonthermal effect): Any effect of electromagnetic energy absorption not associated with or dependent on the production of heat or a measurable rise in temperature.

3.15 attenuation: A general term, expressed as a ratio, used to denote a decrease in magnitude of a field quantity in the transmission from one point to another.

NOTE—The attenuation may be expressed as a ratio or, by extension of the term, in decibels.

3.16 average power ($\bar{P}$): The time-averaged rate of energy transfer:

$$\bar{P} = \frac{1}{t_2 - t_1}\left(\int_{t_1}^{t_2} P(t)dt\right)$$

3.17 average power density: The instantaneous power density integrated over a specific time duration. The time duration could be source related, e.g., the source repetition period, or use related, e.g., the averaging time specified in exposure guidelines. Average power density is expressed in units of watts per square meter (W/m^2).

NOTE—In speaking of average power density in general, it is necessary to distinguish between the spatial average (at a given instant) and the time average (at a given point).

3.18 backward scatter: Energy directed (scattered) into the rear hemisphere with respect to the direction of incident energy.

3.19 bolometer: A device capable of absorbing radiant energy and of using the heat so developed to change its electrical resistance, thus indicating the amount of energy absorbed.

3.20 conductivity: The ratio of the conduction-current density in a medium to the electric field strength. The unit of conductivity is siemens per meter (S/m).

3.21 dielectric constant: *See:* **permittivity**.

3.22 diode: A semiconductor device having two terminals and exhibiting a nonlinear voltage-current characteristic; in more restricted usage, a semiconductor device that has the asymmetrical voltage-current characteristic exemplified by a single p-n junction.

3.23 dipole: (A) Any one of a class of antennas producing the radiation pattern approximating that of an elementary electric dipole. **(B)** A linear radiator, usually fed in the center, producing a maximum of radiation in the plane normal to its axis. The length specified is the overall length.

NOTE—Common usage considers a dipole antenna to be a metal radiating structure that supports a line-current distribution similar to that of a thin straight wire, a half-wavelength long, so energized that the current has a node only at each end.

3.24 driving-point impedance: *See:* **antenna terminal impedance**.

3.25 duty cycle: Deprecated. *See also:* **duty factor**.

3.26 duty factor: The ratio of the pulse duration to the pulse period of a periodic pulse train.

3.27 duty ratio: The ratio of average to peak pulse power.

3.28 effective aperture: *See:* **antenna effective aperture**.

3.29 effective area: *See:* **antenna effective aperture**.

3.30 electric dipole: A pair of equal and opposite charges separated by an infinitesimal distance. When the charges are oscillating, the dipole becomes an elementary radiating electric dipole.

3.31 electric field (general): A vector field of electric field strength or of electric flux density.

NOTE—The term is also used to denote a region in which such vector fields have a significant magnitude.

3.32 electric field strength (E): (A) (General): At a given point, the magnitude (modulus) of the vector limit of the quotient of the force that a small stationary charge at that point will experience, by virtue of its charge, to the charge as the charge approaches zero in a macroscopic sense. **(B)** (Signal-transmission system): The magnitude of the potential gradient in an electric field expressed in units of potential difference per unit length in the direction of the gradient. **(C)** (Radio wave propagation): The magnitude of the electric field vector. The electric field strength is expressed in units of volts per meter (V/m).

3.33 electric field vector: The force on a stationary positive charge per unit charge.

NOTE—This may be measured either in newtons/coulomb or in volts/meter. This term is sometimes called the electric field intensity, but such use of the word intensity is deprecated, because intensity connotes power in optics and radiation.

3.34 electrical length: The length of any electrical conductor, such as an antenna or transmission line, expressed in wavelengths, radians, or degrees.

NOTE—When expressed in angular units, it is distance in wavelengths multiplied by 2π to give radians, or by 360 to give degrees.

3.35 electric flux density (displacement): A vector equal to the product of the electric field strength and the permittivity of the medium. In an anisotropic medium, the permittivity is a function of direction; hence, the electric flux density is not necessarily in the same direction as the electric field strength. Electric flux density can be considered as a surface charge density and is expressed in units of coulombs per square meter (C/m^2).

3.36 electromagnetic field: Electromagnetic phenomena expressed in scalar or vector functions of space and time.

3.37 electromagnetic radiation: The propagation of energy in the form of electromagnetic waves through space. (Not intended to describe propagation along waveguides and other transmission lines.)

3.38 equivalent plane-wave power density: The normalized value of the square of the electric or the magnetic field strength at a point in the near field of a radiating source. The value is expressed in W/m^2 and is computed as follows:

$$S = |E|^2/(120\pi) = |H|^2 \times 120\pi$$

3.39 far-field region: That region of the field of an antenna where the angular field distribution is essentially independent of the distance from the antenna. In this region (also called the free-space region), the field has a predominantly plane wave character, i.e., locally, very uniform distributions of electric field strength and magnetic field strength in planes transverse to the direction of propagation. For larger antennas especially, the far-field region is also referred to as the Fraunhofer region.

3.40 finite difference time domain (FDTD) method: The FDTD method is a numerical algorithm for solving Maxwell's differential equations of electromagnetic field interactions in the time domain by discretizing the problem space into unit cells where the space and time derivatives of the electric and magnetic fields are directly approximated by simple, second-order accurate central-difference equations.

3.41 half-power beamwidth: In a plane containing the direction of the maximum lobe of the antenna pattern, the angle between the two directions in which the radiated power is one-half the maximum value of the lobe.

3.42 heat capacity: The amount of heat necessary to raise the temperature of a given mass of a substance one degree. Heat capacity is expressed in joules per kg kelvin (J/kg K) or joules per kg degree Celsius (J/kg ºC).

3.43 horn antenna: An antenna consisting of a waveguide section whose cross-sectional area increases toward the open end that is the aperture through which electromagnetic energy is radiated or received.

3.44 horn radiator: *See:* **horn antenna**.

3.45 incident wave: A wave, traveling through a medium, in a specified direction, which impinges on a discontinuity or a medium of different propagation characteristics.

3.46 insertion loss: The loss resulting from the insertion of a component in a transmission system. It is the ratio of the power delivered to the load when connected to the generator, to the power delivered to the load when the component is inserted. Insertion loss is usually expressed in decibels.

3.47 internal body current: The current that is induced in a biological subject that is exposed to low-frequency radio frequency fields.

3.48 intrinsic impedance (of free space): The ratio of the electric field strength to the magnetic field strength of a propagating electromagnetic wave. The intrinsic impedance of a plane wave in free space is equal to $1.20\pi\ \Omega$ (approximately 377 Ω).

3.49 ionizing radiation: Any electromagnetic or particulate radiation capable of producing ions directly or indirectly in its passage through matter. Examples are X-rays and gamma rays.

3.50 isotropic: Having the same properties in all directions.

3.51 isotropic antenna: An antenna capable of radiating or receiving equally well in all directions, and equally responsive to all polarizations of electric and/or magnetic fields.

NOTE—In the case of transmitting coherent electromagnetic waves, an isotropic antenna does not exist physically, but represents a convenient reference antenna for expressing directional properties of an actual transmitting antenna.

3.52 loss tangent: The ratio of the imaginary component of the complex permittivity of a material to the real component of the complex permittivity.

3.53 magnetic dipole: A magnetic field moment caused by current flowing in an infinitesimally small loop. When the current is oscillating, the dipole becomes an elementary radiating magnetic dipole.

3.54 magnetic field strength (H): The magnitude of the magnetic field vector, expressed in units of amperes per meter (A/m).

3.55 magnetic field vector: A field vector that is equal to the ratio of the magnetic flux density to the permeability, expressed in units of amperes per meter (A/m).

3.56 magnetic flux density (magnetic induction): The vector quantity $\bar{B}$ producing a torque $\bar{T}$ (in Newton meters) on a plane current loop in accordance with the relation $\bar{T} = LA\bar{n} \times \bar{B}$, where $\bar{n}$ is the positive unit

vector normal to the loop, A is its area in m^2, and I is the loop current in amperes. Magnetic flux density is expressed in units of Teslas (T), formerly webers per square meter.

NOTE—The tesla is often defined as equal to a weber per square meter (Wb/m^2), but as can be seen from the above equation for T, the tesla is also equal to a newton per ampere meter ($N/A \cdot m$).

3.57 maximum normalized field strength: The value of the maximum spatial electric field strength E or the maximum spatial magnetic field strength H under a set of specific near-field exposure conditions (in a prescribed volume of space) that is equal to the corresponding value of E or H associated with a plane wave of given power density.

NOTE—The maximum normalized field strength concept is used to aid in the assessment of the relationship between exposure of an object to external near-fields and the resulting internal SAR.

3.58 maximum permissible exposure (MPE): The rms and peak electric and magnetic field strengths, their squares or the plane-wave equivalent power densities associated with these fields and the induced and contact currents to which a person may be exposed without harmful effect and with an acceptable safety factor. In some guidelines, they are referred to as investigation levels or reference levels.

3.59 microwaves: A term used rather loosely to signify radio waves in the frequency range from about 300 MHz upward.

3.60 modulation: The process, or result of the process, whereby some characteristic of one wave is varied in accordance with another wave or signal.

NOTE—For the purpose of this recommended practice, continuous wave (CW) operation is considered to be a special form of modulation, that is, zero modulation.

3.61 multipath error: The error caused by the reception of a composite signal that arrives via two or more different paths.

3.62 multipath transmission (radio propagation): The propagation phenomenon that results in signals reaching the receiving antenna by two or more paths.

3.63 near-field region: A region in the field of an antenna, located near the antenna, in which the electric and magnetic fields do not have a substantially plane-wave character, but vary considerably from point to point. The term is only vaguely defined and has different meanings for large and small antennas. It is further subdivided into the reactive near-field region, which is closest to the antenna and contains most or nearly all of the stored energy associated with the field of the antenna, and the radiating near-field region. If the antenna has a maximum overall dimension that is not large compared with the wavelength, the radiating near-field region may not exist. For antennas large in terms of wavelength, the radiating near-field region is sometimes referred to as the Fresnel region on the basis of analogy to optical terminology.

NOTE—For most antennas, the outer boundary of the reactive near-field region is commonly taken to exist at a distance of one-half wavelength from the antenna surface.

3.64 nonionizing radiation: Any electromagnetic radiation incapable of producing ions directly or indirectly. Microwaves and radio frequency energy are forms of nonionizing radiation.

3.65 nonthermal effect: *See:* **athermal effect**.

3.66 parabolic antenna: An antenna consisting of a parabolic reflector and a source at or near its focus.

3.67 passive or parasitic re-radiator: Electrically conducting structures that, when illuminated by a primary radio frequency source or ambient electromagnetic fields, act as a secondary radiating source

because of currents induced in the structure. In some cases, re-radiators can produce localized electromagnetic fields significantly more intense than the fields at the location of the re-radiator that are associated with the prime source.

3.68 peak power density: The maximum instantaneous power density occurring during the interval when power is transmitted.

3.69 peak power output: In a modulated carrier system, the output power averaged over a carrier cycle, at the maximum amplitude that can occur with any combination of signals to be transmitted.

3.70 peak pulse amplitude: The maximum absolute peak value of a pulse excluding those parts considered to be unwanted, such as spikes, provided that the energy is small (5% or less) compared with the total energy at the pulse.

NOTE—Where such excursions are made, it is desirable that the amplitude chosen be illustrated pictorially.

3.71 peak spatial-average specific absorption rate (SAR): The maximum local SAR averaged over a specified volume or mass, e.g., any 1 g or 10 g of tissue in the shape of a cube. SAR is expressed in units of watts per kilogram (W/kg).

3.72 penetration depth: For a plane electromagnetic wave incident on the boundary of a medium, the distance from the boundary into the medium along the direction of propagation in the medium, at which the field strengths of the wave have been reduced to 1/e of their boundary values. Penetration depth is expressed in meters (m).

3.73 permittivity (complex): The ratio of the electric flux density in a medium to the electric field strength at a point. The permittivity of biological tissues is frequency dependent. Permittivity is expressed in units of farad per meter (F/m).

3.74 polarization (radiated wave): That property of a radiated electromagnetic wave describing the time-varying direction and amplitude of the electric field vector; specifically, the figure traced as a function of time by the extremity of the E-field vector at a fixed location in space, as observed along the direction of propagation.

NOTE—In general, the figure is elliptical and it is traced in a clockwise or counterclockwise sense. The commonly referenced circular and linear polarizations are obtained when the ellipse becomes a circle or a straight line, respectively. Clockwise sense rotation of the electric vector is designated right-hand polarization and counterclockwise sense rotation is designated left-hand polarization.

3.75 power: A physical quantity describing the rate of delivery or transmission of energy. In this document, power will refer to radio frequency power with units of watts (W).

3.76 power density: Power per unit area normal to the direction of propagation, usually expressed in watts per meter squared (W/m^2) or, traditionally, mW/cm^2. *See also:* **Poynting vector**.

NOTE—$10\ W/m^2 = 1\ mW/cm^2$

3.77 power gain: Of an amplifying device, the ratio of the radio frequency power delivered to a specified load impedance to the radio frequency power absorbed by its input. *See also:* **antenna gain**.

NOTE—Power gain is usually expressed in decibels.

3.78 power level: At any point in a transmission system, the ratio of the power at that point to some arbitrary amount of power chosen as a reference. This ratio is usually expressed as decibels referred to 1 mW (dBm) or decibels referred to 1 W (dBW).

3.79 Poynting vector: A vector $\bar{P}$, defined as the vector product of the electric and magnetic field vectors at the point in question, that is, $\bar{P} = \bar{E} \times \bar{H}$.

NOTE—$\bar{P}$ is expressed in units of watts per square meter and, for a uniform plane wave, represents the electromagnetic energy flow per unit area per unit time across a given surface element.

3.80 probe: A minimally perturbing device used for measuring a component of a radio frequency field in a medium. A probe contains the following components:

a) An electrically small (in the medium) sensor (or sensors) for detecting the radio frequency field component of interest

b) A means for converting the RF signal to a proportional dc or slowly varying ac signal

c) A balanced high-impedance resistive transmission line to extract the rectified signal

3.81 probe antenna-length: The maximum physical dimension of the sensing element, e.g., dipole or loop of an electric or magnetic field probe, respectively, or the dimension of the largest sensing element in a multiple array.

3.82 pulse repetition frequency (PRF): In a pulse-modulated radio frequency system using recurrent pulses, the number of pulses per unit of time.

3.83 pulse repetition rate: *See:* **pulse repetition frequency**.

3.84 pulsed radio frequency (PRF): A continuous-wave radio frequency carrier signal that is amplitude-modulated at a known PRF with a controlled duty factor.

3.85 radar: A system that radiates pulsed or frequency-modulated electromagnetic waves and utilizes the reflection of such waves from distant objects to determine their existence and/or position.

NOTE—The name is derived from initial letters of the expression "radio detection and ranging."

3.86 radiation intensity: In a given direction, the power radiated from an antenna per unit solid angle in that direction. The units are watts per steradian (W/sr).

3.87 radio beam: Radiowaves whose energy is essentially confined within a relatively small angle in at least one plane.

3.88 radio frequency (RF): The frequency in the portion of the electromagnetic spectrum that is between the audio-frequency portion and the infrared portion.

NOTE—The present practicable limits of radio frequency are roughly 10 kHz–300 GHz. Within this frequency range, electromagnetic radiation may be detected and amplified as an electric current at the wave frequency.

3.89 radio frequency protection guide (RFPG): Deprecated. *See:* **maximum permissible exposure (MPE)**.

3.90 radio frequency radiation hazard meter (monitor): An instrument that is capable of measuring spatially localized electric and/or magnetic field strengths under near- and far-field conditions. The instrument consists of a sensor with an antenna suitable for the wavelength under study, plus a means for transmitting information from the sensor to a suitable field strength indicator.

3.91 reactive field: Electric and magnetic fields surrounding an antenna or other electromagnetic devices that result in storage rather than propagation of electromagnetic energy.

3.92 reflected wave: A wave in a medium produced by reflections from objects or discontinuities in the medium or from a boundary of a different medium.

3.93 re-radiated field: An electromagnetic field resulting from currents induced in a secondary, predominantly conducting object by electromagnetic waves incident on that object from one or more primary radiating structures or antennas. Re-radiated fields are sometimes called "reflected" or, more correctly "scattered fields." The scattering object is sometimes called a "re-radiator" or "secondary radiator." *See also:* **re-radiator**.

3.94 response time: The time required for a field-measuring instrument to reach some specified percentage of the final value after being placed in the field to be measured. In this document, 90% of the final value is assumed.

3.95 separation distance: As applied to the measurement of electric and magnetic fields, separation distance means the distance between a source and the nearest point on the probe sensing elements.

3.96 scattering: The process that causes waves incident on discontinuities or boundaries of media to be changed in direction, frequency, phase, or polarization.

3.97 skin depth: *See:* **penetration depth**.

3.98 spatial average: As applied to the measurement of electric or magnetic fields for the assessment of whole-body exposure means the root mean square of the field over an area equivalent to the vertical cross section of the adult human body. The spatial average can be measured by scanning (with a suitable measurement probe) a planar area equivalent to the area occupied by a standing adult human (projected area). In most instances, a simple vertical, linear scan of the fields over a 2 m height will be sufficient.

3.99 specific absorption rate (SAR): The time derivative (rate) of the incremental energy (dW) absorbed by (dissipated in) an incremental mass (dm) contained in a volume element (dV) of a given density (ρ).

$$SAR = \frac{d}{dt}\left(\frac{dW}{dm}\right) = \frac{d}{dt}\left(\frac{dW}{\rho dV}\right)$$

SAR is expressed in units of watts per kilogram (W/kg).

NOTES

1—SAR can be related to the electric field at a point by

$$SAR = \frac{\sigma |E|^2}{\rho}$$

Where

σ is the conductivity of the tissue (S/m),

ρ is the mass density of the tissue (kg/m^3),

E is the rms electric field strength (V/m).

2—SAR can be related to the increase in temperature at a point by

$$SAR = \frac{c\Delta T}{\Delta t}$$

Where

ΔT is the change in temperature (°C),

Δt is the duration of exposure (seconds),

c is the specific heat capacity (J/kg °C).

This assumes that measurements are made under "ideal" non-thermodynamic circumstances, i.e., no heat loss by thermal diffusion, heat radiation, or thermoregulation (blood flow, sweating, etc.).

3.100 specific heat capacity: *See:* **heat capacity**.

3.101 standing wave: A spatially periodic or repeating field pattern of amplitude maxima and minima that is generated by two equal-wavelength propagating waves traveling in different directions. For any component of the field, the ratio of the amplitude at one point to that at any other point does not vary with time.

3.102 standing wave ratio: The ratio of maximum field strength to minimum field strength along the direction of propagation of two waves traveling in opposite directions on a transmission line.

3.103 thermocouple: A pair of dissimilar conductors so joined at two points that an electromotive force is developed by the thermoelectric effect when the junctions are at different temperatures.

3.104 waveguide: An enclosed system capable of guiding electromagnetic waves from one place to another. A waveguide usually consists of a hollow metallic tube or a solid dielectric material.

3.105 waveguide component: A device designed to be connected at specified ports in a waveguide system.

4. Measurement problems associated with RF hazard assessment

4.1 Characteristics of RF EM radiation

4.1.1 Parameters determined by the source

Sources of EM radiation have widely different characteristics that impose a requirement for versatility on the monitoring equipment. Pertinent characteristics are the following:

a) *Modulation*—The specific characteristics of the signal in both the time and frequency domains.
b) *Radiation pattern*—In the near field, patterns change with distance from the source, whereas in the far field, no significant change with distance occurs. At any given point in space, the field strength continually changes if either mechanical or electronic scanning techniques are used.
c) *Frequency*—Energy may be present over several decades of frequency and may be predominately associated with either the E- or H-fields.
d) *Polarization*—In the far field of a single radiating source, only one polarization exists over a broad physical area (vertical linear, horizontal linear, elliptical, or circular). However, in the near field, any one of these polarizations may exist at any given point, and the polarization changes with small variations in location from the RF source.

4.1.2 Interference patterns

In any environment where RF measurements are to be made, field strength will commonly vary with position. Such variability is caused by interference patterns produced by the combining of energy received directly from the source(s) and reflections (or re-radiation) from natural or manmade objects (multi-path radiation). Because the phase of the reflected signal can be at any angle with respect to that of the direct signal, the effect of the reflection can enhance or diminish the signal strength that would be found at the measuring location in the absence of a reflected signal. The distances between maxima and minima are a function of wavelength, and so they may vary from a fraction of a centimeter to many meters. At locations with emitters operating at various frequencies, the field strength pattern is likely to be particularly complex.

Scanning sources, such as radars and other sources that operate intermittently, introduce time variations with their own interference patterns. Planning of measurement programs should take into account both spatial and

time variations. That need is important from both the viewpoints of collecting all data pertinent to the objective and ensuring that personnel are protected from excessive exposure.

4.1.3 Radiation leakage

Radiation leakage from electronic equipment presents special problems because the source of energy may not be clearly defined *a priori*. It could emanate from a crack in a shielding cabinet or from poorly joined or non-shielded connecting cables or sections of waveguide. The polarization of the EM field and the location of the leak are not generally known. This is a special case of the general near-field situation, and the same problems can exist for all near-field measurements, whether the emitted fields are intentional or accidental. Whereas RF antennas (dipoles, horns) include structures intentionally designed to radiate or receive EM energy efficiently, devices designed to process materials with RF energy (RF-dielectric and induction heaters, electrosurgical devices, and arc welders) are not intentionally designed to radiate, but may contain structures that can function as antennas. Workers operating such equipment can receive very intense exposures because of their proximity to these radiating elements.

A completely general theoretical treatment of the leakage problem is very difficult and is beyond the scope of this recommended practice. The survey techniques differ from those associated with the radiation fields from antennas. In the leakage case, the location of the source is generally found by trial and error. A nondirectional, nonpolarized “isotropic” detector is generally desirable in order to probe in the immediate vicinity of the equipment where directive pickup antennas would give inaccurate readings because of their inability to respond to multipath signals and because of inaccurately known gain-reduction factors in their near field. However, at microwave frequencies, a somewhat directive system consisting of a small horn or waveguide probe, thermistor, attenuator, and power meter is easy to assemble, and may be useful for locating a source of leakage when accurate knowledge of the level is not required. However, both the vertical and horizontal polarization components should be measured separately by rotating the probe 90° about its axis.

In the case of leakage sources that produce highly nonuniform exposure of personnel, measurements of induced currents may be a more accurate indicator of exposure than the magnitude of the electric and magnetic field strengths. Induced currents provide a measure of the capacitive coupling between the source and a nearby individual that field strength alone cannot. For example, in a case where the hands are exposed to particularly strong EM fields, the induced current flowing in the fingers, hands, and wrists may become the limiting factor, when interpreted in terms of the resulting SAR.

4.1.4 Reactive near field

The reactive near field is the region close to the radiation source where energy storage fields are important. In this region of space immediately surrounding the leakage source or antenna, reactive components of the field predominate over the radiating near-field and radiating far-field components. Reactive fields can be inductive (low E/H ratio) or capacitive (high E/H ratio) in nature, and either field component can dominate. The characteristics of reactive fields relate to the inductance and capacitance of the radiating structure. Part of the associated electromagnetic energy is stored; i.e., it is not propagated beyond the near-field region. This stored energy is transferred periodically between the radiating structure and the near field. Although the extent of the reactive region varies for different equipment, the practical outer limit is of the order of a few wavelengths. For example, at a distance of between two and three wavelengths from an ideal dipole, all reactive components are less than 10% of the radiating components. Although the reactive components do not contribute to the net flow of radiated energy, they can couple into biological or other material and, thus, affect energy absorption. Consequently, for many hazard assessments, it is important that the reactive fields be measured using the appropriate instrumentation and measurement techniques (see 6.3). Furthermore, both the electric and the magnetic fields should be measured to fully evaluate the hazard potential, because both contribute to the induced SAR in biological objects [B170].

4.1.5 Passive, parasitic, or secondary re-radiators

Conducting objects that are illuminated by RF energy, either in the near or the far field of a primary source, are termed passive or parasitic re-radiators. High E- and/or H-fields (with respect to ambient RF fields) can usually be measured in close proximity to a re-radiator. These are generally reactive fields that decay rapidly with distance, as discussed in 4.1.4. A passive re-radiator can theoretically and physically be replaced by an equivalent transmitting antenna (reciprocity) because an antenna has the same field pattern whether it is transmitting or receiving. The magnitude of the near and far fields produced by a re-radiator depends on the RF currents induced on it by the primary source. The size and orientation (with respect to the primary source) also determine the magnitude of the induced currents and, hence, the local fields.

Examples of passive re-radiators are electrically large, linear, metal objects, such as flag poles, metal sign posts, and electrical house wiring. Closed loops, such as metallic automobile steering wheels and metal window frames are examples of a second type of re-radiator. Large metal surfaces, such as metal fences, metal signs, and the walls of metallic buildings are examples of a third type of re-radiator. Each individual re-radiator has a unique scattering cross section that determines the amount of energy intercepted from an ambient RF field. The scattering cross section of any single object is dependent on the frequency and polarization of the incident radiation and the physical configuration of the object. Resonances and focusing at specific frequencies may occur in a given object that results in significantly enhanced re-radiated fields.

There are virtually no data in the literature that relate to the SAR induced in a person exposed to the near fields of a passive re-radiator. In spite of this fact, near-field theory, antenna theory, and published dosimetric data associated with active radiators can be utilized to draw some general conclusions. Potential hazards to personnel due to passive re-radiators are “reduced” or “enhanced” with respect to exposure to plane waves of equal maximum normalized field strength. Caution should be exercised when interpreting so-called, localized “hot spots” caused by re-radiating objects because the amount of energy that may be coupled to an individual contacting the re-radiator may be very small, despite the existence of relatively high-surface field strengths. This subject is discussed further in 6.6.

4.1.6 Other considerations

In the near field, three orthogonal components of the electric field with arbitrary relative phases and amplitudes exist. Similarly, there are three orthogonal components of the magnetic field with arbitrary phases and amplitudes. The electric field is elliptically polarized in an arbitrary plane, and the magnetic field, in general, is elliptically polarized in another plane. Consequently, in the near field, measurements of the phase and amplitude of each of the three components of the electric (magnetic) field generally do not provide sufficient information to determine the magnetic (electric) field at the same point. Thus, use of instruments capable of measuring either the electric or the magnetic field and that respond simultaneously to all polarizations is desirable. Field measurement devices utilizing three orthogonal dipoles or loops that detect the amplitude, but not the phase of the electric or magnetic field, cannot provide complete information about the elliptically polarized field. Specifically, the maximum instantaneous field vector is not measured with these types of devices. Only an averaged total field strength is measured, with the averaging occurring over one cycle of the oscillation of the field (the carrier frequency). Currently available hazard instrumentation does not provide both phase and amplitude measurement capability. This means that power density is not actually measured under these circumstances even when power density is the quantity displayed, but is only inferred from measurements of $|E|^2$ and $|H|^2$.

An RF radiation monitoring instrument can respond to pulsed fields in an entirely different manner than it responds to CW fields. For low-duty factor pulsed fields, the instrument may become a peak detector and produce meter indications that exceed the actual, time-averaged field values by factors of 10 dB–20 dB.

When characterizing potentially hazardous EM fields, a distinction should be recognized between emission levels and exposure levels. An emission standard specifies the maximum field strength or power density at a specified (usually small) distance from an emitting source; an exposure standard generally specifies the

maximum field strength or power density to which personnel should be exposed as a function of exposure duration. In most cases where an emission standard applies, the sources are small apertures, e.g., localized leakage around the periphery of a microwave oven door. In these situations, the radiated fields follow approximately an inverse-square law reduction of power density with distance or an inverse dependence of field strength with distance. Such inverse-distance dependence has been verified for leakage emission from microwave ovens for distances of 5 cm to about 1 m. The inverse-square relationship may not apply, however, close to an electrically large aperture.

In general, the maximum level of exposure to personnel will not be equivalent to the measured emission level of a source of RF energy. Furthermore, the exposure area will generally decrease as one approaches the source. Thus, as the source is approached, a plane should be scanned by personnel surveying a leakage field to determine the location of the localized leakage radiation beam.

4.2 Summary of the measurement problem

4.2.1 Time and spatial averaging

4.2.1.1 Time averaging

Many contemporary guidelines and standards, including IEEE Std C95.1-1991, specify the maximum permissible values of the RF field strength or power density as averaged over a specified averaging time, e.g., any continuous 6 min or 30 min interval. The time-averaging provision permits exposures that exceed the MPEs for continuous exposure when the exposure duration is less than the averaging time. For example, if the MPE is 10 W/m^2 (1 mW/cm^2) averaged over any 6-min period, the time-averaging provision permits exposures that exceed 10 W/m^2 provided the following is met:

$$S(\mathrm{W/m^2}) \times t(\mathrm{min}) = 60\,\mathrm{W\ min/m^2}$$

$$t \leq 6\ \mathrm{min}$$

Thus, for example, if the exposure duration is only 3 minutes in any 6-minute period, a maximum power density of 20 W/m^2 is permitted.

Figure 1 illustrates the application of the time-averaging provision of the MPEs. In Figure 1(a), the time-averaged exposure value is 60 W-min/m^2 in both periods 1 and 2. During the remainder of the illustrated 6-min periods, no exposure is allowed in order to keep the time-averaged value from exceeding 60 W min/m^2 (6 mW min/cm^2). In reality, RF exposures usually vary continuously with time due to source characteristics or movement of the individual within the RF exposure field. This is represented by Figure 1(b), where the area under the curve within any 6-min window of time does not exceed 60 W min/m^2. The time-averaging feature of the MPE may introduce substantial complications in determination of compliance, depending on the particular exposure situation. For example, although the time-averaged MPE is not exceeded for either period 1 or period 2 in Figure 1(a), the MPE is exceeded for the 6-min period beginning at 3 min in period 1 and ending at 3 min in period 2. Assessing time-averaged RF exposures in some complex environments may be accomplished accurately only through the use of instrumentation designed to acquire and average the real-time variations in the measured field strengths [B17]. Such measurements may be performed with portable datalogging devices adapted to the averaging time of the MPE [B249], which can provide a “sliding” average over the appropriate averaging time. In less complicated exposure environments, such as when the RF exposure is intermittent but not otherwise varying in level, a datalogger used in conjunction with a broadband RF field-strength meter may suffice for determining the time-averaged exposure values.

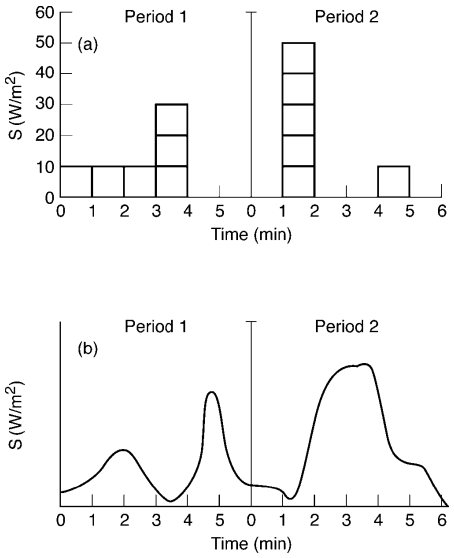

Figure 1—Application of 6-minute time averaging

4.2.1.2 Spatial averaging

The assessment of RF fields that vary substantially with location requires the fields to be spatially averaged in order to specify whole-body-average exposure levels. As applied to the measurement of electric or magnetic fields in the assessment of whole-body exposure, spatial average means the root mean square of the field over an area equivalent to the vertical cross section of the adult human body. The spatial average can be measured by scanning (with a suitable measurement probe) a planar area equivalent to the area occupied by a standing adult human (projected area). In most instances, a simple vertical, linear scan of the fields over a 2 m height through the center of the projected area will be sufficient. In this case, the same approach employed for the measurement of time-averaged exposure levels may be used successfully. For example, Tell [B249] describes a measurement technique using a data-logging device wherein a uniform velocity scan is performed over a linear distance equivalent to the height of an adult human. The resulting value, averaged over the total scanning time, is equivalent to the spatial average of the RF field. Commercially available RF survey meters have provisions for integrated data logging and spatial and time averaging. These instruments offer this capability in smaller packages than previously attainable with separate data logging devices connected to a basic field meter. Spatial averaging of the exposure fields provides a more meaningful description of the exposure, particularly in areas where extremely localized and high-intensity fields may exist, but where only limited exposure of the body actually occurs.

In addition to a straight line linear spatial average, RF exposure fields may be (1) averaged over the projected area of the body or (2) averaged as a volumetric average over the space within which individuals have access. Each of these methods has advantages and disadvantages, and the results in a given situation may differ. When averaging over the actual projected area of the body, the projected area of the body varies with height and the nonuniform fields are weighted accordingly; i.e., the RF fields are not linearly averaged. For example, the projected area of the head represents a relatively small area relative to its vertical extension compared with the torso over an equal vertical dimension. Thus, in cases where the fields may be maximum near the location of the head, and relatively small over the rest of the body, the projected area average will result in a smaller value than would occur via simple linear averaging. However, for fields that are highly variable with spatial maxima in the region of the torso and lower body, the use of projected area averaging may produce higher spatial averages than simple linear averaging. The outcome of the spatial averaging process will also be dependent on the spatial characteristics of the RF fields in relation to the posture of the exposed subject.

The use of spatial volumetric field averaging provides a relatively convenient approach for characterizing RF fields at antenna sites that occupy large areas. In this case, fields are measured by walking about the site moving the RF measurement probe in an up and down oscillatory motion with the probe being moved from near the ground to approximately head height. Combined with walking, this approach permits the probe to sweep out a volume of space and produces a volumetric average that may more realistically represent the typical exposure of individuals in the area than other averaging methods and may be more realistically related to whole-body SAR.

The choice of the most appropriate method for assessing RF exposure relative to whole-body-average SAR should be made by the individual performing the field investigation. With any of the above methods, it may prove useful to determine the relationship between the average value and the spatial peak value of the RF fields measured. Such a relationship may be useful for estimating the average field from simple probing for spatial peak fields. This relationship will be dependent on the frequency of the fields because this will dictate the spatial distance between field minima and maxima caused by reflections.

Preliminary, unpublished data suggest that spatially averaged fields may range between approximately 40% and 60% of the spatial peak field values at VHF and UHF broadcast antenna sites. Individuals performing RF surveys should develop information on these relationships and include such data in field survey reports as well as an explanation for why the specific measurement method was chosen.

Tell [B253] has evaluated the differences between these two methods of spatial averaging for vertical colinear type antennas, common to the type used for paging and other wireless communications services. In an analysis of an 800 MHz band antenna with alternative mounting heights of 0 m, 1.2 m, and 1.83 m, it was found that with the simulated head height configuration, the projected area averaging resulted in an averaged power density almost 29% less than linear averaging.[9] But, for field distributions producing larger fields only slightly higher in elevation, the reduction was determined to be nominally less, about 8% and 1%, respectively. However, for the field distributions of the colinear antennas with 0 m and 1.83 m mounting heights, the projected area approach actually resulted in slightly higher values for the spatially averaged power density, being 7% and 15% greater, respectively.

This finding is not surprising based on the considerably complex situation of reflected fields encountered at telecommunications antenna sites. If the power density of the local field is relatively high in the regions of the trunk of the body, the increased projected area of the body throughout the trunk can result in weighted power densities that are actually greater than if the fields were simply linearly averaged. On the other hand, it is clear that basing spatial averaging on the body's projected area can result, in some cases (especially with highly localized fields), in notably lower values of exposure. Although IEEE Std C95.1-1991 specifies MPEs in terms of spatial averages based on projected areas, the practical complication that this presents for compliance studies is recognized in Clause 6 of the standard, yielding to the acceptability of performing linear averaging. Individuals involved in compliance studies of telecommunications sites should be aware of the possible differences that either technique can have on the results.

4.2.2 External field measurement problems

The EM environment is determined by many factors including the following:

a) The direction of energy propagation from the sources
b) The directions, distances, and relative orientations of the sources and prominent features of the physical environment with respect to the field point
c) The polarization, frequency, type of modulation, and power of the sources

[9] 0 m, 1.2 m, and 1.83 m= 0 ft, 4 ft, and 6 ft)

The variable nature of these factors and their effects on the resulting EM field should be understood to successfully design and operate instruments that measure the EM environment, and to obtain sufficient data to ensure personnel safety.

In general, the character of the near field of an RF source is composed of both reactive and radiation components that exhibit both spatial and temporal variations. These variations will be functions of the physical environment, as well as the properties of the RF source. As a result of the extremely wide variety of possible situations, each of which could be essentially unique, the calculation of near-field intensities for each situation is generally not practical due to the complex nature of near fields. Hence, one should usually rely on measurements. The following material is applicable to both near-field and far-field external fields and SAR measurement applications.

4.2.3 Limitations in the use of near-field instruments

An undesirable situation often arises when a hazard survey is performed using isotropic survey instruments when attempts are made to assess the degree of hazard using only field strength data taken in the near field of a radiating RF source or a passive re-radiating object. The surveyor measures a high field strength that decays rapidly as the probe is moved away from the source. At distance of a few centimeters, the measured field strength may exceed the applicable MPE expressed in units of far-field electric or magnetic field strength or equivalent plane wave power density. However, the coupling of these localized RF fields to any absorbing object (such as a person) may not exceed the SAR value upon which the MPE was based. The possibilities for estimating RF absorption using only external field measurements are discussed in Clause 6 (see 6.6). However, the estimate will often be so inexact that it is useless to attempt to determine the degree of potential risk using external field measurements.

One such situation is the high E-field strength near the tip of the monopole antenna of a hand-held transmitter operating at a wavelength that has similar dimensions as the human head. Very high field strengths (relative to contemporary MPEs) can be measured but only within a few centimeters of the antenna tip. It can be shown that RF absorption may indeed be high if a person's head is placed a few centimeters from the antenna tip, but it is not possible to predict the local SAR in the head using only the measured external field strength. This and many other situations should be assessed through the use of SAR measurements (dosimetry) or induced current measurements in realistic models of the part of the anatomy that is immersed in the local high fields. The use of dosimetric analysis via physical or mathematical models is a well-accepted technique in ionizing radiation health physics and tools and models to perform RF dosimetry are also commercially available. These dosimetric techniques should be used as the principal means for hazard assessment under circumstances where the risk or the economic scale of an RF exposure issue make the relatively high cost and complexity of the dosimetric techniques worthwhile. Such techniques are discussed in detail in this document to enable persons responsible for RF hazard assessment to utilize the available dosimetric technology.

4.2.4 In- and out-of-band interference in RF hazard meters, including cable pickup

In-band interference associated with RF pickup in the cable connecting the probe with the readout of an RF hazard meter often occurs. Errors of as great as 10 dB can occur at frequencies below a few MHz in improperly designed instruments. See 5.4 for more detailed information.

Out-of-band performance of RF radiation hazard monitors becomes increasingly important in areas where multiple signals are present. When illuminated only by frequencies within its designated band, a monitor may provide accurate measurement results; signals outside this band, however, may produce uncalibrated meter responses giving rise to false characterization of the fields actually present. In the case of frequencies higher than the upper usable frequency, erroneously high responses associated with the probe structure generally produce this form of error. For frequencies below the operating band, the instrument response to the reactive field, or a scalar potential field, may produce false indications [B181]. This type of error can be minimized by avoiding measurements close to energized low-frequency elements, where capacitive coupling

to the survey instrument may produce this type of false response. Techniques developed for 60 Hz field strength measurements, e.g., IEEE Std 1460™-1996 [B135], where the potential effects are canceled [B188] can, in some situations, be utilized to correct for this error. The effect of low-frequency interference can be determined at the measurement site using the technique described in 6.3.5.

4.2.5 Effects of sensor size and measurement distance

When an isotropic, near-field probe is used to make RF measurements close to an RF radiator, or near a reflecting or re-radiating object, several types of errors arise. The errors can readily exceed many decibels if the following effects are not avoided.

a) *Field gradients*—Measurement data can be distorted when using an isotropic "near-field probe" to map steep spatial gradients close to the radiating elements of an RF emitter (an antenna or an unintentional radiator). These gradients may cause the amplitude of the field being measured to vary significantly over the volume of space occupied by the probe's antennas. This introduces measurement errors due to spatial averaging. This problem imposes limits on the maximum size of the array antennas or sensors in the probe. Also, a minimum distance exists where accurate measurements can be made of the near field, for a given probe size.

b) *Interaction of an active source with the probe*—Coupling of reactive near fields to the measurement probe can result in erroneously high measured values when a near-field probe is used in proximity to an active radiator or a passive re-radiator. The degree of probe interaction (or coupling) is a function of the size of the probe's antennas (or sensors) and the separation distance between the RF source and the probe.

c) *Probe-antenna loading effects from nearby objects*—When the probe is close to a reflecting object or re-radiator, a probe-loading error is produced. This effect alters the "source impedance" of the probe's antennas and changes the equivalent electrical circuit of each antenna and its respective detector. For a given type of detector, this loading error is dependent on the size of the antenna, the distance to the reflecting object and the frequency of the field being measured.

4.3 SAR measurement problems

The measurement of SAR in exposed biological subjects at radio frequencies is a challenging task, both under near- and far-field exposure conditions. In the far-field case, internal fields are highly dependent on the size, shape, orientation (with respect to polarization), and composition (complex permittivity) of the object. In a sphere (such as the human head) or cylinder (such as the arm or leg), resonances may occur, causing large gradients in the internal field-strength distribution [B124] with focal points, or hot spots, occurring near the center of the sphere and standing waves throughout the volume of the exposed object. However, the SAR on the "front" surface of the sphere will typically be high, and it is usually the maximum value of local SAR. Under localized (partial body) near-field exposure conditions, the internal fields decay exponentially with distance from the exposed external surface. The rate of decay depends on the conductivity of the tissue. Thus, the determination of SAR is easier for this class of near-field exposure, compared with far-field exposure, because the internal fields are confined primarily to the volume directly adjacent to the exposure aperture of the apparatus [B124]. In both the near- and far-field cases, internal regions with differing permittivities create reflections and standing waves and, thus, complicate the measurement problem [B141]. Also, when the whole body of a person or laboratory animal is exposed to plane-wave or near-field RF energy, localized regions deep within can be heated selectively. The resulting intense, local "hot spots" are due to resonant conditions existing in these localized regions where the local SAR (E^2) may exceed the average whole-body SAR by a factor of 100 [B87], [B240].

4.3.1 SAR measurement accuracy and limitations

The local SAR values and the SAR distribution in biological objects cannot be measured without producing relatively large measurement uncertainties, regardless of the instrumentation used. Under ideal plane-wave

exposure conditions, the maximum local (point) SAR can be up to 100 times greater than the whole-body-averaged SAR [B236]. Thermodynamic factors and large gradients in the internal E-fields increase the magnitude of the SAR measurement error whether it is measured with thermal instrumentation or with implantable E-field probes. A measurement uncertainty of about ± 1–2 dB is usually the best that can be achieved when attempting to determine the maximum and minimum internal EM fields or the SAR that exists anywhere within an irradiated biological object. Calorimetric measurements of the whole-body-averaged SAR can be performed with absolute accuracy and precision that is better than 10% [B210]. However, the whole-body-averaged SAR, as well as the local SAR at various points in an exposed object varies significantly as the position of the object is changed with respect to the exposure-field vectors. Therefore, measured SAR data should be expressed with realistic precision (no more than two significant figures) and the limits of uncertainty of the SAR measurement should be stated explicitly.

4.4 Induced current measurement problems

Measurements of induced body currents are at present practically restricted to determining the induced currents caused by electric fields (see 1.5.3). The measurement of induced currents is discussed in Deno [B67], Gandhi *et al*. [B91], Guy and Chou [B108], Hill and Walsh [B123], and Tell [B248]. In practice, a current measuring device is placed in series with the feet or hands and the current that then flows to earth or some other grounded surface is measured. A method for determining the current induced in the arms of tower climbers has been described [B74] in which a broadband, thermocouple type RF milliammeter is used. A narrowband measurement technique in which the RF voltage (that is proportional to the current flowing in the body) developed across a low-impedance resistor is measured with a high sensitivity tunable receiver is discussed in Tell *et al*. [B254]. By using this method, the currents induced at different exposure frequencies can be distinguished. The use of clamp-on type RF current transformers is an alternative method for measuring induced or contact currents.

5. Instrumentation

5.1 Instrumentation for external field measurements

5.1.1 RF survey instruments

RF radiation hazard meters (monitors, survey instruments) are usually the preferred means for measurement and assessment of potential RF hazards. As shown in Figure 2, an RF survey instrument can be divided into three basic parts: probe (sensor), leads, and metering instrumentation. The probe consists of an antenna in combination with a sensor or detector. The design and characteristics of the probe determine to the greatest extent the performance and application of the unit. The detected output from a probe with a flat frequency response is a direct measure of the EM-field strength. One exception is the specially designed hazard probe that has a frequency-shaped response that conforms to a particular MPE (see 5.4.6); i.e., the detected output is appropriately weighted at each frequency. The “leads” refer to that part of the instrument that carries the detected signal to the metering instrumentation. To accomplish this without causing perturbation of the field, the leads may take the form of high-resistance wires, or if they are metallic, they should be carefully oriented so as to minimize coupling with the field. They may also take the form of an optical fiber [B30], [B32], [B266]. Metering instrumentation includes signal-conditioning circuitry and display devices.

To make meaningful near-field measurements, the following conditions should be satisfied:

a) The probe should respond to a particular electromagnetic field parameter and not have spurious responses (for example, it should respond to the E-field with no spurious H-field response).
b) The dimensions of the probe sensor in its surrounding medium should be much less than a wavelength at the highest operating frequency.

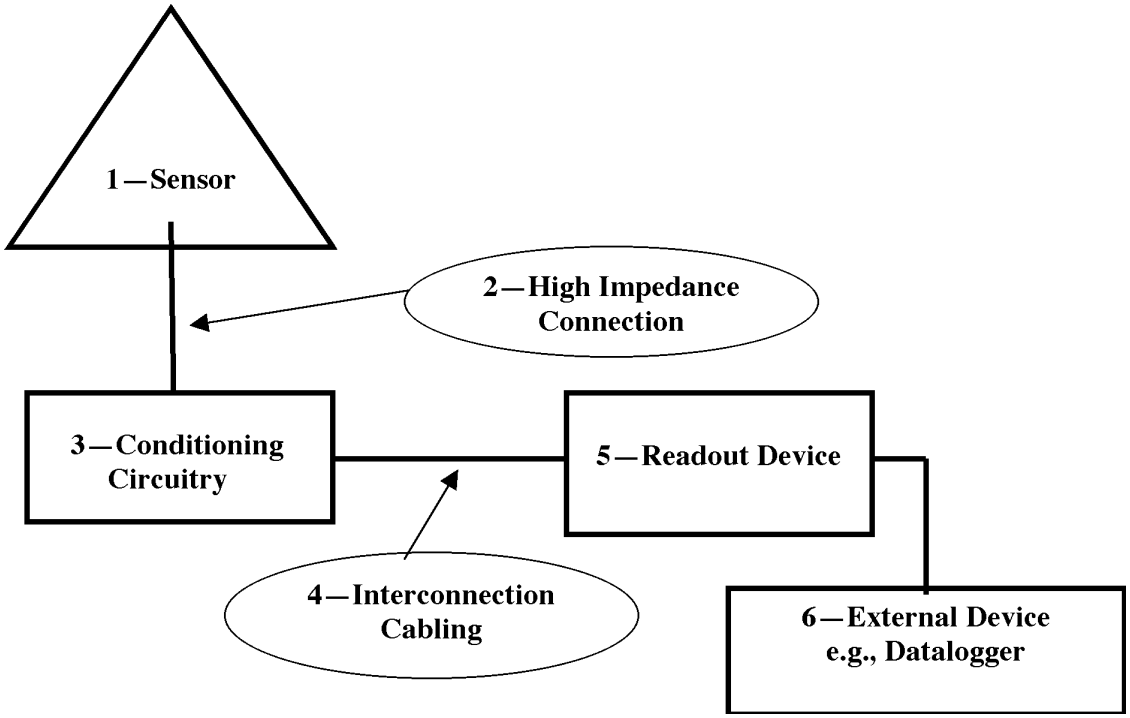

1—*Sensor*: Generates an electrical signal proportional to field strength or the square of field strength.

2—*High impedance connection*: Minimizes interaction between the field and the connection circuit, i.e., isolates the sensor from the conditioning and readout circuitry.

3—*Conditioning circuitry:* Provides signal conditioning, which may include filtering, amplification, digitizing, etc. The sensor, high impedance connection, and conditioning circuitry, in combination, is often referred to as the "probe." The conditioning circuitry may also be combined with the readout device.

4—*Interconnection cabling:* Connects the conditioning circuitry with readout and can be an optical connection for increased electromagnetic isolation between the probe/sensor and readout/surveyor or may be a conductive cable.

5—*Readout device:* A digital or analog readout to display field strength information. The readout device may include logging, averaging, or other data conditioning capabilities. With suitable interconnection modules, the readout device may be a PC (computer).

6—*External device:* The readout may connect through a conductive or optical fiber cable to a remote readout or data collection (logging) device.

Figure 2—Basic components of any RF survey instrument

c) The probe should not produce significant scattering of the incident electromagnetic fields

d) The probe response should be isotropic (independent of orientation), nondirectional, and nonpolarized. A probe with a nonisotropic response is useful if the polarization of the measured quantity (E or H) is known, or if some provision is made to rotate the probe to find the orientation for maximum output.

e) The leads from the sensor to the meter should not interact significantly with the field or conduct RF current from the field to the sensor.

5.2 Desirable electrical performance characteristics

5.2.1 Power supply

The instrument should employ a self-contained power supply that is isolated from external fields by appropriate shielding and filter decoupling. If batteries are used, provision should be made for indicating their condition. The instrument should be capable of at least 8 hours of operation within its rated accuracy before battery replacement or recharging becomes necessary.

5.2.2 Polarization

The combination of probe antennas should be responsive to all polarization components of the EM field. This performance may be accomplished either by inherent design using multiple dipoles or loops or by physical rotation of a single antenna about its axis.

5.2.3 Quantities and units

For the assessment of potential hazards to personnel, the instrument should indicate one or more of the following parameters [B260]:

a) Average "equivalent plane-wave" power density in watts per square meter (W/m^2) or milliwatts per square centimeter (mW/cm^2)
b) Mean-squared electric field strength in volts squared per square meter (V^2/m^2)
c) Mean-squared magnetic field strength in amperes squared per square meter (A^2/m^2)
d) Field strength in amperes per meter (A/m) or volts per meter (V/m)

Average power density (W/m^2 or mW/cm^2) is displayed by some survey meters intended for use primarily above 300 MHz; such meters are often used in near-field and reactive-field regions where true power density is neither measurable nor the most meaningful quantity (E^2 or H^2 are preferred). Some instruments indicate "equivalent plane-wave" power density as derived from the field quantity being measured. Instruments having a probe with a shaped frequency response should read in terms of "percent of exposure limit" based on the MPE of interest, e.g., IEEE Std C95.1-1991.

5.2.4 Range

An adequate dynamic range for instruments with a shaped frequency-response is –10 dB to + 5 dB (10% to 300%) relative to 100% of the exposure limit, as defined by the MPE. For flat frequency response probes, the minimum recommended dynamic range of the instrument is 10 dB below the lowest value and 5 dB above the highest value of the MPE. Either a single logarithmic range or a number of linear ranges can be used to obtain the desired dynamic range.

5.2.5 Recorder output

The instrument should be equipped with a recorder output or other means that will enable the measurement of potentially hazardous fields without endangering the operator, and will facilitate spatial and time averaging. Alternative provisions to avoid endangering the operator may be extension cables between the probe and the meter or a maximum-hold mode of operation where the maximum measured value is maintained until the instrument is re-zeroed by the operator.

5.2.6 Shielding

The instrument housing and antenna cables should provide adequate shielding to ensure that the measurement uncertainty remains within stated limits when the instrumentation portion or accessory cables

(that may act as unintended receiving elements) are exposed to the same field strength as the probe. This shielding should be effective under conditions in which the maximum coupling or "pickup" occurs for the unintentional receiving elements.

5.2.7 Modulation

The instrument should indicate rms parameters, independent of any modulation. However, it is permissible to have a detector or indicator time-constant switch for the CW and amplitude-modulated continuous-wave (AM-CW) modes. Also, the instrument should be capable of averaging the narrowest pulse-modulated envelope of a noncontinuous wave field that is expected to be encountered by the surveyor.

5.2.8 Static electricity

The instrument should not indicate false levels due to a response to static electric charges. These static charges are often induced on the probe of the survey instrument, or on the system being surveyed, e.g., cathode-ray tube displays. As an example, when making measurements during windy conditions and/or low humidity, static charge on the operator can influence the readings of the survey instrument.

5.2.9 Response to other radiation

The specified accuracy of the instrument should include effects of exposure to ionizing radiation, artificial light, sunlight, or corona discharge.

5.2.10 Response time

The response time is generally defined as the time required for the instrument to reach 90% of its final value when exposed to a step function of CW RF energy. The user should know the response time. Multiple operator-selectable response times are desirable with a fast response time no greater than 1 s.

5.2.11 Special functions

It is desirable that the instrument is provided with one or more of the following functions:

a) A maximum-hold function that indicates the maximum reading during the measurement period.
b) An audio signal function that is proportional to the measured field strength and/or an audible indication that a preset level has been exceeded.
c) A data-logging function that can provide an average, maximum, and minimum value of the field quantity being measured. These data are stored for later utilization. This feature could also provide a real-time average of the measured fields with an averaging time specified by the user, e.g., 6 min. This average value should be updated every few seconds, providing the user with an indication of the behavior of spatial or time varying fields.
d) A time-averaging function with relatively long time constants (of the order of minutes) that, for a flat-frequency response probe, averages the measured quantity over a known time period. The output of a probe with an appropriately shaped frequency-response, averaged over an appropriate period, e.g., 6 min, is a direct measure of that portion of the corresponding current MPE.
e) Analog or digital interfacing capability with a personal computer or other data-acquisition equipment, including the appropriate software.

5.2.12 Stability

The instrument should exhibit stability sufficient to permit accurate measurements of the RF exposure fields over periods of time that are consistent with the times normally required for the particular measurement. In practice, the instrument should be capable of operating for 10 min–30 min without the need for re-zeroing

the meter (in the absence of RF radiation) on the range necessary for the measurement. Automatic electronic zero-circuitry can be used to avoid the requirement of shielding the sensitive probe from ambient RF fields during the zeroing process. Automatic zeroing is desirable, particularly when performing RF surveys in difficult environments such as on communications/broadcast towers, where an RF-free location may not be available or where a surveyor, climbing a tower, may not be able to move freely or have the use of both hands to reset the zero level of the instrument. The instrument should be insensitive to thermal variations within the range of normally encountered temperature extremes. The instrument specifications should state the maximum zero drift for each range.

5.2.13 Accuracy and precision considerations

The instrument should be provided with calibration data that permit the user to assess the maximum uncertainty in determining RF field strength or power density when using the instrument in various types of fields of different frequencies. Calibration data should also include the sensitivity of the instrument to frequencies beyond the intended useful range (out-of-band response). A meter sensitive to out-of-band fields should not be used in an environment where such fields may be present at other than negligible levels. Absolute field strength calibration uncertainties (accuracy) of no greater than ± 1 dB are desirable but difficult to achieve. Uncertainties of ± 2 dB or even greater may be acceptable if the levels are well below the limits of the MPE, but as the MPE is approached, measurement uncertainty becomes of greater importance. In any event, the uncertainty factor should be known and included in the measurement report. The instrument specifications should address the instrument's ability to respond to amplitude modulated (AM) fields, such as pulsed radar signals, as well as a multiplicity of signals that might simultaneously illuminate the sensing probe (see 5.4). The instrument readout should permit resolution (precision) of the measured field strength to within 5% of the full-scale value or less.

5.3 Desirable physical characteristics

5.3.1 Portability

The instrument should be portable to permit convenient operation under restrictive conditions (e.g., climbing a tower).

5.3.2 Weight

The weight should be kept as low as is practicable in keeping with current engineering technologies.

5.3.3 Volume

The volume should be as small as is practicable and convenient for hand-held operation (see 5.3.1).

5.3.4 Dependence on temperature, humidity, and pressure

Specified accuracy of the instrument should include the effects of temperature, humidity, and pressure variations, and the operating ranges for these parameters should be indicated.

5.3.5 Durability

The indicating meter and other system components should be rugged enough to withstand vibration and shock resulting from transport. A carrying case is desirable.

5.3.6 Readability

The meter dial markings should be large enough to be easily read at arm's length. The reading corresponding to the applicable protection guide should appear within the central one-third of the full scale reading of the dial if the readout is of the analog type. If more than one range of sensitivity is provided, the full-scale value of the selected range should be indicated, and the units of interest should be readily interpretable. In any case, the analog or digital readout should provide a clear indication of the units being displayed.

5.3.7 Ease of adjustment

The instrument should have a minimum number of controls. They should be clearly labeled as to their functions. There should be no requirements for moving two controls at the same time. For mechanical meter movements, the electrical zero point should be coincident or upscale from the mechanical zero of the indicating meter.

5.3.8 Ease of use

Complicated operating procedures should be avoided. An average technician should be able to make accurate measurements with only the information supplied in the instruction manual.

5.4 Instrument types for external field measurements

The instruments described in the following clauses are limited to those types that can provide reasonable accuracy in both near-field and far-field situations. Instruments that have large scattering areas (in terms of wavelength) are not included here.

5.4.1 Diode rectifier-based instruments

In these instruments, single or multiple diodes terminate small antennas. Multiple diodes and linearly polarized antenna elements arranged in suitable configurations can be used to sum all field components and enable measurements to be made independent of polarization and direction of incidence. A minimum of three elements in an orthogonal arrangement is required for an isotropic instrument that can be used in any orientation with respect to the field.

Some units now in use employ a single diode in combination with an electrically short dipole or small loop antenna. These instruments respond to only one field component and, consequently, should be oriented to read the maximum value, a process that can be tedious and time consuming. Such instruments are, however, useful for measuring individual field components.

A crossed-dipole or multiple dipoles arranged in a single plane will respond correctly to signals arbitrarily polarized in the plane of the sensor, but not to the total field. Such units should be oriented so that the resultant (maximum) field vector is in the plane of the sensor.

Two-dimensional H-field probes, which consist of two concentric orthogonal loops with diameters of 5.4 and 5.5 mm directly loaded with diodes [B224], are commercially available. The resistive lines have been realized using thick-film technology enabling excellent decoupling of the lines from the loop with a filter. The loops are not resistively loaded; i.e., the detected signal is directly proportional to the square of the frequency (when the diode operates in the square-law region). Although this makes the probe unsuitable for measuring broadband fields, it provides a higher sensitivity and better accuracy for narrow-band signals of known frequency. The sensitivity is of the order of 1 A/m at 1 GHz decreasing to 0.1 A/m at 100 MHz. Such probes can be used to measure surface currents on conductors if held orthogonal to the surface. Single-axis probes with a loop diameter of 3 mm and frequency range of 100 MHz–2 GHz have also been developed and

are commercially available. Fiber optic H-field sensors are currently being studied, but probes based on this approach are not known to be available commercially.

Diode instruments are basically nonlinear with respect to power density or field strength. At low levels, the rectified voltage is proportional to power density, or the square of *E* (or *H*). At higher levels, the rectified voltage becomes directly proportional to *E* (or *H*) [B147]. This change in characteristic requires the range of operation of the diode to be restricted to low levels to provide a true indication of total power density. When the diodes are operated at higher levels, the output voltages of the individual elements are required to be modified (generally squared) prior to their summation. When diode instruments are used in pulsed fields, they usually change from an average to a peak-detecting device, and hence, measurement errors may be large in fields of high peak to average ratio. The exception is when saturation of the diode takes place at very high peak field strengths or when circuitry is added to minimize the effects. Such linearization of the square-law response can be very effective for the measurement of single frequency fields, but may introduce errors when subjected to multiple frequency fields. The instrument manufacturer should provide information about the true rms response of the probe over its range of operation.

Two errors are associated with measurements made with any diode-based probe. The first error arises with the use of any electrically short dipole antenna with a diode load and an RF filter transmission line. This is the multiple-source, multiple-frequency error [B214] that is typically 1–3 dB, but in some circumstances can exceed 10 dB. The second error arises from an effect discussed in 5.4.2. This is due to the fact that typical high-resistance signal-carrying leads act as a more efficient antenna at low frequencies, e.g., 540 kHz–1700 kHz used for AM broadcasting, than the short dipoles in the probes. Alignment of the leads with the E-field can result in erroneous measurements.

Schottky (metal barrier) diodes, in general, exhibit some photovoltaic effect. Beamlead hybrid types exhibit this effect to a much greater extent and may produce erroneous readings when illuminated by sunlight or strong incandescent light. Therefore, optically opaque encapsulation is required to eliminate this effect.

When adapted to broadband operation, the upper frequency range of a diode-based E-field instrument is presently above 26 GHz [B128], [B150], the low-frequency limit is below 400 kHz, and the burn-out level can be in the thousands of W/m^2 range.

Diode detectors, depending on design, may exhibit a marked dependence on ambient temperature. Variations in output with ambient temperature will typically be less than 0.05 dB per degree Celsius. Diode units also may be modulation sensitive if the square-law region is exceeded, resulting in errors dependent on the form of modulation.

5.4.2 Active antenna

It is difficult to make accurate, broadband E- and H-field probes that cover the long-wavelength (above about 100 m, i.e., frequencies below about 3 MHz) region, using the conventional means cited above. This is due to the fact that the source-impedance of an electrically small (10 cm) dipole antenna is extremely high, and the sensitivity of a small (5–10 cm diameter) loop antenna is very low. In order to provide a dipole probe with a flat frequency response and adequate sensitivity, the load impedance of the detector and the high-impedance lead in combination should be greater than the antenna (source) impedance. One solution is to provide a high-impedance RF buffer amplifier that is connected directly to a monopole or loop antenna and that acts as the load. This is accomplished by placing the amplifier and battery in a metal enclosure that serves as a cubical “ground plane” or asymmetric dipole element. In commercially available units, the size of this cube is small enough (10–15 cm on a side) so as to not unduly perturb the field under test or the receiving pattern of the device [B197]. This is practical for frequencies between 10 kHz and several hundred MHz. Commercially available magnetic and electric field probes, using active electronics, operate at frequencies as low as 60 Hz [B60].

A second problem associated with probes without active electronics is that of isolating the signal-carrying leads from the antenna/detector combination. This problem may become severe below about 100 MHz, and particularly below 10 MHz. This is due to the fact that the typical high-resistance signal-carrying leads serve as a low-pass filter, and their ability to separate the low-frequency detected signal from the RF field being measured becomes more difficult as the two frequencies approach each other. This results in excessive sensitivity and poor antenna patterns in passive probes. Finally, at frequencies above about 300 MHz, when "free-space" or uniform irradiation conditions exist, both the sensor and the metal enclosure of the survey instrument can be exposed to similar levels of RF [B147] and scattering from the enclosure to the sensor (probe) can cause significant measurement errors.

Active electronic probes eliminate the use of such leads entirely by including the visual display (readout) with the metal box containing the active electronics. Instruments are available commercially that use a fiber-optic data link to connect the box containing the active electronics (located at the base of the probe) to a remote readout.

5.4.3 Displacement current sensors

In addition to short dipoles and monopoles, a form of parallel plate capacitor, called a displacement-current sensor [B107], can be used to measure electric fields normal to its surface or normal to any large conducting surface. An example of an instrument designed primarily for measuring fields associated with video display terminals, is based on the displacement-current sensor concept [B133]. The sensor is a double-sided circuit board 30 cm in diameter. On one side, the front, an annular ring electrically isolates a smaller circular area. The smaller area, approximately 10 cm in diameter, is the active area; the larger annular ring serves as a guard ring to eliminate errors associated with fringing fields. The smaller area is connected through an integrator (an operational amplifier with capacitive feedback) to the backplane of the sensor, which serves as a reference ground. When a time varying electric field is normally incident on the front surface of the device, the induced surface charge produces a current that flows to the backplane through the integrator circuit. This current, called a displacement current because it is proportional to the time derivative of the electric displacement, is also proportional to the time derivative of the incident electric field strength. Integration of the displacement current results in a voltage at the output of the operational amplifier that is directly proportional to the incident electric field strength (and the cross-sectional area of the smaller circular area). The output of the operational amplifier drives a true rms-voltmeter located within a shielded electronics package. The electronics package, which contains a microprocessor, digital readout, and an optical fiber telemetry system for remote monitoring, is mounted to the edge of the sensor. Displacement-current sensors are typically used at frequencies in the LF and VLF regions, e.g., from dc to a few hundred kHz, but they may be used effectively at frequencies as high as a few hundred MHz.

5.4.4 Electro-optical (photonic) sensors

This type of electromagnetic field sensor utilizes a nonmetallic, passive sensing element (electro-optic modulator) with a very broadband response (dc to 20 GHz) that converts electromagnetic field strength information to instantaneous modulation of a laser beam. The laser energy is transmitted via fiber optics to a modulator. The modulator impresses amplitude modulation on the laser beam, in proportion to the instantaneous amplitude of the RF electromagnetic field to which the modulator is exposed. The amplitude-modulated laser beam is then carried from the modulator to a photodetector that converts the modulated optical beam to an electrical signal that represents the instantaneous amplitude of the RF field strength.

The above system has been used with electrically small dipoles [B31], [B185], [B186] as an electric field sensor, as well as without antenna elements (where the electro-optic modulator serves as the E-field sensor) [B193]. In addition, conventional antennas can be connected to a commercially available electro-optic modulator via a short lead, to provide a nonmetallic, passive RF link to the antenna [B266].

5.4.5 Thermocouple

Thermocouple-type radiation monitors generally utilize thin-film thermocouples as the detection elements, with parts of the film performing the function of the antenna element. These units exhibit extremely good adherence to square-law characteristics in that the dc output from the thermocouple is proportional to the square of the electric field strength. These units, while relatively independent of ambient temperature, are generally less stable than diode type detectors. Hot and cold junctions of the couple are in close proximity to reduce the drift due to the gradient in temperature. Variation in sensitivity is of the order of 0.1% per degree Celsius. The major limitation of the element is the burnout level, which in terms of average values may be about three times full scale. The full-scale ratings depend on the basic probe sensitivity. The utilization of thin resistive films provides very broad bandwidth.

Some commercial probes arrange alternate hot and cold thermocouple junctions in a continuous series in a linear arrangement to form a dipole or in a circular arrangement to form a loop. If any single thermocouple junction fails because the probe is subjected to fields well in excess of the maximum rating of the probe, the probe will be nonusable.

Some thermocouple devices utilize dual modes of operation for extreme bandwidth. They may function as a linear resistive dipole at frequencies typically below 18 GHz [B11], [B14], [B127], and as a traveling wave or phase effect antenna above 18 GHz. Such devices have an upper frequency limit that exceeds 95 GHz [B231].

5.4.6 Shaped frequency response

Contemporary MPEs are frequency dependent, and they require determination of the ratio of the exposure field to the corresponding MPE incurred within each frequency interval. In order to comply with the MPE, the sum of such fractions must not exceed unity. Probes containing dipole–diode elements separately or in conjunction with thermocouple elements have been designed to have a sensitivity versus frequency characteristic that is the inverse of specific MPEs [B13]. This allows the summation and weighting of multiple-frequency signals in conformance with frequency-dependent MPEs. The resultant readout for this equipment is usually expressed as a "Percent of the Standard." The probes are tailored to specific MPEs such as those specified in IEEE Std C95.1-1991.

Shaped frequency response probes may cover only a portion of the frequency range of typical MPEs. Additional probes may be used to complement each other and provide a wider measurement range. When complementary probes are used, it is necessary that their out-of-band performance is well defined; preferably, the instrument should be insensitive to out-of-band signals. Overlapping of frequency bands will also add to the uncertainty of the measurement.

5.4.7 Combined electric and magnetic field probes

Probes described in 5.4.1 through 5.4.6 have utilized one probe to measure the electric field and a second, separate probe to measure the magnetic field. In the near field of an RF source, the relative values of E and H vary considerably with respect to one another and as a function of distance from the source. Also, under typical usage situations, potentially hazardous fields may change rapidly with time. Both of these factors present practical measurement problems. For example, in order to measure both electric and magnetic field strengths that vary over time and space, an E-field probe and an H-field probe should be placed at exactly the same point, at exactly the same time. If done sequentially, the fields under study may change during the finite time that elapses between the performance of successive measurements resulting in a measurement uncertainty.

Instruments for simultaneous and mutually independent measurement of RF electric and magnetic field strengths have been developed [B19], [B20], [B69], [B148]. A broadband isotropic probe system for measuring the E- and H-fields simultaneously can be produced with a set of three mutually orthogonal

dipole elements and a set of three mutually orthogonal loops that are physically located within the same very small (compared with wavelength) volume (Figure 3). Each antenna has associated circuitry comprising a detector and an optional frequency-response-shaping filter to provide a frequency response that is flat over the desired frequency range. The lengths of the dipoles are kept electrically short so that the fields are not perturbed and the diameters of the loops are kept electrically small so that the E-field pickup of the loops will be negligible. Mutual coupling between any of the probe elements is also minimized by the use of electrically small antennas. Detectors based on the use of square law operated diodes or thermocouples are used to provide a signal to the electronic circuits, which include an arrangement for analog or digital summing and data processing. An analog or digital display, data-logger, and/or recorder can be incorporated as the final stages of this system. If three loop antennas are arranged with a common center, an isotropic response is achieved [B16]. Probes of this type are commercially available.

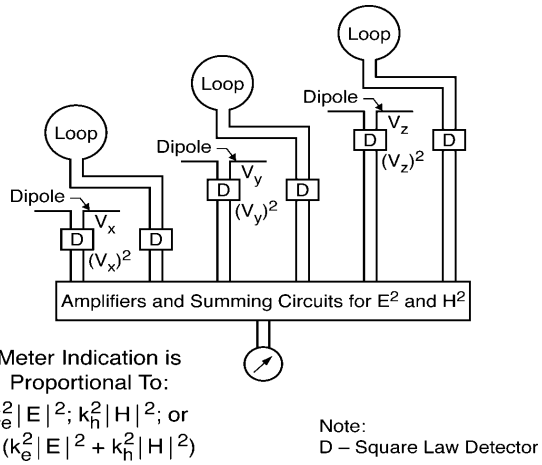

Figure 3—Schematic representation of three-dimensional isotropic E/H probe

5.4.8 Personal monitors

Personal monitors are typically small, portable broadband detectors, suitable for attachment to workers' clothing, which are equipped with an alarm feature for alerting the wearer to the presence of high-level RF fields that may approach the MPE of interest. Some personal monitors provide an alarm with an adjustable or preset threshold, e.g., 50% of the applicable MPE [B251]. In the region between 1–100 GHz, resistive thermoelectric dipoles are used as sensors with a background of lossy material to reduce the effect of scattering from the body. Electrically short dipoles with diode detectors as sensors may cover a portion of this range.

In the frequency range of 3–1000 MHz, the sensors respond to the magnetic and/or electric fields. Although magnetic field sensors are less susceptible to the effects of scattering from the body, various techniques may be employed with E-field monitors to reduce their susceptibility to these effects.

In the range of 0.1–30 MHz, surface charge detection is used and the monitors, therefore, respond to the radial fields which predominate near re-radiators in this frequency range. Personal monitors may incorporate sensors for both electric and magnetic fields and some contain frequency dependent sensors that automatically weight the detected RF fields in accordance with frequency-dependent RF exposure limits. This feature makes them especially useful in multiple frequency environments such as broadcast and wireless telecommunications antenna sites.

Because personal monitors respond to the RF fields at the position where the monitor is located on the body, some care should be used in its placement and interpreting exposure during an alarm condition. For example, wearing a belt mounted personal monitor when the predominant exposure is at eye level may not

provide sufficient warning of excessive exposure. Conversely, when used in non-uniform RF field environments, such as VHF and UHF broadcast facilities, an alarm condition may be a very conservative indication of potential excessive exposure since the MPEs of several exposure standards/guidelines are based on spatial averages over the projected area of the body. Encountering fields that trigger the alarm at one point in space may not ultimately lead to whole-body-average exposures exceeding the MPE value. Use of personal monitors can form a valuable component of an RF safety program, but a description of their use should be an integral part of any RF safety training program.

5.5 External field measuring instruments

5.5.1 Calibration methods

Reliable calibration of the various instruments used for measuring EM fields is essential to ensure safety of personnel, to assure compliance with exposure criteria and regulations, and to provide a basis for comparing the results of RF hazard or RF field-calibration research that has been performed by two or more independent groups and laboratories. Existing calibration methods are based on the premise that a known field strength can be established through measurement, calculation, or a combination of both. The device to be calibrated is placed in this standard field, and the meter indication is compared with the known field value. There are three basic approaches for producing a standard calibrating field, as follows:

a) The free-space standard-field method
b) Guided wave methods
c) The standard-probe or transfer-standard method

The most widely used techniques are described in the following subclauses. The choice of technique will depend on the type and size of the probe, frequency range, available facilities and equipment, and the accuracy requirements [B149], [B165], [B194]. Refer to IEEE Std 1309™-1996 [B134] for further information on calibration methods, techniques, and typical grades of calibration used in EMC applications.

NOTE—The RF output of the generator used in all of the following methods should be free of harmonics; i.e., the harmonics should be at least 20 dB below the fundamental frequency. A low-pass filter can be placed on the output port of the generator to accomplish this.

5.5.1.1 Free-space standard field method

There are several variations of this method, but the objective is to establish a known calibration field in free space. The most common experimental arrangement for use at microwave frequencies is shown in Figure 4. The power density S at a point on the axis at a distance d from a transmitting antenna is given by the Friis free-space transmission formula

$$S = \frac{P_T G}{4\pi d^2} \tag{1}$$

Where

P_T is the net power delivered to the antenna,
G is the effective antenna gain with respect to an isotropic antenna

The gain is normally determined in advance, and P_T and d are measured as part of the regular calibration procedure.

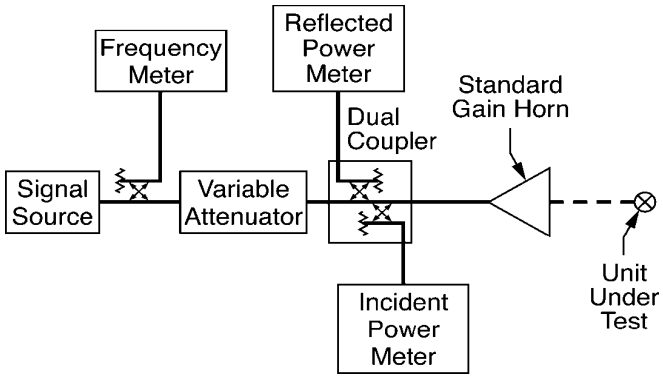

Figure 4—Free-space standard-field calibration method

The most convenient method for determining P_T is by means of a dual directional coupler, as indicated in Figure 4. The incident power P_i and the reflected power P_r are monitored at the coupler sidearms, and P_T is obtained from the relationship

$$P_T = P_i - P_r$$

High-quality, broadband couplers are available, along with methods for calibrating and using them to determine P_T [B37], [B72], [B73], [B129], [B130]. The methods cited are for calibrating power meters, but the same techniques can be applied to antennas if corrections are made for impedance mismatch effects. The method of Bramall [B37] allows the use of a low-power, calibrated bolometer to provide accurate determination of high transmitted power levels. P_T can be determined to within 1% or 2% if mismatch corrections are included (as they should be for accurate measurements).[10] One way of accounting for mismatch effects utilizes the power-equation technique [B72], [B73], which also permits use of directional couplers that are not restricted in terms of directivity and do not require precision connectors. The power-equation technique and cascaded-coupler method were combined [B29] for the precise determination of transmitted absolute power from an antenna used to calibrate near-field instruments.

Alternatively, modern automatic network analyzers with built-in microprocessors for real-time correction of system errors may be used to determine P_r as well as P_T / P_r. All components used in the system being calibrated should use precision connectors and coaxial-to-waveguide adapters. This includes the high-power coaxial and waveguide directional couplers and adapters that are used during actual generation of far-field calibrated power densities.

The foregoing assumes that the device being calibrated is sufficiently small and far enough away from the transmitting antenna that the amount of energy reflected back into the transmitting system is insignificant. If this condition cannot be met, it is possible to obtain a correction for the effect of the reflected energy by varying d, observing the (approximately) sinusoidal variations in P_r, and then averaging P_r over at least one full cycle.

5.5.1.1.1 Sources of error

The principal sources of error in the free-space method are multipath interference, reflections from metallic or dielectric objects used for measuring the fields in the calibrating system, and uncertainties in the antenna gain determination. Multipath effects are often overlooked, but every calibrating facility will have some scattering associated with the walls, equipment, and even dielectric probe-support structures. They may

[10]The uncertainties stated here are intended to include all known, significant sources of error and correspond roughly to 95% confidence limits. However, uncertainties quoted from the published literature should be interpreted as indicated in the original articles.

cause the power-density in the calibration region to be significantly different from that predicted by Equation (1). Calibration errors due to multipath effects can be reduced by observing the probe response as a function of position and averaging the results. Useful discussions of methods for the reduction of multipath errors are given by Swicord [B243] and Tell [B248] Additional errors can be caused by backscatter from cables, metering components, and so on, which are a fixed distance behind the probe-under-test. The effects of this type of scattering can be reduced by multiple-position averaging if the probe can be moved with respect to the source of scattered energy (see 6.3.2 and Swicord [B243]). Alternatively, absorbing material should be placed in front of all such items that could reflect energy in the direction of the probe.

5.5.1.1.2 Antenna gain determination

Problems associated with the determination of antenna gain (G) add to the measurement difficulty. It is relatively easy to obtain accurate gain values at large distances, but large distances require greater transmitter power and the multipath situation is often worse. On the other hand, there are some fundamental difficulties associated with accurate gain determinations at short distances.

The effective gain G of an antenna is a function of distance and approaches a constant G_∞ as d approaches infinity. This is illustrated in Figure 5, which shows the estimated gain reduction for a representative example [B145] plotted as a function of the parameter $n = (\lambda d)/a^2$, where a is the largest aperture dimension and λ is the free-space wavelength. In establishing a calibrating field, one should use the correct value of G for the specific distance involved; otherwise, significant errors can result. The far-field gain G_∞ of pyramidal horns can be calculated with sufficient accuracy (≈0.3 dB) for many purposes [B39], [B138], [B145], [B223], [B228] and may be measured to within about 0.1 dB if necessary [B57], [B154], [B198], [B230], [B256]. As indicated in Figure 5, the measured values of G_∞ obtained by these methods hold for distances greater than about $(8a^2)/\lambda$ ($n > 8$). It may also be possible to calculate G to within about 0.3 dB for pyramidal horns [B146], [B165] at distances down to $(2a^2)/\lambda$; however, the accuracy of these near-zone calculations has not been definitely established.

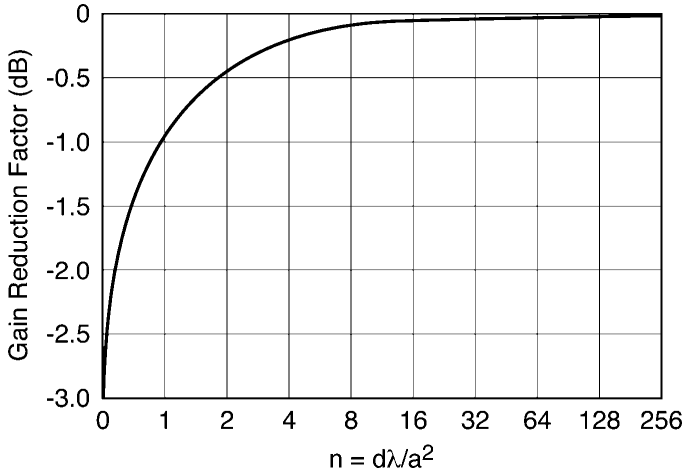

Figure 5—Estimated gain reduction for a representative antenna

There are also problems in experimentally determining the near-field gain. The usual far-field gain measurement approach involves measuring the power transmitted between a pair of antennas and applying Equation (2)

$$G_T G_R = \frac{P_R}{P_T}\left(\frac{4\pi d}{\lambda}\right)^2 \quad (2)$$

Where

P_R	is the received power,
G_T and G_R	are the gains of the transmitting and receiving antennas, respectively,
d	is the distance between the antennas.

Equation (2) holds rigorously only in the far field. At shorter distances, G_T and G_R cannot be separated into the individual factors [B230]. Nevertheless, since one can measure the ratio P_R/P_T, it is tempting to apply Equation (2) to the case of two identical antennas in the near field and obtain

$$G_a^2 = (P_R/P_T)(4\pi d/\lambda)^2$$

Where

G_a	is the measured apparent near-field gain of the two antennas

However, G_a obtained in this manner is not the correct near-field gain. In other words, G_a will not yield the correct on-axis power density when used in Equation (1). This fact can perhaps be seen intuitively. P_R is the result of an integration (or averaging) of the incident field distribution over the receiving aperture and unless the incident field is a plane wave, there is no simple relationship between G_a and the desired on-axis power density. The error decreases as d becomes larger. The near-field gain error can be approximated empirically by plotting measured data (smoothed to eliminate standing wave oscillations) and comparing it with a theoretical curve that falls off as $1/d^2$. By determining the deviation from $1/d^2$, the smoothed, experimental data can be evaluated.

For rectangular apertures

$$S = \frac{\eta P_T}{n^2 A}\left(\frac{b}{a}\right)^2 \quad (3)$$

Where

S	is the power density at the receiving aperture,
$A = ab$	is the physical area of the aperture,
a and b	are the aperture dimensions (a being the larger),
h	is the aperture efficiency defined as A_e/A, with A_e the effective aperture area.

Equation (3) is simply a modified form of Equation (1) obtained by use of the relations $G = (4\pi A_e)/\lambda^2$ and $\eta = (\lambda d)/a^2$. For horns of a given geometric and electrical design, e.g., a family of "standard gain horns" from a particular manufacturer for use at the various waveguide operational frequency bands, the ratio b/a and η are approximately constant, and according to Equation (3), the power density for a particular value of n is inversely proportional to the aperture area. It is desirable to have η as large as possible to reduce the gain uncertainty; therefore, if P_T is limited, it is necessary to use smaller apertures in order to achieve the required calibration field strength.

Hence, if one desires to calibrate antennas at short distances, because a long-distance range is not available, or to avoid the expense of high-power systems and to avoid the complications caused by standing waves due to multipath reflections from an imperfect anechoic chamber, the near-zone gain should be known. Two

possible techniques for determining the near-zone gain follow. If one antenna is small (an open-ended waveguide, for example) and its far-field gain is known, it can be used to determine the effective on-axis gain of a larger antenna at relatively short distances by means of Equation (2). The measurements should be reasonably accurate (≈0.5 dB) so long as d is greater than $(4a^2)/\lambda$ for the small antenna. With respect to distance from the larger antenna, the primary considerations are that the field gradients must be small in the calibration region and the wavefront should approximate a plane-wave. These conditions will be satisfied reasonably well at distances greater than a a^2/λ for the large antenna. The dimensions of the receiving aperture or the sensing elements of the probe being calibrated should also be less than the aperture dimensions of the small antenna. This procedure was followed by [B264], which claims an overall uncertainty in the calibrating field of ± 0.5 dB from 1 GHz–18 GHz and ± 1 dB up to 35 GHz.

5.5.1.1.3 Small apertures

In view of the discussion in the two preceding paragraphs, there is no advantage in using a large antenna as a source. In fact, one can operate at closer distances with less transmitter power if the source antenna is kept relatively small. Open-ended waveguides are perhaps the smallest practical source antennas. They are readily available, do not have serious mismatch problems, and yet have sufficient directive gain to concentrate the energy in the calibration region and facilitate the suppression of scattered energy in the test chamber. Further, one can easily operate at distances greater than four a^2/λ. However, an open-ended waveguide antenna should consist of a section of waveguide whose aperture end extends several wavelengths from any flanges or bends. Also, the aperture (radiating) end should be very cleanly cut in the plane perpendicular to the axis of propagation of the guide. For common open-ended waveguide apertures with a two-to-one aspect ratio, i.e., $a/b = 2$, the far-field gain is approximated by Equation (4) [B151]

$$G = 21.6fa \tag{4}$$

Where

f is the frequency (GHz),
a is the width (larger dimension) of the waveguide aperture (m).

When it is necessary to calibrate a large number of nominally identical hazard meters, the extrapolation method described in [B198] is useful when applied as follows. Let B_d be the meter indication with the probe at an arbitrary near-field distance d, and B_o be the indication with the probe at a large distance d_o where far-field conditions hold. One can write the relations

$$B_o = KS_o \tag{5}$$

$$B_d = KS_d$$

Where

S_o is the far-field power density,
S_d is the equivalent plane-wave power density in the near field,
K is a proportionality factor that relates the meter indication to the incident power density.

In the extrapolation technique, B_d is measured over a range of distance d, and a power series is fitted to the product $B_d d^2$ over the measurement interval. This series is then used to determine $B_o d_o^2$ by extrapolation. One can then obtain the near-field correction factor F_d from

$$F_d = \frac{B_d d^2}{B_o d_o^2} \tag{6}$$

F_d can also be determined without recourse to the extrapolation method if a long enough range is available to measure $B_o d_o^2$ directly. Combining Equation (5) and Equation (6) yields

$$S_d = F_d W_o \left(\frac{d_o}{d}\right)^2 = \frac{F_d P_T G_T}{4\pi} \tag{7}$$

since

$$S_o = (P_T G_T)/(4\pi d_o^2)$$

P_T can be measured and G_T (the far-field gain of the transmitting antenna) can be obtained by the extrapolation method or other methods previously referenced. The near-field correction factor F_d is a function of d, and should be determined for every combination of radiator and probe type. However, once F_d has been obtained for a given probe, it can be used to calibrate other probes of the same type with little additional error.

Using the methods above practical near-zone calibration facilities can be established for use at frequencies above about 300 MHz. Standard-gain horns are normally used as radiators above 1.1 GHz (that is, WR650 and smaller waveguides). The transmitter power required to produce a 100 W/m^2 (10 mW/cm^2) calibration field is only 10 to 20 W. Between approximately 300 MHz and 2.6 GHz open-ended waveguides (WR2100-WR430), are more suitable for the radiating elements because, as shown in Equation (7), less power is required to produce a calibrating field of sufficient power density and uniformity with known on-axis gain. In this case, transmitter powers of 50 W or less will produce a 100 W/m^2 field. Note that the near-field gain calculations for horns do not yield accurate results for waveguides, so the near-field gain should be measured. A good discussion of free-space methods of calibrating hazard meters from 500 MHz–20 GHz is given by Bowman [B36], which indicates that an overall uncertainty of ± 1.0 dB or less can be achieved if sufficient care is taken.

5.5.1.2 Calibrations using rectangular waveguides

The fields inside a rectangular waveguide can be calculated and, in some cases, are sufficiently uniform to be considered for calibration purposes. The main advantage of such a system is that considerably less power and space are required. One disadvantage is that the maximum transverse dimension of a rectangular waveguide should be less than the free-space wavelength at the highest calibration frequency in order to avoid higher order modes that result in complicated field distributions. Hence, the method is generally used only for frequencies below 2.6 GHz (WR430) since the device being calibrated should be small compared with the guide dimensions. The field would decay rapidly with distance from the radiator, and only the probe sensor would experience the major effect of the field, i.e., the handle and cable are illuminated by a much smaller field. Therefore, waveguide calibrations provide a good calibration technique for the isolated probe sensor (tip). In contrast, calibrations in a plane-wave field result in uniform illumination of the the entire probe and its attached cables. A careful error analysis of this problem has not been completed, but it appears that if the maximum probe dimension is less than one-third the smallest waveguide dimension, the total uncertainty will not exceed ± 1 dB [B12], [B264].

NOTE—Care must be taken to preclude placing metallic objects into the waveguide that could disturb the mode pattern.

Figure 6 shows how a section of rectangular waveguide can be used for calibrations. A reflectionless load is connected to the output end to prevent standing waves that would cause serious errors in the calibration. The probe to be calibrated is usually inserted into the waveguide through a hole in the sidewall (as in Figure 6) and positioned in the center of the guide where the field is most nearly uniform. (Entry through the top wall is not recommended because spurious pickup by the leads that are then aligned with the E-field is greater.) The access hole should be as small as possible to minimize perturbation of the field distribution. Equations for calculating the field distribution from P_n (the net power delivered to the section) and the guide dimensions can be found in Hill [B120] and Larsen [B165]. The “equivalent power density” can be

determined in terms of E^2 (not $\overline{E} \times \overline{H}$) at the center of a rectangular guide in which the width a is twice the height *b* from

$$S = \left[\frac{4P_n}{a^2}\right]\left[1 - \left(\frac{\lambda}{2a}\right)^2\right]^{-\frac{1}{2}} \quad (8)$$

A slide and slot in the sidewall of the guide may be used to evaluate and reduce the uncertainty produced by any standing wave within the guide. P_n is determined in the same way as P_T in Equation (1). It is difficult to estimate the total uncertainty of this method in general because the field strength at the probe sensor being calibrated will be modified by the size and nature of the probe. The influence of the conductive walls on probe calibration in a waveguide is analyzed and evaluated in John [B140]. The error assessment of the probe voltage for dipoles of lengths of 20 and 30 mm having terminations of 100 ohms in a WR430 waveguide is 1% and 2.5%, respectively. (The 100 ohm termination impedance is typical for thermocouple, but not for diode-based probes used for microwave oven leakage measurements). Woods [B264] describes a system that operates from 400 MHz–600 MHz with an estimated uncertainty in power density of ± 12% (0.5 dB). Later results at 2450 MHz have been reported by Aslan [B12], which claim an accuracy of ± 5% (0.2 dB). In this case, the probe diameter was 1.6 cm compared with the narrowest guide dimension of 5.46 cm.

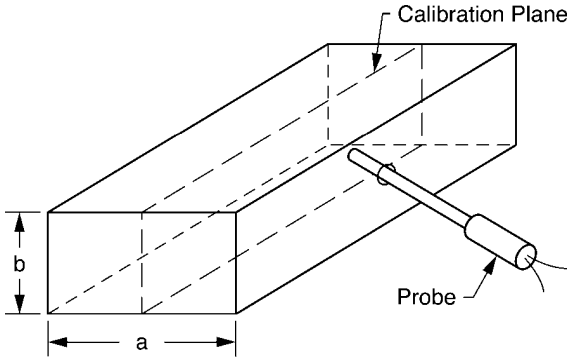

Figure 6—Rectangular waveguide calibration system (TE_{10} mode)

5.5.1.3 Calibrations using TEM cells

Another guided wave method suitable for calibrating EM-field probes below frequencies of about 500 MHz is the use of a transverse electromagnetic or TEM cell. Like the rectangular waveguide, this device is fully shielded and does not emit energy that may be potentially hazardous or cause interference with nearby electronic equipment. Other advantages are excellent long-term stability of the calibration system and moderate cost (compared with an anechoic chamber). The basic TEM cell is a section of two-conductor transmission line operating in the transverse electromagnetic (TEM) mode, hence, the name. As shown in Figure 7, the main body of the cell consists of a rectangular outer conductor and a flat center conductor located midway between the top and bottom walls. The dimensions of the main section and the tapered ends of the cell are chosen to provide a 50 W characteristic impedance along the entire length of the cell [B61]. When the cell is properly designed and terminated in a reflectionless load, the input voltage-standing-wave ratio (VSWR) is usually less than 1.05 for frequencies below the cutoff limit. In the center of the calibration zone, halfway between the center conductor and the top (or bottom) wall, the E-field will be vertically polarized and quite uniform. Also, the wave impedance (*E* /*H*) will be close to the free-space value of 120π ohms. Introduction of the probe into this region will alter the field distribution in the vicinity of the probe, but the total uncertainty in the field strength is less than 1 dB [B61], [B62], [B180] if the maximum probe dimension is less than *b*/3, where *b* is the distance from the top wall to the center plate. Cells can be made in various sizes to suit particular needs and to cover specific frequency ranges. However, since the width (surface parallel to the surface of the center plate) should be less than a half-wavelength to avoid higher

order modes in the cell, the upper useful frequency of a TEM cell is approximately 500 MHz unless the cell walls are lined with RF absorbing material [B101] (see 5.5.1.3.6).

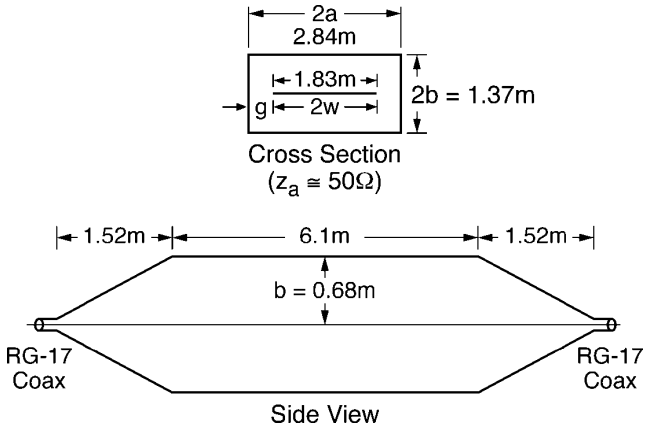

Figure 7—Typical large transverse electromagnetic (TEM) cell

For proper use of TEM cells, several factors should be considered, including the following:

a) The electrical characteristics of the cell
b) Higher order modes
c) Relative size of the probe being calibrated with respect to the plate separation
d) Stability and calibration of the voltmeter, directional couplers, and power meters used in conjunction with the cell to produce field strengths with an absolute, known value

Several of these issues have been considered in more detail by Hill [B121] and by Mantiply [B180].

5.5.1.3.1 Electrical characteristics

The rectangular TEM cells available commercially are designed to have a characteristic impedance of approximately 50 ohms. This value can be calculated from Equation (9):

$$Z_o \cong \frac{30\pi}{\frac{w}{a} + \frac{2}{\pi}\ln\left(1 + Coth\frac{\pi g}{2b}\right)} \tag{9}$$

Where the dimensions w, b, and g are given in Figure 8 [B179]. The characteristic impedance can be measured with a time domain reflectometer (TDR). The TDR can also be used to check for and correct impedance mismatches, particularly at the transitions. The fields at the test point, i.e., the geometrical center of the center plate (septum) and midway between the center plate and the upper (or lower) wall of the cell, can be calculated from

$$E = V/b = \frac{\sqrt{P_n Z_o}}{b} \tag{10}$$

$$H = E/(120\pi)$$

Where V is the voltage at the input or output port of the cell, Z_0 is the real part of the characteristic impedance of the cell, and b is the distance from the upper wall to the center plate. P_n (the net power

delivered to the cell) is determined in the same way as P_T, and the discussion in 5.5.1 applies. The equivalent plane wave power density S can be calculated from

$$S = E^2/(120\pi)\ (\mathrm{W/m^2})$$

or

$$S = 120\pi H^2\ (\mathrm{W/m^2}) \tag{11}$$

These field values apply only at the test point for a well-matched cell, and significant variation will be seen closer to or farther from the septum.

5.5.1.3.2 Higher order modes and standing waves

The maximum operating frequency of a cell is determined by calculating the cutoff frequencies for the higher order modes. The TE_{10} cutoff frequency f_c is given by the relationship

$$f_c = (75/a)\sqrt{1 + (4a)/(\pi b)\ln(8a)/(\pi g)} \tag{12}$$

Where f_c is expressed in megahertz and a, b, and g are the cell dimensions in meters. The TEM cell should be used well below this frequency to assure proper operation for probe calibration. Actually, some difficulties may be presented by the TE_{01} mode that can be determined by methods published in Gruner [B104] or Weil *et al*. [B262]. However, if the frequency of operation is limited to one-half the TE_{10} cutoff frequency, problems should not occur, and uniform fields should be obtained if the cell is properly designed. (Additional analyses on higher order modes have been performed by Hill [B121].) However, slight errors in design or construction may sometimes lead to impedance discontinuities in the cell, particularly in the tapered regions. These mismatches can produce standing waves, which generate errors in the values of the fields at the calibration point. To assure proper cell operation, field maps at each desired frequency of operation should be performed in a plane above the septum, halfway between the septum and the outer wall of the cell. Maps can be made by using E-field and H-field probes with small sensors. When using the cell, forward and reflected power measurements should be made at the input port. Constant values assure consistent cell calibration. The error due to standing waves can be estimated by calculating the ratio of the field at the test point to the average field above the septum, the average being taken from one end of the cell to the other along the centerline.

5.5.1.3.3 Probe sensor size with respect to plate separation

If the sensor being calibrated occupies one-third or less of the distance b (from septum to the top or bottom of the cell), field perturbation error is less than 10% for the E-field and can be corrected to within 1% using methods described in Crawford and Workman [B63]. However, as the sensor size is increased, the probe response is increased over that expected from the calculations. This field enhancement is due to loading of the chamber. Since there is no accurate way to correct for this error, one should limit the space used to less than $b/3$, effectively eliminating the problem. This limits the useful range of a TEM cell to frequencies below 500 MHz for probes with sensors having a diameter of 5 cm.

5.5.1.3.4 Power measurement stability

The accuracy of probe calibrations using a TEM cell is directly related to the accurate determination of the cell voltage or the power flow through the cell. There are basically two ways to measure power flow through the cell. The first uses directional couplers to measure input, reflected, and output power, thereby determining the net power delivered to the cell. This method ensures that the accuracy of the field strength is associated with the power meter and coupler calibrations that usually have less than 1% uncertainty. The other method involves use of a high-power attenuator that is attached to the load end of the chamber, and a

power meter that is attached to the attenuator to measure the power flow through the chamber. The uncertainty of this measurement (approximately 1%) is associated with the attenuator and power meter calibrations. As long as all components remain constant, this is an accurate method for cell calibration. However, since changes in the cell power or power measuring instruments cannot be detected with a single power measurement at the cell output, this is not the preferred method.

5.5.1.3.5 TEM cell operated with a termination impedance different from 50 Ω

If a transmission line (other than a waveguide) is terminated in its characteristic impedance, only the TEM mode is present and the intrinsic impedance (*E*/*H* ratio) has a free-space value of 377 Ω . However, a TEM cell can be operated without a resistive termination at frequencies up to about 30 MHz. When the cell is open-circuited, it acts as a parallel plate capacitor rather than a transmission line, and produces a field with a high intrinsic impedance (high *E*/*H* ratio). Large E-fields can then be produced by connecting a broadband step-up transformer at the cell input terminal. By contrast, when the cell is short-circuited, it acts as a single turn loop and produces a field having a very low intrinsic impedance. This configuration is useful for producing large H-fields.

5.5.1.3.6 Wideband TEM cells

If a TEM cell is "loaded" in strategic locations with microwave absorbing material (such as the carbon-filled foam that is used in anechoic chambers), higher order modes can be suppressed. The resulting cell can therefore generate a calculable, relatively pure TEM mode, at frequencies that are much higher than would be possible using standard TEM cells [B62]. This condition degenerates whenever reflecting (metallic or dielectric) objects are introduced in the cell. For calibrating probes with very small sensors and nonperturbing leads (resistive or fiber optics), specially designed absorber-loaded TEM cells may be useful over a very broad range of frequencies (dc-18 GHz) [B156]. Careful design, testing, and error-analysis should be performed for each specific combination of TEM cell and sensor under test, to ensure reasonable performance at any frequency in the range where undesirable higher order modes may exist.

5.5.1.3.7 Gigahertz TEM (GTEM) cells

Another transmission line structure for calibration electromagnetic field probes is known as the GTEM cell, shown in Figure 8 [B157]. The GTEM cell consists of a tapered asymmetrical rectangular coaxial transmission line, similar to a lengthened input section of a TEM cell. Cross-sectional dimensions are selected to maintain a constant 50 Ω characteristic impedance along the length. A GTEM cell can be constructed to have a much larger working volume than a TEM cell. There are no geometrical discontinuities, as in a standard TEM cell, and therefore, higher order modes should not exist over the useful frequency range (dc-18 GHz). The septum (or center plate) is terminated in a series/parallel 50 Ω resistor array, which dissipates fields and currents up to low megahertz frequencies. Pyramidal absorber covering the back wall dissipates the approximately plane wave fields at higher frequencies.

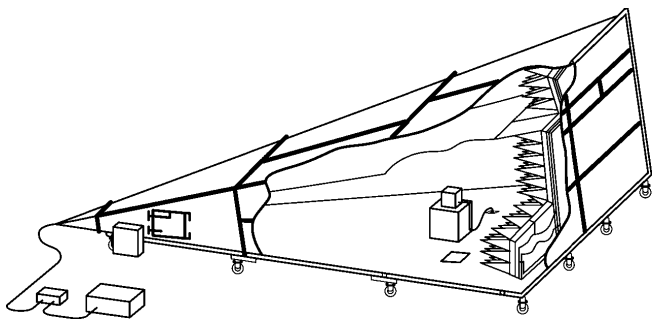

Figure 8—Typical gigahertz transverse electromagnetic (GTEM) cell

The GTEM characteristic impedance and quasi-static field are approximately calculated using asymmetric TEM theory [B255], [B263]. For most GTEM sizes, the quasi-static field calculations are most accurate up to a few hundred megahertz. At higher frequencies, the measured field may vary up to about ± 4 dB. At present, a rigorous method of GTEM field calculations for all frequencies is not available. For these reasons, it is recommended to use the transfer method when calibrating probes in a GTEM cell. Moreover, since the ratio of the E- and H-fields may not equal 120π ohms, the transfer method should include the field of interest.

Standard methods are used for measuring power delivered to the GTEM cell. Note that due to the changing spacing between the septum and the outer walls, the field components in the Z direction (direction of field propagation) are not zero. This effect must be accounted for when calibrating isotropic probes.

5.5.1.4 Magnetic field generators using coils

At low frequencies, the axial magnetic field (in A/m) at the center of a circular loop of wire is simply the current (in amperes) divided by the loop diameter (in meters). For a single-turn coil in free space, a loop becomes self-resonant when the circumference approaches the free-space wavelength. For multiturn coils, the resonant frequency is lower because of capacitance between the turns. For a flat coil (all turns in a single plane), the following relationships hold: Using a coil with a total wire length less than $\lambda/10$, the input impedance is very low, and the field strength value is easily calculable and given by

$$H = \frac{NI}{D} \tag{13}$$

Where

H is the magnetic field strength at the center of a flat coil (A/m),
N is the number of turns in the coil,
I is the rms current (A),
D is the diameter of the coil (m).

The magnetic field at points on the axis of a flat coil is

$$H = \frac{NIr^2}{2(r^2 + d^2)^{3/2}} \tag{14}$$

Where

r is the radius of the coil (m),
d is the distance along the axis from the coil center to the field point where the H-field is to be computed (m).

This type of coil is useful for probe calibration purposes up to about 30 MHz. Figure 9 is a sketch of a coil arrangement that consists of two flat coils on the same axis, both carrying current in the same direction. The arrangement is known as a Helmholtz arrangement when the two coils are of equal diameter, each with the same number of turns and are separated by a distance equal to the common radius of the two coils. This type of coil system generates a more uniform H-field over a larger volume than the single coil. For the purpose of generating a uniform H-field in which a typical hazard probe can be calibrated, Helmholtz coils are useful up to about 10 MHz. This frequency limit is dictated by the dimensions of the coil, which should be small compared with a wavelength. The wave impedance (E/H ratio) is low for frequencies below self-resonance.

In general, the axial field strength H_x at a point on the common axis of the two coils is given by [B134]

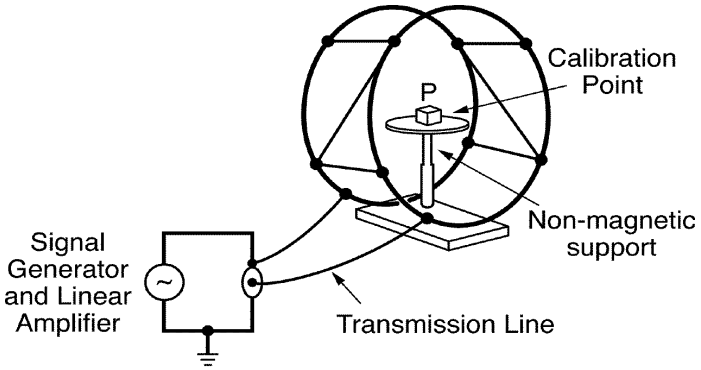

Note: P is the device under test

Figure 9—Helmholtz coils for generating an H-field to calibrate hazard probes at frequencies below about 10 MHz

$$H_x = \frac{N_1 I r_1^2}{2(r_1^2 + x_1^2)^{3/2}} + \frac{N_2 I r_2^2}{2(r_2^2 + x_2^2)^{3/2}} \tag{15}$$

Where

H_x is the magnetic field strength along the common axis of the coils,
N is the number of turns on each coil,
I is the current in each coil, in amperes,
r is the radius of the coils, in meters,
x is the axial position of the magnetic field, in meters, from the center of the coil set [B172].

For the special case where $r_1 = r_2$ and $N_1 = N_2$, the magnetic field at the center of the coil set ($x = 0$), Equation (15) reduces to

$$H_0 = \frac{2NI}{r(2)^{3/2}} = \frac{0.715NI}{r}$$

or

$$H = 1.43\frac{NI}{D} \tag{16}$$

Where

D is the diameter of each coil (m).

Since $B = \mu H$, it is possible to calculate the magnetic flux density B in microtesla from Equation (17)

$$B = 180\frac{NI}{D} \tag{17}$$

Where

B is the magnetic flux density at the midpoint (in μ T).

The volume within a Helmholtz coil where probes can be calibrated accurately is about 0.6*r*, where *r* is the coil radius. A large probe made of magnetic materials may, however, load the coils and concentrate the fields in its vicinity. If inserting a probe into the test space of a Helmholtz pair causes the coil current to change by more than a few percent, it is likely that the field will be distorted and the calibration may not be accurate even when the current is adjusted to the correct value. The coil current should always be adjusted with the system empty and then reset after the probe being calibrated is inserted. If field distortion is suspected, a larger coil set should be used.[11]

5.5.1.5 Standard probe method

This method is the simplest, and may be the best method of calibrating hazard meters for general field use. The principle of this method is to have a stable and reliable probe that has been calibrated accurately (by one of the previously discussed techniques) for use as a "transfer standard." The standard probe is used to measure the field strength produced by an arbitrary RF field-generating device, e.g., antenna or TEM cell, over a particular region in space (or in a waveguide system). Then an uncalibrated probe is placed at the same location in the field that the standard probe occupied, and the uncalibrated probe's meter reading is compared with the known, measured value of the field, based on data obtained with the standard probe. The transmitter and field-generating device used during this process should generate a field that has the desired magnitude and that is constant with time, and the field should be uniform over the region where the unknown probe is placed. Accuracy of about ± 2–3 dB is readily attainable with this method, and improved accuracy is possible if special care is taken. The advantages of this approach are convenience, reliability, and simplicity. A potential source of error when using the transfer standard to calibrate another probe is the possible difference in the receiving patterns of the two probes. Also, in the near field of a radiator, the size of the probe's sensor is important. Ideally, the standard and unknown probes should be nominally identical and the calibration should be conducted in a field relatively free of spatial variations due to multipath interactions among the probe, the radiator, the anechoic chamber, and other field-generating components, and near-field gradients. In TEM cells or parallel plate transmission systems, capacitive coupling between the probe and the center plate and walls of the cell can create calibration errors.

The transfer standard probe should be stable, rugged, and not easily burned out; it should have a large dynamic range, cover a broad frequency range, and possess an isotropic response. Organizations that cannot justify the construction and maintenance of a calibration facility could have a transfer standard (probe) calibrated by a reputable laboratory. This secondary reference standard can then be used to calibrate a field-generating system at the user's facility. The system, in turn, can be used to calibrate other probes. The transfer standard should be recalibrated at intervals appropriate to the particular standard, based on experience with the stability of the calibration factor with time. See Annex A for additional calibration techniques.

5.5.2 Evaluation of field survey instruments

In order to determine electric and magnetic fields accurately, the characteristics of the survey instruments used should be defined in some detail. A series of tests, when properly performed, define worst-case uncertainties that can occur when that instrument is used to make field strength measurements. The tests also indicate what operational procedures can be used to minimize measurement errors. Details of tests for microwave instruments (for frequencies greater than 0.9 GHz) can be found in Herman and Witters [B119], and details of electric and magnetic field probe performance evaluations at 27 MHz can be found in Nesmith and Ruggera [B197]. The minimum test parameters that should be observed are as follows:

a) *Absolute calibration*—Should be performed at field strengths that produce indications that equal or exceed the instrument's mid-scale readout display.
b) *Instrument linearity*—Measurements should be made at 25%, 50%, 75%, and 100% of full scale, on each range of the instrument's readout device.

[11]For a detailed discussion of Helmholtz coils used in generating magnetic fields, including uncertainty calculations, refer to [B134].

c) *Amplitude-modulation response*—This test should be tailored to the desired instrument usage conditions. For example, if the modulation of concern is from unfiltered power supplies, such as in industrial microwave heaters, 60 or 120 Hz modulation with a 50% duty factor would be appropriate. If the instrument is to be used around radar equipment, duty factors as low as 0.001 should be used during the evaluation process.

d) *Frequency response*—The response of the instrument over the frequency band of interest should be determined. The response should be relatively flat over the design frequency range (1–3 dB).

e) *Out-of-band response*—The sensitivity of the instrument, probe, cable, and readout should be evaluated for exposure to fields at frequencies far from the specified usable range of the instrument. This is important when instruments are used in multiple-frequency fields.

f) *Near-field response*—The response of an instrument in very high- and low-impedance fields (*E*/*H*) should be investigated to determine the instrument's response to extraneous fields. For example, the H-field response of an E-field instrument, or E-field response of an H-field instrument, should be evaluated with appropriate field-generating devices.

g) *Polarization ellipticity*—The variation in response as the probe is rotated about the axis of its handle should be defined.

h) *Receiving pattern isotropy*—Variations in response can occur as the handle of a probe is rotated through the E-plane so that one position during the test should be with the handle parallel to the E-field.

i) *Lead pickup*—Tests to detect and quantify extraneous pickup by the probe handle are important (see 5.4.2) [B181].

j) *Temperature response*—Changes in the instrument's response to a given field strength over the temperature range of interest should be determined.

k) *Supply-voltage response*—Several commercially available RF hazard survey instruments utilize one or more batteries, including single battery-packs with several separate voltage terminals. It has been found that deviations from the nominal voltage rating of one or more of the batteries can cause errors in the overall accuracy of the instrument [B119]. Therefore, adequate battery-voltage testing is important for battery-operated RF survey meters.

l) *Radio frequency interference (RFI)*—The response of the instrument readout device and cable should be determined with the probe, cable, and readout device exposed to E- and H-fields whose magnitudes lie in the range of use for the probe during typical hazard surveys.

m) *Drift and noise*—Short-term and long-term stability of the instrument should be determined with respect to full scale on each measurement range of the instrument, in the absence of EM-fields.

Based on all of the above tests, a worst-case error analysis can be performed. As in any experiment, care should be taken to design each test to measure only the parameter of interest, while all other parameters are held constant.

5.5.3 Practical measurement accuracy

Several methods for calibrating hazard meters have been discussed, and the uncertainties associated with each method were estimated. It is important to understand that one cannot expect to achieve the same accuracy when using the meters for practical measurement applications. Some of the reasons are as follows:

a) Hazard meters are usually calibrated in nominally plane-wave or uniform fields. Such fields are seldom encountered in practice, and the sensor may not respond in the same way to nonplanar fields (fields with large spatial gradients).

b) In most calibration methods, only the sensor (probe) is exposed to the field, while, in practice, the complete system, including the indicating unit and connecting cable, is immersed in the field. Significant errors can result from spurious responses from other parts of the instrument including readout meter (case) and cable.

The overall uncertainty added by the above factors is difficult to assess and will vary with the type of meter and usage situation. However, if good measurement procedures are followed, accuracy of ± 1–3 dB can be expected in practice, with greater uncertainties in near-field situations and at higher frequencies (shorter wavelengths), or in areas where large reflecting objects are present. Measurements with an accuracy <1 dB can be made at frequencies above a few gigahertz, (centimeter wavelengths) near high gain aperture antennas. At lower frequencies, particularly at HF frequencies and below 30 MHz, the surveyor and instrumentation can perturb the fields and the surveyor must exercise great care in order to make accurate measurements. Use of nonperturbing fiber optic cables and nonconducting stands is recommended. Standard field intensities at these frequencies transferred from the US National Institute of Standards and Technology (NIST) have a stated uncertainty of ± 1 dB [B122]. To this uncertainty must be added the uncertainty or repeatability of the calibration facility and techniques used.

5.6 Instruments for measuring induced (body) current

Body currents are generally taken to be the induced current associated with exposure of the body to RF fields, but without any direct contact with objects other than the ground upon which the subject may be standing. The measurement of RF body current is, in many cases, required to assure compliance with contemporary safety standards and guidelines that specify induced current limits, e.g., IEEE Std C95.1-1991. Induced current meters can also be used for determining SAR in the ankles or wrists (see Annex C.2). Several common techniques are used for measuring induced currents, including clamp-on “loop” type current transformers for measuring current through the ankle or calf, and parallel plate “stand-on meters” for measuring currents that flow to ground through the feet.

Commercially available lightweight clamp-on current transformer instruments have been developed that may be worn (with care) about the subject’s lower leg [B112], [B113], [B209]. A readout module, either mounted directly on the transformer or connected through an optical link for remote reading, provides a display of the current flowing through the aperture (primary circuit) of the transformer. Current sensing in these units may be accomplished using either narrowband techniques, e.g., spectrum analyzers or tuned receivers (which offer the advantage of being able to determine the frequency distribution of the induced current in multisource environments [B254]), or broadband techniques, e.g., diode detection or thermal conversion. If diode sensing is used, care must be taken to ensure that the diodes are operated in their square-law response region to achieve a true rms current indication. Sometimes additional circuitry is provided to extract the square root for linear indications of current. This mode of operation produces true rms indications in the presence of multiple frequencies and/or amplitude-modulated waveforms.

True rms current detection is usually achieved with thermal sensors that respond accurately to the simultaneous flow of currents at different frequencies and to low duty cycle pulsed currents. In most current transformers, there is a tradeoff between the size of the opening (aperture) and the reliable high-frequency response. Generally, as the aperture size increases, the high-frequency response decreases. Therefore, current transformer-type instruments must be used with care since operation at frequencies above their specified high-frequency limit can result in erroneous measurements. Air-core transformers, as opposed to the typical ferrite-core transformer, have been used to help extend the upper frequency response of these instruments. The lower weight of the air-core sensors makes them useful for long-term measurements. Air-core instruments, however, tend to be significantly less sensitive than ferrite-core devices.

An alternative to the clamp-on device is the parallel plate stand-on meter. In this instrument, the body current flows through the foot (feet) to a conductive top plate, through some form of current sensor to the bottom plate, and then to ground. The current flowing between the top and bottom plates may be determined by measuring the RF voltage drop across a low impedance resistor and using Ohm’s law to relate the measured voltage to the corresponding current. Alternatively, a small aperture RF current transformer may be placed around a conductor that is placed between the two plates, and with appropriate circuitry (which includes narrowband instruments), the current can be determined. Chen and Gandhi [B46] have described a parallel plate type of system in the form of bilayered printed circuit board, in the shape of human feet. Another

alternative is a direct reading RF thermocouple ammeter placed in series between the plates. This method is entirely passive since power supplies or other associated circuitry are not required. Two factors that may reduce the effectiveness of the thermocouple ammeter are its physical size and sensitivity to burnout.

Another device that can be used when measuring induced current is the "human equivalent" antenna [B86]. This device simulates a standard person to permit the measurement of induced currents without requiring the person to be subjected to exposure to fields that induce the current. This device also reduces the variability of the measurements with people of different stature. The frequency range of one commercially available device is 50 Hz–100 MHz. These devices also have low sensitivity to radial electric and magnetic fields and thus require the use of a correction factor where such fields predominate.

5.6.1 Calibration of induced current meters

Induced current meters can be used for determining SAR in the ankles or wrists. Calibration is accomplished using current injection and power measurement techniques in a terminated RF circuit. To calibrate a stand-on meter, an RF source is connected, through a suitable series resistance, to electrodes that contact the upper and lower plates of the induced current meter. (See Figure 10.) An RF current transformer (CT) is used to measure the current applied to the induced current meter (unit in test—UIT), and the output of the transformer is monitored using an RF voltmeter [B251].

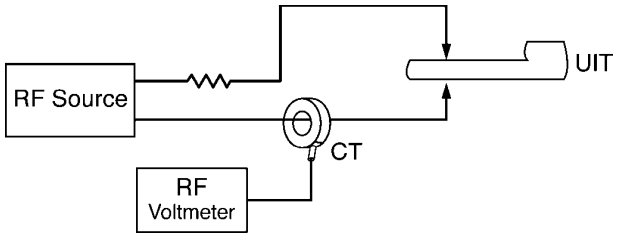

Figure 10—Current injection method for calibrating stand-on induced current meters

The clamp-on induced current meter is calibrated in a manner similar to that used for common RF current transformers. A special fixture is used that connects to a 50 Ω coaxial line and expands the outer shield to allow access to the inner center conductor (similar in principle to a TEM cell). The size of the fixture must accommodate the larger dimension of the clamp-on induced current meter when it is connected around the center conductor of the test fixture. (See Figure 11.) An insulating spacer is often used to center the conductor within the aperture of the induced current meter. RF power from a suitable source is transmitted through the fixture to a termination with a means for measuring total transmitted power, e.g., a feed-through termination. The current flowing in the coaxial line and, hence, through the aperture of the induced current meter is calculated using Ohm's law.

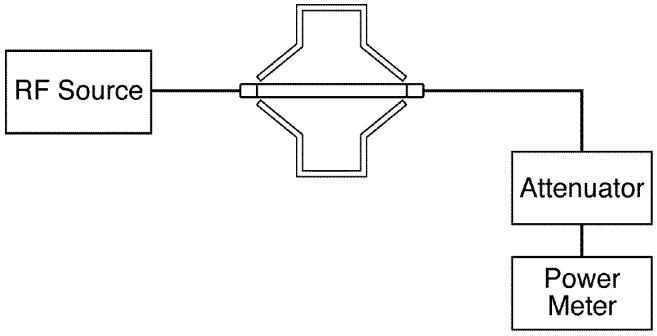

Figure 11—Method used for calibrating clamp-on induced current meters

5.7 Instruments for measuring internal fields and SAR

5.7.1 Implantable E-field probes

Implantable E-field probes provide the ability to measure the local electric field strength in tissue at a specific point, or they can be used to obtain a continuous real-time or linear scan in tissue. A typical isotropic device consists of three orthogonally arranged dipoles that are directly loaded with Schottky (metal-barrier) diodes at the feed point. The RF signal is rectified by the diodes, and the dc signal is transmitted to a data conversion unit by high resistance (RF transparent) lines. The high resistance lines have been realized either by carbon impregnated Teflon strips or by thin- or thick-film technology on a ceramic or quartz substrate. A typical probe (see Figure 12 for a single-axis probe) consists of a thin-film dipole, 0.6–3 mm in length, and a pair of high-resistance leads placed on a thin plastic or glass substrate and encapsulated in a low-dielectric constant insulating material. A beam-lead diode is placed across the gap of the dipole to provide RF detection capability of the order of 1 mV per mW/cm^2 in free space [B32]. Typically, a 1–5 mm spherical or cubical volume is required to house the three orthogonal dipoles of an isotropic internal E-field probe. This means that field strength and, hence, SAR data may be obtained with a spatial resolution of better than several millimeters. This is about one-half of a wavelength in high-water-content tissue such as muscle, brain, or internal organs at a frequency of 3 GHz. A low-frequency limit of about 100 MHz is achievable. The lower limit is due to the fact that the high-resistance leads cannot reject RF pickup adequately at low frequencies (as discussed in 5.4.2). Implantable E-field probes with 1.5–2.5 mm long dipoles have been produced in small quantities by several commercial firms. Reviews of the theory of this type of probe are discussed in Bassen and Smith [B32] and Schmid *et al*. [B224].

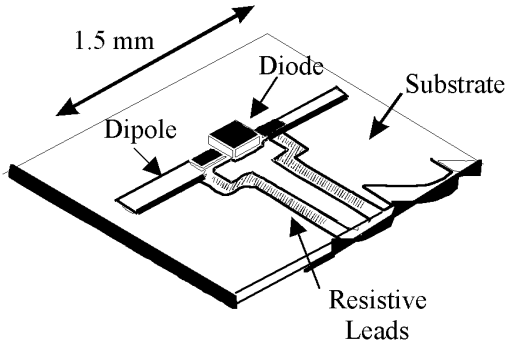

Figure 12—Elements of a typical implantable E-field probe (single-axis)

Recent improvements in decoupling the diodes from the high resistance line have led to the realization of true rms sensors. The improvement is achieved by employing thick-film techniques, which allows the use of multiple sheet resistances on the same substrate, to provide high-resistance lines of several kΩ/square. Measurements have shown that the dielectric material around classically designed probes can significantly disturb the reception pattern, leading to deviations from an isotropic pattern that are larger than ± 2 dB in air. In tissue the deviation will be reduced to typically ± 0.9 dB. Possibilities for optimization have been studied using numerical modeling. Solutions have been found that will reduce the deviation from an isotropic response in all planes and polarizations to better than ± 0.35 dB [B212].

5.7.1.1 Implantable E-field probe calibration techniques

The response of E-field probes implanted in biological tissue or tissue simulating material is enhanced by a factor that depends on the dielectric properties of the material. Therefore the implantable E-field probe should be calibrated in lossy dielectric media at points where the absolute value of E is known. Calibrations have been performed in spheres [B28], [B239] and in waveguides filled with lossy dielectric liquids, e.g., salt water [B120]. These lossy media are exposed to a known external E-field while placed in a dielectric object in which the internal E-field distribution has been calculated using electromagnetic field theory. The

internal E-field calibration factor for the probe is determined from its response compared with the calculated internal field. If this is done at several frequencies for a specific probe design, the calibration uncertainty will be typically 1–2 dB when implanted in any lossy, high dielectric-constant object, such as biological tissue that contains a large percentage of water (muscle, brain, and internal organs, but not bone or fat). (See also 6.5.1.) Care should be taken when calibrating the probe in a region of the lossy dielectric object where SAR spatial gradients are large. This is often the case for probes calibrated at the higher microwave frequencies in high-dielectric constant media (e.g., saline-based phantom materials).

5.7.1.1.1 Waveguide techniques

Another technique for calibrating probes in tissue-equivalent material is based on the boundary condition that the tangential component of the electric field is continuous across any interface [B120]. This technique utilizes a waveguide section with a thin plastic septum separating two segments, one containing air and the other segment containing the tissue simulant. (See Figure 13.) Various recipes for tissue-equivalent material can be found in the literature, e.g., Chou *et al*. [B56] and Hartsgrove *et al*. [B118].

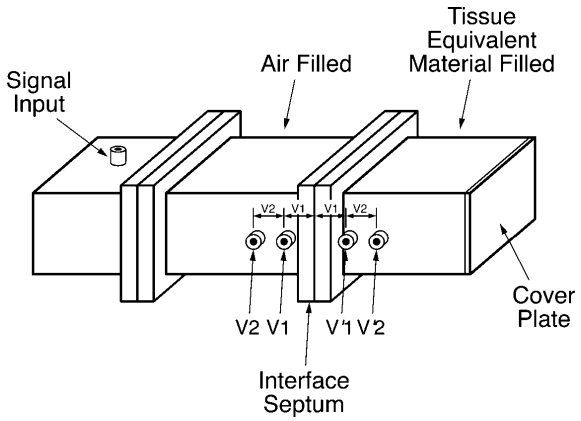

Figure 13—Boundary condition method for calibrating implantable E-field probes in tissue-equivalent material

The fields are measured with the probe being calibrated at a number of positions on each side of the septum, and the resulting curves are extrapolated to the septum interface. The field in the tissue-equivalent material decays exponentially, while the field in air varies sinusoidally due to reflections at the air-tissue simulant interface. To minimize interaction with the field, the probe is passed through the narrow wall of the waveguide with the probe axis and lead wires normal to the E-field. Measurements should be made as close as possible to the interface. The resulting curves should plot as straight lines on semi-log paper.

When distances between the measurement points and the distance between the septum interface and the closest measurement point are equal, Equation (18) may be used to measure the probe-tissue enhancement factor F_{TE}

$$F_{TE} = \frac{V_0}{V_0^t} = \left(\frac{V_1}{V_1^t}\right)^2\left(\frac{V_2^t}{V_2}\right) \tag{18}$$

Where

F_{TE} is the tissue enhancement factor,

V_o^t is the voltage measured in air,

V_o' is the voltage measured in tissue,

V_1, V_1', V_2, V_2' are the voltages measured with the probe under calibration at the locations indicated in Figure 13.

Another waveguide calibration setup consists of an appropriate size rectangular waveguide with its axis of propagation oriented vertically (z-direction). A dielectric separation plate allows the tissue simulating solution to be filled from the top. To minimize reflections from the interface between the tissue simulant and air, the impedance of the dielectric spacer should be equal to the geometric mean of those on the two sides and the thickness should be equal to one-quarter wavelength (determined at the phase velocity of the wave in that region), i.e., a quarter-wave matching section [B213]. The transverse field distribution in the liquid corresponds to the fundamental mode with an exponential decay in the vertical direction (z-axis). (The symmetry of the construction and high losses in the liquid ensures that the dominant TE_{10} mode propagates in the tissue simulating liquid, although higher order modes are theoretically excitable.) The liquid must be sufficiently deep to ensure that reflections from the liquid/air interface (top surface) do not affect the calibration field. The SAR in the liquid can be determined from the waveguide dimensions and the measured forward and reflected power. The expression for the SAR along the waveguide axis in the liquid is given by

$$SAR = \frac{4(P_{fwd} - P_{ref})}{ab\delta\rho} e^{\frac{-2z}{\delta}} \tag{19}$$

Where

ab is the cross-sectional area of the waveguide,
P_{fwd} is the forward in the lossless section of the waveguide,
P_{ref} is the reverse power lossless section of the waveguide,
δ is the penetration depth,
ρ is the mass density of the liquid.

The penetration depth in the liquid is given by

$$\delta = \left\{ \sqrt{(\pi/a)^2 + j\omega\mu_0(\sigma + j\omega\mu_0\varepsilon_r)} \right\}^{-1}$$

Where

ω is the radian frequency (2pf),
μ_0 is the permeability of the liquid,
σ is the conductivity of the liquid,
ε_0 is the permittivity of free space,
ε_r is the relative permittivity of the liquid.

The field is measured at a number of points in the liquid along the vertical center axis of the waveguide by moving the probe under calibration away from the dielectric separation plate in small steps from the contact position. The analytical fields at the measurement points are used for the probe calibration. The probe should be rotated around its axis and the measured probe response averaged in order to average out any axial isotropy errors in the calibration.

5.7.1.1.2 Transfer method

An alternative method for calibrating implantable E-field probes is to measure the SAR in an irradiated object with a precisely calibrated temperature probe, and then place the E-field probe at the exact location where the SAR was measured. Techniques for calibrating temperature probes are given in 5.7.2.1.

5.7.2 Implantable temperature probes for SAR measurements

Certain temperature probes can be used successfully to make SAR measurements. The minimum requirements are that the temperature sensor and associated leads should be nonperturbing to the EM-fields, and the SAR should be large enough to produce a measurable temperature rise during a period of less than about 30 s. The first requirement is usually satisfied by using highly resistive materials or fiber optics, instead of metal components, for the temperature-sensing element leads [B42], [B125]. The second requirement entails the measurement of SARs no lower than a few Watts/kilogram. This lower limit exists because the resolution of most temperature probes is typically 0.01°C–0.1°C, and the longest practical duration of irradiation that allows reasonably accurate SAR measurement is typically 5–30 seconds. Irradiation of an inert, lossy dielectric object for longer durations causes local "hot spots" to lose their thermal energy to the surrounding area via conduction and convection. In living biological systems, active thermoregulation also degrades accuracy. It is acceptable to use an ordinary metal-wire temperature probe for RF and microwave dosimetry when the probe is not in place during irradiation, but is put in place immediately before and after. Such a method has limited application, but has been used successfully in small laboratory exposure systems, e.g., waveguide exposure systems. The use of metallic probes during irradiation is not acceptable because of their significant field perturbation. Even when the probe's metallic leads appear to be oriented orthogonal to the incident electric field vector, the depolarization of fields within finite sized dielectric objects induces errors. Limitations of many nonperturbing temperature probes include fragility and high cost. Without the strength of wire leads and rugged insulation, nonperturbing devices are much less durable than ordinary thermistor and many thermocouple probes. Also, high-resistance leads in temperature probes can be easily destroyed by local heating when the leads are in air and are exposed to high E-fields and high E-field gradients along the length of the lead. Additional methods for determining SAR are given in Annex C.

5.7.2.1 Temperature probe calibration techniques

For accurate determination of SAR with nonperturbing temperature probes, the precision with which small temperature changes can be measured must be optimized. Calibrations to assure maximum precision must be performed at regular time intervals, the length of which is dependent on the type of temperature probe to be calibrated. Some must be calibrated daily (especially certain fiber optic probes), whereas some can be calibrated monthly with minimal loss in accuracy. A capability to resolve temperatures within tenths of degrees Celsius is required for calibrating temperature probes, and in clinical settings with human subjects, even higher precision is needed [B41]. For comparisons to reference thermometers, the ability to produce a stable thermal environment over the range of approximately 10 °C–50 °C is also required.

In earlier years, it was impractical for a small laboratory to possess a standard platinum resistance thermometer (SPRT) along with the bridge circuitry developed by the National Institute of Standards and Technology. Therefore, many laboratories maintained ultrastable standard reference thermistors from which highly accurate comparisons were conducted using four-lead resistor-measurement circuits with current-reversing switches and thermal "calibration blocks" to ensure near-zero temperature gradients inside a controlled water bath [B125]. During the past 10 years, however, self-contained and self-calibrating platinum resistance thermometers have become commercially available such that tedious resistance measurements that were fed into a computer-based curve-fitting program of the thermistor equation [B233] became unnecessary.

Still required is an insulated, stirred water-bath to provide a homogeneous environment for probe-to-probe comparisons. Sufficient measurement time is also a significant factor in the accuracy of thermal probe

calibrations. To avoid the negative effects of stray thermal gradients between the compared probes, several minutes, at least, should elapse before recording new thermal levels.

Two approaches may be used in performing these calibrations. First, absolute calibrations can be performed at regular time intervals at several temperature points over the range of interest. This is accomplished by comparing the temperature probe being calibrated with a standard thermometer, usually a platinum or thermistor type. The platinum resistance thermometer has good long-term stability, but the thermistor type has a smaller sensing element and thus has a smaller thermal mass. This smaller thermal mass minimizes the creation of temperature gradients in the calibrating water bath and thermal lag problems caused by use of a large metallic temperature probe with its inherently large thermal mass and long time constant. If a dynamic temperature calibration technique is used, a well-stirred water bath should be used. Also, the rate of water temperature rise must be adjusted so that it is much slower than the time constants of either of the probes. The unknown and the reference probes should be placed in intimate contact at their sensor-areas (usually the first few centimeters near the tip). It is best to use an automated data acquisition system to ensure reliable, instantaneous, and simultaneous readings from all temperature probes. If absolute calibrations of the unknown thermometer can be performed with accuracy approaching the resolution of the instrument being calibrated, this type of calibration is preferred. In some cases, an instrument under calibration will not accurately indicate absolute temperature but will correctly measure a change in temperature ΔT . In this case, the ratio $(\Delta T_{\text{absolute}})/(\Delta T_{\text{measured}})$ is determined over the range of interest. If this value is constant over the range of temperatures to be studied and over a reasonable period of time, e.g., from week to week, accurate SAR data can be obtained even when absolute temperature can not be precisely defined.

With either the dynamic or static calibration technique, it is useful to perform two calibrations of ΔT . The first was described above: a temperature rise in a water bath. The second calibration should be performed using a temperature decrease in a water bath. If a difference in the calibration factors exists for the unknown probe when determined by the two methods, the thermal time constant of one or both of the probes may have been longer than the time period that elapsed between the thermometer readings taken during one or both of the calibrations. To correct this, the calibration process should be repeated, using a slower rate of temperature increase or decrease in the bath.

6. Measurement of potentially hazardous exposure fields

6.1 Preliminary considerations

6.1.1 Source and propagation characteristics

Before carrying out a survey of potentially hazardous EM fields, it is important to determine as many of the known characteristics of the sources of these fields as possible and estimate their likely propagation characteristics. This knowledge will permit a better estimate of the expected field strength and, consequently, a more appropriate selection of test instruments and test procedures. A checklist of source characteristics should include the following:

a) Type of RF generator and the output power.
b) Carrier frequency(ies), signal duty factor, pulse width, pulse-repetition frequency, etc.
c) Modulation characteristics, e.g., peak and average values, waveform, etc.
d) Intermittency, e.g., scanning beams, operational duty factors.
e) Number of sources: If more than one source is present, are some or all of the signals coherent? Are intensities likely to add linearly or will they create interference patterns (standing waves etc.)?
f) Spurious frequencies including radiated harmonics.

A checklist of propagation characteristics may include the following:

— Distance of source to test site
— Type of antenna and properties including gain, beamwidth, orientation, scanning program, physical size with respect to the distance to the area being surveyed, i.e., near field, etc.
— Polarization of the E- and H-fields (linear, elliptical)
— Existence of absorbing or scattering objects likely to influence the field distribution at the test site

A review of such a checklist is a necessity if the surveyor is to avoid some simple, but often surprising, situations. For example, it is necessary to know the location of the source and RF propagation path during surveys with hand-held probes. Only then can an appropriate assessment of the effect of the presence of the surveyor's body be made, and measurement errors avoided. Another example common in leakage situations is the possibility that the levels of the EM fields may be potentially hazardous to the surveyor and may produce RFI in the survey instrument electronics if it was not designed for operation in the presence of such fields.

6.1.2 Estimate of expected field strength

If the fields are far fields or radiating near fields of an antenna, then the material on theoretical calculations of exposure fields (Annex B) can be used to obtain field strength estimates. General references on antennas and hazard surveys are useful [B88], [B140], [B143], [B226], [B251], [B253].

If more conservative values for the on-axis power density maxima S_m are desired for parabolic reflector antennas with tapered aperture distributions, the curves in Annex E can be used. However, one should always keep in mind that equations in Annex B and the curves in Annex E are only suitable for obtaining approximate power densities for estimation purposes. More definitive values will require careful measurements.

Field enhancement due to ground reflections could increase S by as much as a factor of four times and even more if focusing effects are present. It should be recognized that such fields measured in the absence of a person may be misleading relative to potential hazards. For example, a person exposed in front of a reflecting planar surface reduces the magnitude of the standing wave by his or her absorption.

In the case of low frequencies or small-aperture antennas, the existence of potentially hazardous reactive near fields becomes relevant. These fields can be accurately calculated only for well-defined antennas of simple geometry. Since radiator geometries are rarely simple or well defined for low-frequency (1 MHz–300 MHz) sources in commercial use, measurements of E and H are usually required. However, one can always utilize the general property [B155] that reactive fields predominate at distances d close to sources where $(2\pi d)/\lambda \ll 1$. Reactive near-field amplitudes diminish as $1/d^2$ or faster, whereas radiation far-field amplitudes diminish as $1/d$. General texts [B155] can sometimes be used to estimate E- and H-field values at these lower frequencies, and specific literature [B43], [B58], [B64], [B66], [B116], [B248] on the propagation characteristics of various broadcasting and communication antennas can be used to estimate either near or far fields from these sources.

6.1.3 Determination of type of instrument required

Although many instruments designed for potentially hazardous fields are broadband in nature, there are none that cover the entire frequency range of interest and all parameters of potential interest. Some general considerations in the selection of an instrument include the following:

a) *Frequency*—Frequencies should be determined in advance so that proper instruments and measurement methods can be selected. The presence of several frequencies dictates the use of a broadband device with true rms response. (If the operating frequency cannot be readily determined, e.g., from the equipment label or user information, the use of a spectrum analyzer, field-strength meter, or frequency counter should be used to determine the frequency.)

b) *Response time*—It is usually desirable to begin a survey using a hazard instrument with a response time (integrator time-constant) of 1 second or less (the "fast" setting on some commercial instruments). This enables a coarse measurement or the detection of pulse-modulated or intermittent fields, e.g., those created by a scanning radar beam. A "peak hold" feature on some survey instruments can provide an accurate indication of moderately fast bursts of RF energy (duration greater than several milliseconds). Once a high- field-strength zone is located, a slower time constant (3 s or more) should be used to obtain the time averaged value of the field strength. If the hazard meter still indicates that an intermittent field exists, other means of recording and averaging should be used. Data-logging systems are available specifically for use with RF hazard meters.

c) *Peak power limitations*—A knowledge of the peak power limitations of the instrument is necessary to protect probes from damage in some low-duty-factor pulsed fields, such as those associated with radars.

d) *Polarization*—A knowledge of the polarization of the fields enables a surveyor to use a nonisotropic probe for hazard surveys. In the absence of such knowledge, an isotropic probe is highly desirable both for ensuring accuracy and ease of performance of the survey in a reasonable period of time.

e) *Dynamic range*—The maximum anticipated field strengths should be estimated before measuring emissions from an RF source. A survey instrument capable of withstanding continuous exposure to field strengths (E^2 or H^2) of at least ten times the predetermined value should be chosen in order to avoid destruction of the probe sensing elements or the high-resistance leads connected to those elements. In addition, adequate sensitivity is required to ensure a reasonable signal-to-noise ratio when the minimum expected field strengths are being measured.

f) *Near-field measurement capabilities*—If a leakage situation exists, or if the fields in close proximity to a source are to be measured, care should be taken to select a suitable instrument (see 6.3.4).

6.2 Safety precautions

Personnel should take appropriate safety precautions while conducting surveys, and the degree of care exercised should increase in proportion to the power levels associated with the systems being surveyed. The nature of the precautions will also differ for leakage surveys compared with measurements of deliberate radiating systems (antennas).

6.2.1 Potential hazards not directly associated with the survey

Before discussing precautions directly related to the surveying process, it is worthwhile to consider potential hazards, other than RF exposure, which might be associated with the electronic equipment or system being surveyed.

a) *High voltage*—Electrical and electronic equipment can present potential and lethal shock hazards. Ordinary precautions, such as not defeating interlock protection systems, exercising care around necessarily exposed high voltage leads and terminals, and avoiding working alone near high-voltage systems, should be employed. It should be noted that, in many high-power systems, a prime RF-leakage source may be the high-voltage electrodes of the transmitting tubes. Additional caution is advised when performing measurements in the vicinity of conductive structures, such as tall cranes or long vertically suspended cables, which are located near high-power, low-frequency RF sources. In such circumstances, large open-circuited voltages can exist on the structures that are exposed to ambient RF fields; these voltages may reach levels of several kilovolts and have the potential for arcing to a grounded body, leading to strong startle responses and, in some cases, severe RF burns. Appropriate precautions should be exercised before contacting improperly grounded objects in strong RF fields.

b) *X-ray hazards*—In high-power systems utilizing high-voltage transmitting or other high-power tubes (greater than about 20 kV), there is generally the potential for X-ray emission. It, therefore, may be desirable to first conduct a survey of X-ray emissions before an RF survey is conducted in close

proximity to such devices. One should take care that the X-ray survey instrument is not susceptible to RFI.

c) *DC magnetic fields*—Very high-power systems may include sources of strong static and low-frequency magnetic fields. In order to avoid exceeding the MPEs for static magnetic fields, e.g., ACGIH [B1], survey personnel should avoid sustained close proximity to such sources. Also, tools have been known to fly out of the surveyor's pockets, etc., causing personnel injury.

d) *Indirect RF hazards*—It is important to remember that the presence of RF fields can produce hazards, or at least undesirable effects, besides those arising from exposure of body tissue. Since surveys may be conducted not only in controlled laboratory conditions, but also near mobile transmitters, in industrial situations, and even in homes, one should at least be aware of the following possibilities:

   1) Serious hazards are associated with the potential exposure of electroexplosive devices (EEDs), combustible gas, or flammable materials to EM fields. IME 20-2001 [B8], or IEEE Std C95.4™-2002 [B137], on safe exposure distances for EEDs relative to various transmitters should be followed.
   2) It is generally important to realize that potential EM interference to electronic devices or systems often occurs at levels far below those that cause bodily harm. This interference may be only an annoyance, for example, the effects of low-elevation radar operation on TV or consumer electronic devices in homes, or it may be more serious, such as causing the possible reprogramming or "upsets" of microprocessor-controlled medical devices, e.g., cardiac pacemakers, or causing errors in digital computers controlling industrial processes. In any case, such interference is undesirable, and care should be exercised when operating systems (particularly in abnormal modes of operation) that may be useful for survey purposes. A clear assessment of the impact of potential interference problems should always be made before beginning a survey. It is also understood that surveys are to be made with responsible adherence to the rules of the Federal Communications Commission and other bodies that regulate against RF interference.

e) *Burns (associated with high-power fields)*—One should take care to prevent RF burns resulting from handling conducting objects exposed to these fields or RF cables with exposed connectors [B216]. In addition, one should follow ordinary precautions in the operation of RF heating systems and plastic sealers during surveys, e.g., avoid handling test loads, sealing bars, and superheated liquids.

f) *Abnormal modes of operation*—One should be aware that electronic systems have the potential for abnormal modes of operation in which spurious frequencies and unintended leakage radiation are generated at significant power levels. The operation of a system should not be attempted by the surveyor without qualified personnel present to assess the normality of operation, in order to avoid such situations.

g) *Fall hazards*—Personnel performing RF field surveys must always be aware of the potential for falling from rooftop or tower antenna sites, elevated antenna pedestals, etc. The use of safety lines and climbing harnesses is recommended.

6.2.2 Precautions during the survey process

Serious precautions are clearly required when surveying radiating systems, such as a high-power radar. Such precautions include the following:

a) Based on known parameters of the system, the survey process should be planned so as to limit exposure of all personnel to levels below the MPEs found in the applicable exposure guidelines or standards, e.g., IEEE Std C95.1-1991. This limitation relates not only to power density, but also exposure duration. If survey personnel are exposed to field strengths in excess of those specified in the guides for continuous exposure, they should be accompanied by other personnel who can ensure that the exposure duration does not exceed the time recommended in the MPE for exposure to higher level fields (see 4.2.2). In such situations, it may be desirable to conduct the survey with RF-emitting

equipment operating at a reduced power level and use power scaling to compute the corresponding field levels that would exist during full-power operation.

b) The operation of movable or scanning antennas should be done with full allowance for safety precautions. These precautions range from avoiding injury from bodily collision with rotating or moving structures, to avoiding start-up operation of RF generators with antennas pointed in the direction of personnel. Before a survey begins, antennas should be adjusted far from the most potentially hazardous position with the surveyors approaching from out of the beam path toward the beam. Furthermore, if measurements are to be conducted while the antenna is scanning, one should first determine whether or not the response time of the instrument is fast enough to respond to the scanning beam. In addition, one must be aware of the burnout characteristics of thermocouple type probe-elements that can reach their burnout limit in a pulsed field without reaching the rms limit of the probe.

c) A theoretical examination of the antenna radiation patterns should be made before beginning actual system operation or conducting the survey.

d) Antennas should not be pointed toward metal structures, and metal objects should not be inadvertently located close to antennas. These not only create scattering and multipath situations, but are also a potential source of RF burns. However, if the normal area of transmission includes such metal objects, measurements should be conducted in those areas with the objects in place. The presence of secondary structures such as towers, guy wires, fences, reflecting surfaces, etc., can enhance the fields and produce RF hot spots. Allowance for such effects should be made when undertaking a survey. During the survey, the surveyor should be in continual communication with the operator of the RF source so that the source may be controlled in accordance with survey requirements.

When performing leakage surveys, the following precautions should be taken:

— The possibility of leakage exists at the site of the RF generator, along any transmission line or waveguide conveying power from the generator (particularly at waveguide joints), and at all access doors and panels of enclosures housing the generator. Normally, leakage energy drops off as the inverse square of the distance. Therefore, in conducting a survey, one should begin by approaching the generator, antenna, or any unintended radiating/leaking structures from a “safe” distance. The survey instrument should be set to a “high” range to alert the surveyor to the possibility of being exposed to levels exceeding the applicable MPE.
— The possibility of RF burns exists, so contact should be avoided with any metallic structure on or near a point where high field strengths could exist.
— When opening access doors or panels to insert or remove a test load (for example, in a microwave oven or RF-exposure test chamber), the equipment should be shut down first and the interlock systems left operative.
— In checking for possible inoperative interlocks at an RF enclosure access port, one should ascertain leakage levels while the source is on and the port is closed. Then the surveyor may slowly open the port to observe any increase in leakage and possible interlock failure.
— Foreign objects (especially metallic objects) should not be inserted into any opening or port of the RF enclosure. This applies particularly in the case of high-power industrial systems that use conveyor belts carrying materials through ports of the RF enclosures.
— With the source switched off, the surveyor should visually inspect all flexible waveguides that carry high power. This inspection should determine signs of fatigue, aging, damage at joints, lack of adequate support, etc.

6.3 Measurement procedures for external fields

6.3.1 General considerations

Prior to making measurements, one should estimate the expected field strength and determine the type of instrument required, as discussed in 6.1. Additional approaches and equations for calculating field strength in various situations are given in Annex B. The measurement procedures to be used may differ, depending on the source and propagation information available.

If the information is adequate, then the surveyor, after making estimates of expected field strengths and selecting an instrument, may proceed with the survey. The surveyor should use a high-power (least sensitive) probe with the range switch set on the most sensitive scale. The high-intensity field areas, e.g., the main beam of a directional antenna, should be approached from a distance to avoid probe burnout. The surveyor then gradually proceeds to move progressively closer to the regions of higher field strength. Extreme care should be exercised to avoid overexposure of the surveyor and survey instrument. For low frequencies, the E-field should be measured first since it represents a greater potential hazard.

On the other hand, if the information is not well defined (for example, reports of strong, intermittent interference), then it may be difficult to make a hazard survey without first conducting an empirical, hazard assessment. A survey for potentially hazardous fields of unknown frequency, modulation, distribution within an area, etc. may require use of several instruments. Examples of such instruments are spectrum analyzers or field-strength meters that display frequency-domain information with a means to analyze amplitude modulation characteristics, and which have a wide dynamic range, e.g., 60 dB in power. After this preliminary procedure is performed, it may be possible to continue a more meaningful survey with isotropic hazard survey instruments.

6.3.2 Far-field, single-source conditions

The measurement of a linearly polarized plane-wave field whose source location, frequency, and polarization are known may be performed with a tunable field-strength meter of acceptable accuracy that covers the frequency range of interest. This instrument is used with a calibrated conventional antenna such as a standard-gain horn or dipole. Alternatively, an isotropic hazard probe may be used.

Multipath reflections may create highly nonuniform field distributions, particularly at frequencies in excess of 300 MHz. To judge the level of exposure at any specific location, a series of measurements should be made over a square surface whose sides are approximately 1 or 2 m in extent. The spatial average of the square of the fields within that area, e.g., over an area equivalent to the vertical cross section of the human body, should be considered as the appropriate value for comparison with whatever protection guide is being employed as a criterion. Measurements near re-radiating metallic objects should be made with the edge of the probe at least 3 “probe lengths,” e.g., 20 cm, from the object (see 6.3.6.1).

In an analysis of RF field measurement data obtained during a field survey in a metropolitan area adjacent to a large antenna farm, Tell [B252] discussed the degree of variability in the measured field magnitudes obtained at the same measurement location, using the same instrumentation with measurements performed by the same individual but with different orientations of the observer relative to the measurement point. A broadband electric field probe equipped with a datalogger was used to acquire the minimum, maximum, and average square of the RF field strengths along a vertical path 2 m in height, with the observer facing the measurement point from four different directions. Measurements were performed at 171 different locations along neighborhood streets near a broadcast site containing six FM radio antennas. Observer-induced field perturbations accounted for a mean value of 71% (2.3 dB) variation in the spatial average measurement of the RF fields (ratio of maximum spatial average to minimum spatial average obtained from four successive vertical scans at each measurement point). RF fields were found to be nonuniform over the body dimension with a mean value of the maximum to minimum field readings of 10.3 (10.1 dB). These variations in

measured fields should be carefully considered when interpreting measurements used for demonstrating compliance with exposure limits.

While mounting or holding the measuring antenna or probe, care should be taken to avoid reflections or perturbations of the field by support structures or by the operator's body. Where required, to avoid field perturbation, metallic portions of the measuring device, or support structure, should be covered with absorbing material of appropriate quality. Where possible, probe interconnect cables should be oriented normal to the electric field. When that is not practical, or where severe multipath effects produce fields originating from multiple directions, metallic cables should be covered with absorber unless tests demonstrate that the cable position does not affect the measurement. Dielectric fixtures should be as small as possible (minimum reflection cross section) and should be of low dielectric-constant material, or be less than one-quarter wavelength in effective thickness T_E. The effective thickness is given by

$$T_E = T(\varepsilon_r)^{\frac{1}{2}} \tag{20}$$

Where T is the physical thickness and ε_r is the relative permittivity. Even dielectric slabs ($\varepsilon_r > 2$) can significantly alter plane wave fields if the effective thickness is greater than 0.1 wavelength.

For highest accuracy, sources of error can be accounted for so that the true field strengths may be ascertained with less than ± 2 dB uncertainty. To obtain this level of accuracy at frequencies above approximately 300 MHz, a scanned measurement or many fixed-point measurements per wavelength should be performed in order to obtain information on the variations in field strength in that area due to multipath and other reflections.

6.3.3 Far-field, complex sources

When measuring the fields from multiple, distant sources of unknown frequency, polarization, or direction of propagation, a broadband isotropic probe is required. Since standing-wave effects and multiple-source field interactions should be accounted for, it is necessary to scan a volume of space in the zone of interest. The area should be divided into a grid of 1 m – 3 m squares (depending on the size of the area of interest), and measurements should be taken at each grid intersection. Scans should also be made in the vertical plane at grid intersection points.

In the case of multiple sources of unknown polarizations, a single-axis probe (linear dipole) cannot be used to provide accurate data in a reasonable length of time, since measurements with three orthogonal orientations of the probe are required to ensure that all components of the field are accounted for. If a single-axis probe or linearly polarized antenna must be used, one should be sure that the field being measured is time invariant. Even if an isotropic probe is used, it should be relatively free of sources of measurement error caused by reflections from the probe, cables, readout case, and the surveyor. The use of long (many meters) high-resistance or fiber-optic probe interconnect cables will minimize the reflection problems mentioned above.

6.3.4 Near fields

Since large field gradients exist in the near field of an active radiator or passive re-radiator, their measurement requires the use of a probe with an electrically small array of three orthogonal dipoles and, for frequencies below approximately 300 MHz, an array of three electrically small orthogonal loops, in order to provide satisfactory performance for the resolution of these spatial gradients. (See 6.3.6.5 for effects of magnetic field averaging over coil probes.) Otherwise, a spatially averaged value will be measured by a large probe (one with an effective area greater than one-quarter wavelength in cross section). In addition, a small antenna array produces minimal perturbation of the field and the radiation characteristics of the source are not modified (alteration of reactive near fields). Since the polarization of the fields in near-field situations is

usually unknown, under most circumstances, an isotropic probe should be used. If the frequency and polarization are known, a broadband instrument is not required. Instead, a narrowband probe with uniform response in a single plane (similar to some commercial, microwave-oven survey instruments with two-orthogonal dipoles) may be used (see also 6.3.5).

6.3.5 External field-measurement instrumentation-usage considerations

The scattering effects of the operator, cable, support structure, and readout device have been mentioned. These problems are most significant when a spatially uniform field (plane wave) illuminates all of these objects and the probe sensor with the same approximate field strength. This produces reflections that are directly related to the scattering cross section of the various objects and their distance from the probe. Scattering from the operator's body may introduce errors in the equivalent plane-wave power density of more than 2 dB [B44]. Reflections from readout cables aligned with the incident plane-wave electric field and placed approximately 30 cm behind the sensor of an isotropic probe can cause measurement variations of ± 1.5 dB at 915 MHz and ± 0.75 dB at 2450 MHz [B27], [B30]. These effects become more significant at lower frequencies where the cable length and RF wavelength are comparable. The magnitude of the reflections from a cable, the operator, or other objects increase as frequency decreases for a fixed geometrical relationship between the probe and the cable. Therefore, greater care should be taken at frequencies below 1000 MHz to avoid large errors when measurements are performed in spatially uniform fields. Orientation of the cable perpendicular to the incident electric field, or covering it with absorber, will reduce this problem. One should bear in mind, however, that most absorbers are not effective at low frequencies. Therefore, fiber optically coupled instruments are preferable at frequencies below 300 MHz.

RFI also becomes a significant problem at lower frequencies, since it is more difficult to shield readout electronics and cables at frequencies below about 500 MHz. An operational test of the system can be made by totally shielding and grounding the sensor tip of an electric-field probe with metal foil. This procedure allows the determination of the existence of RFI or capacitive coupling between the cable and readout and nearby radiating objects during the measurement. Similarly, reorienting the probe leads in the field, with the probe sensing element fixed, should not alter the reading of the meter appreciably (± 6 dB) if RFI is not problematic. It is not uncommon to find large errors in readings from older designs of isotropic instruments when they are used to measure electric and magnetic fields below about 1000 MHz, especially when the readout device and probe cable are exposed to a field of the same magnitude as that which illuminates the probe [B31], [B218]. This often is due to faulty RFI gaskets in the readout device or poor system RFI design. Fiber-optic cables, high-resistance cables, or double-shielded coaxial and signal cables can be used by designers of hazard survey instruments to connect the probe to the readout device, in order to minimize the effects of RFI. A self-contained (active antenna) probe with integrated antenna, sensor, and readout in the same housing can minimize the problem of RFI otherwise induced in cables or readout [B32].

Response to the scalar potential field is often mistaken for RFI. This false response can be evaluated by comparing the readings of the probe with the probe sensor area covered with an ungrounded conductive foil. This ungrounded cover will attain the average potential at that point. Any readings with the probe covered will be due to the response of the probe to potential scalar fields, and not due to the force field [B15].

Instrument linearity as a function of the peak-to-average power ratio of amplitude-modulated fields should be considered when performing measurements in an unknown situation. Pulse duty factor or amplitude-modulation waveform can be quantified through the use of a conventional antenna with a coaxial output, e.g., log periodic, dipole, and a coaxial attenuator and diode detector. The detector output can be fed via coaxial cable into an oscilloscope of appropriate bandwidth. The duty factor of pulsed sources and the waveform of the amplitude modulation can then be observed, and the ratio of the peak to average power or energy density can be ascertained. It is not necessary to maintain square-law operation of the detector for the evaluation of 100% rectangular amplitude-modulated waveforms. For other pulse-modulated waveforms, one can only be assured that both the peak and average field strengths are correct if the detector is operated in the square law region [B243]. Also, with square law detection, the ratio of the peak to average equivalent power density (E^2 or H^2) can be quantified.

Measuring the effects of a slowly time-varying field generated by a rotating radar antenna, or a microwave oven with a mode stirrer, can be accommodated by use of the appropriate time constant of the readout instrument. Some instruments provide "fast" and "slow" time constants. Any observable periodic variation of the field strength, as indicated by the instrument in the fast mode of operation, should be considered as low-frequency field modulation and the slow time constant should be used. Care should be taken to avoid mistaking slow variations in reflected signals (due to objects moving in the field) for a true time-varying source modulation. This implies that any movement of the operator, probe, or surrounding objects, should be eliminated during the measurement procedure where time-varying fields are involved.

An ellipticity (nonisotropic reception condition) in the receiving pattern of multi-axis or isotropic probes is always present to a certain degree (typically 2%–20%). Only when the ellipticity of an instrument is accounted for, can highly accurate data be taken. In fields where components do not exist along the direction of the probe handle, a rotation of the probe about the handle axis should be performed during a survey (if the surveyor desires to eliminate this error) at each fixed point of interest within the spatial volume being surveyed. The minimum and maximum values should be recorded and an average value computed. This can be done manually in near-field situations, e.g., microwave oven surveys, without introducing error, if the surveyor's hand is in an area of minimal field strength with respect to the field at the sensor (probe tip). In situations where uniform illumination exists over the entire probe body (tip and handle), larger errors are usually introduced by the presence of the operator's hand, while performing this rotation, than are introduced by probe ellipticity. In this case, if precise data are required, the probe should be supported by a dielectric support and error limits associated with the probe ellipticity should be assigned to the measurement, rather than attempting to manually rotate the probe.

6.3.6 Interaction of RF hazard probes with nearby passive scattering objects (re-radiators) and active radiators

When measurements are made with a hazard probe placed close to conducting or high-dielectric-constant objects (scatterers or "passive re-radiators"), large errors may result. Two situations are addressed in this clause. One situation occurs when a hazard probe with an "electrically large" antenna (larger than about 0.25 wavelength) is placed close to field-perturbing objects such as a person's body, or large conducting objects, e.g., a metal pole or metal shed. A second error-producing situation occurs when measurements are made with the probe antennas less than a few probe "antenna-lengths" or "probe lengths" from an active RF radiator such as the monopole antenna of a mobile radio transmitter or a leaking microwave oven. (The term probe/antenna-length is discussed in 6.3.6.4.)

Inaccurate performance of a hazard probe located near either passive re-radiators or active radiators is due to several factors, including the following:

a) Reflections from a re-radiating object that produces standing-waves (or interference patterns in the EM-fields) that extend a distance of several wavelengths from the scatterer. When a probe is not tightly coupled (via the reactive near-fields of the re-radiator), the techniques of 6.3.2 can be used to minimize measurement errors. These techniques remove the effects of standing-waves through the use of spatial averaging. When the probe is tightly coupled to the re-radiator, the data in 6.3.6.1 can be used;

b) A perturbing object (whether it is an active radiator or a passive re-radiator) "loads" or distorts the measurement characteristics of the probe's antenna/detector combination [B217]. This occurs when the antenna is large compared with the wavelength of the RF energy being measured (6.3.6.1 addresses this situation);

c) An electrically large probe in the reactive near-field of an active radiator alters the fields being radiated by the source and spatially averages the nonuniform near fields being measured. This averaging occurs over the effective aperture area of the probe antenna, i.e., dipole length or loop diameter. (See 6.3.6.5.)

6.3.6.1 The effects on measurement accuracy of the separation distance between survey probes and nearby passive radiators

An analysis can be performed to determine the degree of probe interaction (or coupling) with nearby objects, such as passive re-radiators or scatterers, including exposed personnel. When a probe is tightly coupled to a re-radiator, a probe-loading error has the effect of altering the impedance match between the probe's antenna and its detector. Although this loading error is dependent on two electrical parameters of the antenna and detector equivalent circuits, the ratio of the antenna's "source impedance" to its "load (detector) impedance" is the critical one. The "source impedance" refers to the complex output impedance of the antenna (at the frequency of interest): The "load impedance" is the complex impedance of the RF detector that is placed at the output terminals of the antenna. For any type of detector, e.g., diode, thermocouple, if the magnitude of the complex impedance of the load (detector) is "high" (about ten times larger than the source antenna impedance), the probe will be less susceptible to performance degradation due to a small separation distance between it and a large field perturbing object.

Analyses and specific calculations have been performed to quantify the probe-to-passive- re-radiator effects discussed above. Estimations have been made to quantify the errors caused when measurements of field strength are made with a hazard probe that is in close proximity to a large, passive re-radiator. A thorough analysis has been carried out for the situation where a dipole-based hazard probe is used to measure a plane-wave field close to an infinite, conducting plane [B229]. The effect of proximity of the conducting plane to the electric field probe was studied analytically, and confirmed experimentally. The degradation of the measurement is quantified in terms of the true field-strength distribution (including the standing-wave) along a path normal to, and close to, the large reflector. Two cases were studied for dipole-diode probes of total lengths equal to 0.2 and 0.4 wavelengths. (It should be noted that in [B229], the results are expressed in terms of the half-length of the dipole antenna, while the following will relate the results to the full "probe antenna length.")

The performance of the antenna/detector combination was analyzed as a function of distance between the antenna and the reflecting plane and the results quantified the probe error with respect to the true electric field (including the large standing wave associated with the reflector). The errors associated with the measurement of the E-field were examined for very high- impedance (open-circuit) antenna-terminal loads (detectors), and for very low-impedance (short-circuit) loads. The measurement error of the dipole/detector combination was determined by analyzing the behavior of the equivalent circuit of the probe antenna and detector. The analysis performed by Smith [B229], using the assumptions above, yield a fractional E-field measurement error ΔV that is defined as follows:

$$\Delta V = \frac{|V| - |V_0|}{|V_0|} \tag{21}$$

Where

V_0 is the voltage from the E-field detector in the absence of the scatterer,
V is the measured voltage in the presence of the scatterer.

While probes with a complex load (detector) impedance of at least ten times greater than the source (antenna) impedance are less susceptible to errors induced by a nearby field-perturbing object, a low-capacitance, high-impedance diode detector across the antenna terminals will reduce the worst-case errors by a factor of about two.

Results and conclusions of the analysis of measurement errors due to the interaction between a probe and a nearby passive scatterer are presented below. Selected data from Smith [B229] are included in Table 1. Note that errors in equivalent power density or field-strength-squared in Table 1 have been calculated using the relationships shown in Equation (22). For the equivalent power density error, it was assumed that the RF

hazard probe is square law. Here, the fractional error encountered when measuring the equivalent power density with and without the reflecting plane present can be calculated from Equation (21) and expressed as indicated below:

$$\Delta S = \frac{V^2 - V_0^2}{V_0^2}$$

Where

ΔS is the field-strength-squared error (or equivalent power density error), and V and V0 are defined above.

Table 1—Measurement errors for field strength measurements made in close proximity to an electrically large, passive re-radiator (from Smith [B229])

Frequency (MHz)	Probe length (cm/wavelength)	Separation		Measurement error	
		(cm/ wavelength)	(antenna length)	FS (%)[a]	FS^2 (%)[b]
300	20/0.2	20/0.2	1	10	21
3000	2/0.2	2/0.2	1	10	21
3000	4/0.4	5/0.5	1.25	13	28

[a](FS) = field strength
[b](FS^2) = field strength squared or equivalent power density.

The following trends are revealed in Smith [B229]. At frequencies between 300 MHz and 3 GHz, and separation distances between 0.2 and 0.5 wavelengths, field-strength measurement errors were found to be less than 13% (28% for field-strength-squared or equivalent power density) for antennas that are less than 20 cm in length. Data are lacking for dipole antennas used below 30 MHz that are shorter than 200 cm. Therefore, practical hazard probe error analyses cannot be obtained from Smith [B229] for frequencies at or below 30 MHz.

Overall findings from the analysis presented above indicate that worst-case measurement errors, over the frequency range of 300–3000 MHz, are no greater than 10% (21% for field strength squared), under the following worst-case conditions:

a) The detector (load) impedance is low, with respect to the antenna's source impedance, i.e., the detector draws a relatively high RF current from the receiving antenna. In contrast, a low-capacitance, high-impedance diode detector will reduce the probe loading errors by about a factor of two.
b) The perturbing object (passive re-radiator) may have any scattering cross section, i.e., its size can be much greater than several wavelengths at the frequency being measured. Small scatterers will introduce lower measurement errors.
c) The dipole electrical length is less than or equal to 0.4 wavelengths tip-to-tip.
d) The distance between the probe and the perturbing object is greater than 20 cm at 300 MHz (0.2 wavelengths), and greater than 2 cm (0.2 wavelengths) at 3000 MHz.

Tell [B250] described a test designed to evaluate the possibility that a measurement probe might, when placed very close to a strong localized RF source, capacitively couple to the source, thereby altering the

source characteristics and, thus, the fields being measured. In these tests, the electric field near one end of a re-radiating resonant rod was measured with one instrument while other probes were brought near the opposite end of the rod. Any interaction of the probe with the re-radiating rod could conceivably be manifested as changed readings of the field at the other end of the resonant rod. Of the probes used in these tests, only the magnetic field probe and one electric field probe produced any observable change in the electric field being monitored at the other end, and even in this case, the effect was minimal. Data related to the magnetic field probe that produced the greatest interaction are summarized in Table 2.

Table 2—Effect of a 10 cm diameter magnetic field probe on a re-radiating 144 MHz resonant dipole antenna (Tell [B250])

Distance from probe surface to rod (cm)	Change in square of electric field strength (%)
20	0
10	0
5	0
4	1.2
3	1.2
2	3.5
1	7.1
0	17.6

These data show that only when the probe surface was placed in contact with the resonant rod was there sufficient coupling between the probe and the rod to significantly change the electric field strength at the other end. In the case of the magnetic field probe tested, it was observed that the probe has loop windings on its spherical surface. Hence, the windings were essentially placed in direct contact with the source, and consequently, there was no distance isolation afforded as there was with the other probes tested. In the evaluation of a broadband isotropic electric field with a 40 GHz response, direct contact between the probe housing and one end of the re-radiating resonant rod resulted in a maximum change of 2.2% in the field observed at the opposite end.

Other evaluations related to deformation of the pattern of the field probe response due to near-field coupling phenomena were also reported by Tell [B250]. These tests revealed only minor interactions with the re-radiating dipole rod. These test data, when taken collectively, appear to support the remarkable conclusion that measurement probe interaction with RF hot spots does not appear to be a significant issue, at least for the conditions evaluated in this project. For applications in the VHF broadcast band, the test results appear to suggest that no significant interactions occur that would lead to erroneous field strength readings for the most commonly used isotropic broadband probes. This finding seems to hold even for measurements taken with the spherical shell of the probe in direct contact with the source. However, in the case of one magnetic field probe, a 2 cm spacing between the probe and the source appeared necessary to minimize any interaction with the source. It must be emphasized, however, that all of the probes evaluated were small compared with the wavelength of the RF field. Very large field sensors would likely yield significantly different results, and particular care should be used in conducting measurements with large probes.

A set of measurement errors with similar values can be expected for an electrically small loop antenna (H-field probe) due to the impedance "loading" effect from a nearby conducting plane. Here the loop diameter would represent the probe antenna length.

6.3.6.2 The effects on measurement accuracy of the separation distance between survey probes and nearby active radiators

The accuracy of measured data can be affected when using a near-field probe to map large spatial gradients very close to radiating elements of an RF emitter (an antenna or a leakage source). These gradients may cause the amplitude of the field to vary significantly over the volume of space that is occupied by the probe antennas, thereby introducing measurement error due to spatial averaging. As the separation distance between the probe and the radiator increases, the field throughout the entire volume occupied by the probe's antennas becomes more uniform. Based on the fact that the largest field gradients are associated with the reactive or quasi-static E-field near a radiating device, it is possible to predict the minimum distance between a near-field probe and an active radiator that will avoid significant measurement errors. For example, for an infinitesimal electric dipole antenna, the field strength at a point d can be expressed mathematically by [B213]

$$E_r = \frac{I_0 h}{4\pi} e^{-jkr}\left(\frac{2\eta}{d^2} + \frac{2}{j\omega\varepsilon d^3}\right)\cos\theta \tag{22}$$

$$E_\theta = \frac{I_0 h}{4\pi} e^{-jkr}\left(\frac{j\omega\mu}{d} + \frac{1}{j\omega d^3} + \frac{\eta_0}{d^2}\right)\sin\theta$$

$$H_\phi = \frac{I_0 h}{4\pi} e^{-jkr}\left(\frac{jk}{d} + \frac{1}{d^2}\right)\sin\theta$$

Where

$$k = \frac{2\pi}{\lambda}\ (1/\mathrm{m})$$

η_0 is the impedance of free space = $120\pi\ \Omega$ ($\approx 377\ \Omega$),
ε is the permittivity of free space (F/m),
μ is the permeability of free space (H/m,
h is the length of the dipole (m),
I_o is the antenna current (A),
ω is the angular frequency (radians/second),
λ is the wavelength (m),
d is the distance from the center of the dipole to the location of interest (m),
θ is the angle between the axis of the dipole and the unit direction vector from the center of the dipole to the point r.

Examination of Equation (23) shows that the fields decrease inversely with the cube of the separation distance d between the radiator and the point of measurement. An analysis of the magnitude of the E-field components indicates that the reactive field component ($1/d^3$) dominates at distances of less than 0.15 wavelengths from the source.

Further examination of Equation (23) at distances less than 0.15 wavelength provides data that define the range of separation distance over which E^2 varies less than a factor of ± 3 dB. With this as a criterion, Equation (23) can be used to provide a worst-case simplified analysis using the single $1/(\omega d^3)$ term in the

expression for E_θ. The results indicate that the minimum separation distance necessary is 5 receiving "probe-antenna lengths" (see Table 3), e.g., approximately 20 cm or more for typical commercial near-field instruments where the size of the sensor elements is small compared with 20 cm. Here, an antenna length is equal to the tip-to-tip dimension of a simple dipole or the diameter of a loop. A worst-case estimate of the "probe-antenna length" can be readily obtained following the procedure described in 6.3.6.4.

It should be noted that the above worst-case analysis yields errors that are significantly larger than the actual errors encountered for many types of radiators. Specifically, many radiation sources, such as a crack in a microwave oven door, do not produce "radial" components with $1/d^3$ decay with separation distance, even in their reactive near-field region.

6.3.6.3 Conclusions on the minimum spacing between an RF probe and a radiating source or a passive re-radiator

The analyses presented in 6.3.6.1 and 6.3.6.2, and the information contained in 5.5.3, may be applied to the near-field measurement problem. This problem involves the worst-case uncertainties that occur when measurements are made at a minimum distance from an active radiator or passive re-radiator. Table 3 provides information on this subject, in terms of ranges for which the probe sizes and frequencies are valid for the particular analysis technique. Also, the minimum separation distance is expressed with respect to wavelength and in terms of the probe-antenna length (the maximum dimension of a single antenna or the array of orthogonal antennas of the hazard probe).

The data in Table 3 can be used to estimate the errors that will result if the minimum probe to source or scattering object separation distances are not exceeded. The largest error is due to the gradient of the radial field over the probe antenna with which it is aligned. This error is an extreme worst case, and many situations will not produce an error this large, even at smaller separation distances. In general, for a typical hazard probe with an array of 5 or 10 cm dipoles or loops, a separation of 3–5 probe lengths will ensure a maximum error of 3 dB at frequencies lower than 500 MHz, while the maximum error at higher frequencies may be lower due to the fact that the gradients in the radial components are less steep at distances greater than 0.15 wavelengths. Therefore, for most situations, when appropriate near-field survey instruments are used, a minimum separation distance of 20 cm is reasonable for passive re-radiators.

NOTE—Determining the appropriate measurement distance from a near-field source is, at best, a compromise. However, when considering the potential constraints on measurement accuracy caused by inadequate probe-source separation distance and the importance of assessing whole-body exposure levels, a minimum measurement distance of 20 cm from scattering and re-radiating objects is recommended, in accordance with guidance in 6.3.6.3. However, because some generating devices and their associated attachments that meet the field MPEs at distances of 20 cm and greater are capable of producing SARs that exceed the SAR limits, measurements should be made at a distance of 5 cm from any such generating device and its associated attachments. Both E- and H-field measurements may be necessary.

Table 3—Worst-case errors associated with the minimum probe to RF source separation distance

Separation distance				
Analysis method	**Antenna length[a]**	**Wavelength**	**Frequency range (MHz)**	**Error (dB)**
TEM cell	1	< 0.25	< 500	1
Passive radiator	1–1.25	0.2–0.5	300–5000	1
Active radiator ($1/d^3$)	5	< 0.15	<< 470	3

[a]Normalized antenna length.

6.3.6.4 Estimation of the physical size of hazard probe antennas

Although the length of the dipoles or diameter of the loops of most survey instruments are not obvious, the maximum size of a probe's sensing antennas can, nevertheless, be estimated. Since a survey probe has antennas that are physically smaller than the dielectric radome or other physical object surrounding them, the size of the radome can be used to approximate the maximum size of the antennas within. Thus, the diameter of the spherical radome can be used as a worst-case estimate of the size of the enclosed antennas. This, in turn, can aid in determining the minimum separation distance that should be used between the survey probe and any surrounding object.

Several popular broadband RF hazard probes with thermocouple sensors have antenna elements that are almost as large as the diameter of the radome within which they are enclosed. Some active antenna-type hazard probes that have been designed to work below 200 MHz, utilize active electronics to match the impedances of their electrically short-monopole antennas to the RF detection circuitry (see 5.4.2). This type of instrument is equivalent to an asymmetric dipole, with one element (monopole) emerging from the center of a metallic box. The box houses the active electronic impedance-matching circuitry and serves as the "ground plane" or second element of the dipole. Although the overall dipole length is greater than the sum of the length of the monopole receiving antenna and the height of the electronics-containing box, the combined length should be used to define the equivalent dipole length.

6.3.6.5 Errors associated with magnetic field averaging over circular coil probes

Significant errors can also occur during measurements of highly nonuniform magnetic fields that are dipolar in character because of the averaging effects over the cross-sectional areas of circular coil probes. The difference between the magnetic field at the center of a circular coil probe and the average magnetic field has been calculated as a function of the ratio of the distance from the magnetic field source and the radius of the probe. The difference can be considered an error because the center of the probe is usually considered the measurement location. The calculations assume that the single-axis probe is rotated until a maximum reading is obtained. It is also assumed that orientation of the dipole axis is unknown, a situation that is common near some electrical devices. With the above assumptions, probability distributions of errors (which are asymmetric) have been obtained and are shown in Table 4 [B190]. For example, the errors can range from 14.6%–14.1% when the probe is three radii away from the source.

Table 4—Error probability distribution for single-axis coil probe as a function of the ratio of the distance from a magnetic dipole source and the radius of the coil (r/a) [B190]

Normalized distance (r/a)	Most probable values (%)	Extreme values (%)
3	14.1	–14.6/14.1
4	7.5	–8.7/7.5
5	4.7	–5.7/4.7
6	3.2	–4.0/3.2
8	1.8	–2.3/1.8
10	1.1	–1.5/1.1
15	0.5	–0.7/0.5

Corresponding calculations of error probability distributions for three-axis coil probes (with a common center) have been obtained and are shown in Table 5 [B189]. For the three-axis calculations, it is assumed that the orientation of the magnetic dipole and also the three-axis probe are unknown.

Table 5—Error probability distribution for a three-axis coil probe as a function of the ratio of the distance from a magnetic dipole source and the radius of the coil (r/a) [B189]

Normalized distance (r/a)	Most probable values (%)	Extreme values (%)
3	3.0	–19.6/14.4
4	2.0	–10.8/7.6
5	1.4	–6.9/4.7
6	1.0	–4.8/3.2
8	0.6	–2.7/1.8
10	0.4	–1.7/1.1
15	0.2	–0.8/0.5

A "rule of thumb" for making the $1/d^3$ dipole approximation during magnetic field measurements is that the measurement location should be greater than three times the side dimension of the source [B269].

6.4 Induced body current and contact current measurements

6.4.1 Induced body current

There are several issues that should be considered when selecting an instrument for measuring induced current. First, stand-on meters are subject to the influence of electric-field induced displacement currents from fields terminating on the top plate. This means that such meters may produce some indication of current when subjected to strong electric fields, even without a subject standing on the meter. When a subject stands on the meter, however, the electric fields are generally shielded from significant interaction with the top plate, as they preferentially terminate on the surface of the subject. Therefore, when using parallel plate type meters, the displacement current indication, without the subject in place, should be ignored. That is, the induced current reading with the subject in place should be taken as the most accurate indication of the induced body current (the initial background displacement current should not be subtracted).

Another observation is that the sum of both ankle currents measured with clamp-on type meters tends to be slightly greater than the corresponding value indicated with stand-on type meters. This observation can be explained by the fact that fringing electric fields about the periphery of the top plate of the stand-on meter induce charge on the top plate and, consequently, displacement current that does not flow through the current sensing elements of the meter. This phenomenon, which tends to reduce the induced currents for the stand-on meter, is a function the RF frequency and the geometry of the meter. While the current passing through the ankle, just above the foot, may be slightly greater than that passing through the bottom surface of the foot due to displacement current leakage off of the foot, this is not likely to be significant [B26]. The currents measured with a clamp-on current meter should be a more accurate measure of the current actually flowing through the ankle. While the induced-current limits specified in contemporary guidelines and standards, e.g.,

IEEE Std C95.1-1991, are based on limiting the current flow through this region (the smallest cross-section of the leg) to limit the local SAR, the actual limits are specified as foot current, not ankle current.

An additional issue pertains to the problem of accurately relating the induced current indicated by a stand-on meter to the actual current passing through the foot when the subject is standing on a variety of ground surfaces. For example, differing ground conductivity conditions and ground surface textures such as grass, gravel, concrete, steel decking, wood floors, etc., can result in different indicated body currents, for the same electric field strength, when measured with a stand-on meter [B173]. This is because of the differing degree of electrical contact between the bottom metal plate and the actual ground surface; i.e., the flat surface of the bottom plate does not necessarily make uniform contact with many surfaces on which it is placed. Also, the degree of contact can vary according to the weight of the subject. The inherent variability introduced by the stand-on meter suggests that a direct measurement of ankle current using a clamp-on current meter will be subject to less variability due to contact conditions and will yield a more meaningful measure of the current flowing in the ankle under realistic conditions of shoe contact with differing ground surfaces.

When discussing the variability in measurement results, the use of a Human Equivalent Antenna (see 5.6) must be considered. These devices eliminate the variability due to the difference in human physique, stance, and footwear. They also allow current measurements to be made without requiring a person to be exposed to potentially hazardous currents and fields.

6.4.2 Contact current

Measurement of contact currents may be accomplished with the clamp-on type current transformer discussed in 6.4.1. Inserting a current measuring device between the hand and the object to be tested is an alternative technique for measuring contact currents. This may take the form of a metallic probe, one end of which is held by the individual while the other end is touched to the object under test. The contact surface area (and resulting surface impedance) between the subject and the object under test is an unknown variable when using this technique. However, such a measurement method will tend to yield a direct measurement of the actual RF currents flowing between the subject's body and the object.

As a means of protecting the subject from excessive current flow, an impedance network may be used to simulate the body impedance during initial measurements. Kanai *et al*. [B152] and Gandhi *et al*. [B88] discuss electrical models that are intended to represent equivalent body impedances in connection with common objects. The use of body impedance equivalent circuits to prevent excessive contact current from flowing between the subject and object under test must be approached with caution because the electric fields present in some objects can couple directly to the subject's hand, thereby producing RF currents in the hand, arm, and body of the subject while only a portion of the contact current flows through the probe being held by its insulated handle.

It should be noted that there is a possibility of producing a spark discharge when making and breaking contact with conducting objects when making contact current measurements. It is difficult to predict such occurrences, and surveyors should be cognizant of this possibility when making such measurements.

6.5 Measurement procedures for internal fields (SAR)

Phantom models of various tissue geometries and gross anatomies of whole animals or humans can be fabricated. They include stratified layers of muscle and fat of various thickness, circular and irregular cylindrical structures consisting of fat, muscle, and bone, and spheres of synthetic brain tissue to simulate various parts of the anatomy. Various recipes for tissue-equivalent material can be found in the literature, e.g., Chou *et al*. [B56] and Hartsgrove *et al*. [B118]. Liquids are poured to fill rigid, outer shells of simulated subcutaneous fat in the shape of a full-size human [B234]. Miniature implantable E-field probes can be easily moved with mechanical scanners in a continuous path throughout these liquid-filled phantoms. This

provides an efficient means for the mapping of local SAR distributions throughout models with complex shapes, such as the extremities of the human body.

6.5.1 SAR measurement with miniature electric-field probes

Miniature isotropic, implantable E-field probes with high impedance feed lines, which have been commercially available for a number of years [B53], are used to measure SAR distributions in phantom models and in living, anesthetized animals [B28], [B233]. (See also 5.7.1.) These probes have much higher sensitivity than thermal probes and are especially suitable for measuring E-fields within simulated or actual biological tissues of moderate to high water content, i.e., brain and muscle. While it is possible to measure SARs of the order of 1 W/kg using sensitive and precise thermal measurements ($(\Delta T)/(\Delta t) \approx 0.1\ ^{\circ}\text{C}/30$ s), it is well within the domain of E-field probes to measure SARs as low as 10 mW/kg [B24]. SAR can be calculated using Equation (24) and the data in Table 6 and Table 7 that show typical dielectric properties for simulated and actual tissues.

$$SAR = \frac{1}{\rho}\omega\varepsilon_0\varepsilon'' E_{int}^2 \text{ W/kg}$$

$$SAR = \frac{\sigma}{\rho}E_{int}^2 \text{ W/kg} \tag{23}$$

Where

ρ is the mass density (kg/m^3),
ε_0 is the permittivity of free space (F/m),
ε'' is the imaginary part of the complex relative permittivity,
ω is the radian frequency ($= 2\pi f$),
σ is the conductivity (S/m),
E_{int} is the rms electric field strength in V/m at the point in the body, with the subscript "int" used to emphasize the fact that the field inside the body is not the same as the external field strength surrounding the exposed object.

Measurements may be made at individual points within a simulated or actual biological subject. Since there are large spatial gradients and standing waves in most biological objects that are exposed in the near or far field, a sufficient number of data points should be obtained to accurately characterize the SAR distribution. At each site, the sum of the outputs of three mutually orthogonal dipoles and the location of the probe must be recorded. The accurate positioning of the sensing probe is essential to perform repeatable measurements; repeatability can usually only be achieved by means of an automated 3-D positioner—not by hand. To reduce the magnitude of the effort of taking data throughout a volume of tissue, data can be taken while the probe is scanned through the volume. Since the E-field probe has a response time of the order of a few milliseconds, continuous line scans of the internal E-fields may be dynamically recorded as the probe is moved along a path (see 6.5.1.1). Extensive data in an object can, thus, be plotted in a relatively short period of time, and the possibility of missing a local peak is reduced [B28].

There are several inherent sources of error associated with the use of implantable E-field probes for SAR measurements. Regardless of the quality of the specific probe used, calibration (in terms of absolute field strength in high water-content biological tissue or tissue simulant) is difficult (see 5.7.1.1). Large gradients in the internal E-fields and imprecise knowledge of the conductivity and mass density of the biological tissue or tissue simulant add additional degrees of uncertainty. Although implantable probes are commercially available, custom-designed probes are frequently developed, evaluated, and calibrated by the developer or user. Therefore, instrument performance limitations, as well as errors introduced during the measurement procedure, should be understood by the user and steps taken to minimize errors introduced by these factors.

Table 6—Electrical conductivity (S/m) of simulated tissues at RF frequencies

Tissue type	Frequency (MHz)			
	10	**100**	**1000**	**2450**
Muscle	0.7[a]	0.9[a]	1.3[a]	2.2[a]
Brain	—	0.47[b]	0.75[a], 1.2[b]	1.2[a]
Fat and bone	—	0.008	0.07[a],0.12[a]	0.18[a]

Formulations:

[a]Polyethylene powder and TX 150 gelling agent used for muscle and brain simulants.
[b]HEC gelling agent without polyethylene powder used for muscle and brain simulants.

NOTE—Fat and bone simulants are solid versions for both formulations.

Table 7—Electrical conductivity (S/m) of biological tissues at RF frequencies

Tissue type	Frequency (MHz)			
	10	**100**	**1000**	**3000**
Muscle	0.645	0.731	1.006	2.237
Bone (gray matter)	0.29	0.56	0.99	2.22
Brain (white matter)	0.16	0.32	0.62	1.51
Fat	0.029	0.037	0.054	0.130
Bone (cancellous)	0.122	0.172	0.364	1.006
Bone (cortical)	0.043	0.064	0.155	0.506

NOTE—Values are from Furse *et al*. [B81] and Gabriel [B82].

Detailed discussions on the evaluation, calibration and use of implantable probes have been published [B28], [B239]. In summary, SAR measurement uncertainties of the order of ± 2 dB are to be expected, even under optimum measurement conditions.

The high sensitivity of the E-field probes make them ideally suited for the measurement of SARs associated with low-power (of the order of 1 W or less) localized sources such as hand-held radio transceivers, e.g., cellular and personal communications equipment.[12] The low-power output make thermal measurements extremely difficult [B21], [B22], [B23]. Increasing the power of such sources by a factor of ten times so that thermal techniques could be used would entail a substantial modification of the device to the point of being nonrepresentative of an actual transceiver. Since the exposure of concern from such low-power localized sources is within about 5 cm of the antenna, accurate positioning of the sensing probe is crucial for performing repeatable measurements. The probe positioning should be performed by machine, e.g., a 3-D positioner, rather than by hand. The phantom used for such measurements may vary from case to case depending on the specific device being evaluated. For cellular phones, for example, the head and upper part of the torso would usually be sufficient [B24], while a 150 MHz two-way radio strapped to the belt with the antenna operated by remote switching would require a full-size human phantom [B77].

[12]Protocols for determining the peak spatial-average SAR induced by specific products, e.g., hand-held radio transceivers used for personal wireless communications, are developed by IEEE Standards Coordinating Committee 34.

The conductivity of the tissue simulant must be correct for the frequency being tested. The mixing of such materials and the measurement of their corresponding electrical properties present substantial challenges in order to achieve accuracy and repeatability. It is not possible to use a single formulation over a wide frequency range, e.g., more than an octave, without running into relatively large departures (± 5%) from published conductivities for biological tissues. To obtain repeatable results (± 3%), it is advisable to restrict the frequency band and to purchase the primary materials from the same supplier. Well-documented mixing procedures should also be adhered to, e.g., accurate weights of the components, temperature of the liquids during mixing, length of the mixing time, rotational speed of the stirring device. Measurement of the dielectric properties of tissue simulants is also difficult to perform accurately. Acceptable results can be obtained using open coaxial line methods [B18], [B237], but the slotted coaxial line method provides more repeatable results for liquid simulants. Moreover, the slotted coaxial line method provides a means to examine the attenuation of the RF wave as it progresses along the line so that the overall precision of the measurement can be assessed more accurately than that for single surface point measurement of the open coaxial line technique.

Accurate SAR measurements can only be made with probes that have been carefully calibrated in the simulant being used to represent biological tissue (see 5.7.1.1). The calibration process, which is tedious and prone to error, requires simultaneous or subsequent measurement of the magnitude of the E-field and the temperature rise at the same location in a canonical model such as a flat or a spherical phantom of appropriate tissue-equivalent material. The calibration in a flat model is usually performed using a relatively high power source coupled to a resonant dipole placed at a specified distance from the phantom [B162]; calibration in a spherical model can be performed under plane wave irradiation conditions or using a dipole.

As pointed out above, the experimental error associated with SAR measurements can be substantial (± 2 dB) because of the multistep nature of the process. The following factors contribute to the overall experimental accuracy that can be expected to be realized: accuracy of the electrical characteristics of the tissue simulant—± 5% (if the measurements are limited to a narrow band of frequencies); accuracy of the temperature rise measurements during probe calibration and errors associated with calibration—± 3%; accuracy of the RF power measurements—± 5%; positioning errors the nonisotropic response of the probe—± 6%.

NOTE—The overall uncertainty in the measurement is not the sum of the above measurement errors. The overall uncertainty is found by calculating the individual uncertainties, using a root sum square for the system uncertainties and then using a confidence interval of 95% to obtain a multiplier of this sum to obtain the expanded uncertainty—the number usually quoted. Methods for evaluating and expressing uncertainty in measurements can be found in ANSI/NCSL Z540-2-1997 [B9], NIS [B199], and Okoniewski and Stuchly [B200].

Even for a narrow frequency band, the achievement of a total relative error of only ± 2 dB requires specialized equipment for measuring the dielectric properties of the tissue simulant, accurately calibrated RF power meters, temperature probes, and well-trained personnel to measure rises in temperature of the order of 0.10°C with a 0.03°C measurement error. The procedure is time-consuming, and the calibration of a single E-field probe at a single frequency in two different media, e.g., brain and muscle tissue simulant, can take as long as two working days.

6.5.1.1 Automated SAR scanners

The measurement of three-dimensional SAR distributions within a phantom involves measurements at hundreds of points. At higher frequencies, especially with near-field exposures from small localized sources that produce rapid spatial variations in the SAR distribution, the locations of the measurement points with respect to the phantom must be determined precisely. High precision is also necessary to accurately measure the spatial peak SAR. Automated scanning systems allow such measurements to be performed routinely. In order to move a small probe along unrestricted continuous paths, such systems are generally restricted to shell phantoms filled with liquids that simulate human tissue.

Although automated scanners based on temperature probes are possible, the maximum measurement speed would be unacceptably slow. Because of this and the low sensitivity of temperature probes, scanning systems that have been implemented are based on miniature E-field probes. Such systems range from one-dimensional positioners [B59] to three-axis scanners [B235] and, most recently, six-axis robots [B24].

A system designed for testing compliance of hand-held radio transceivers, e.g., cellular phones, with peak spatial-average SAR safety criteria, is described in Schmid *et al*. [B224]. It incorporates a high precision robot (working range greater than 0.9 m and a position repeatability better than ± 0.02 mm), isotropic E-field probes with diode-loaded dipole sensors, an optical proximity sensor for automated positioning of the probe with respect to the phantom surface (within ± 0.2 mm), and sophisticated software for data processing and measurement control. The usable frequency range extends from 10 MHz to at least 3 GHz, the sensitivity is reported to be better than 1 mW/kg, and the dynamic range extends to 100 W/kg. Complex measurements, such as the spatial peak SAR value when starting with an unknown field distribution in the body can be completed within 15 minutes.

6.5.2 Temperature probes for SAR measurement.

The use of a nonperturbing temperature probe for SAR measurements is very simple in principle, but many pitfalls exist to complicate the practical situation if precise data are required. The objective is to measure the time rate of irradiation-induced temperature rise ($\Delta T/\Delta t$) at a specific location in tissue or phantom material. The SAR, which is proportional to ($\Delta T/\Delta t$), can then be determined. When the temperature does not rise linearly during constant irradiation of the tissue or tissue-equivalent material under test, other factors such as heat loss or heat gain by thermal conduction, convection, etc., are important. Therefore, the simplest procedure is to produce a brief and relatively small ΔT (no more than a few degrees Celsius in 30 s) at the location of the temperature probe.

To obtain SAR, the probe indication or analog output is usually plotted or automatically recorded before and during irradiation, and the irradiation-induced rate of temperature rise is either graphically determined or found through the use of a slope-determining algorithm. A graphical record of $\Delta T/\Delta t$, as well as a simultaneously recorded plot of the RF power (to precisely determine when the power is turned off and on with respect to the temperature rise) is helpful in verifying the linearity of the slope. SAR is calculated from the initial linear slope of $\Delta T/\Delta t$ from

$$SAR = \frac{\Delta T \times c}{\Delta t} \tag{24}$$

Where c is the tissue (or phantom material) specific heat capacity, in J/kg °C. Typical values for specific heat capacity are shown in Table 8.

There are several sources of error when using temperature probes for SAR measurements. First, it is difficult to obtain repeatable results at a location of a large spatial SAR gradient. Small changes in probe location can cause large SAR changes in such situations, and the linear portion of the slope of $\Delta T/\Delta t$ is rather brief (with respect to the initiation of irradiation). This is due to the presence of high-thermal gradients and the resulting thermodynamic effects that cause measurement degradation. For these reasons, it is desirable to determine locations in the subject where maximum values of SAR exist. Data should be taken at and on either side of the maxima. Second, regions of relatively high SAR (>20 W/kg) should be scrutinized closely to ensure that the proper value is actually obtained, because such regions often exhibit high-thermal conduction losses, as well as high SAR. In high SAR regions, it is appropriate to halve the irradiation time and ensure that ΔT is also reduced by one-half; if it is not, thermodynamic effects, such as those associated with thermal conduction, are present. It is also important to note that dielectric constants and conductivities will generally change with temperature, which of course will alter the measured SAR. This would be relevant, say, if the measurements were being made inside an animal carcass that was allowed to equilibrate to room temperature to obtain $(\Delta T)/(\Delta t) = 0$ in order to null out the spatial thermal gradients.

Table 8—Specific heat capacity and mass density of tissue-equivalent (phantom) materials and actual biological tissues*

Tissue	Heat capacity (kJ/kg °C)	Mass density ($x10^3$) (kg/m^3)
Muscle simulant[a]	3.7	1.0
Muscle simulant[b]	3.6	1.1
Brain simulant[a]	3.4	0.98
Adipose tissue (fat) simulant[b, c]	1.1	1.4
Muscle *in vitro*	3.5	1.1
Brain *in vitro*	3.5	1.1
Adipose tissue *in vitro*	1.2–1.6	1.05
Bone	1.25–3.0	1.25–1.8

[a]Data for tissue formulated for use at 2450 MHz.
[b]Data for tissue formulated for use at 27 MHz.
[c]Simulated fat material has dielectric properties that are almost identical to living bone.
NOTE—Data for this table was taken from Leonard *et al*. [B167].

Significant errors can occur when SAR is measured, using temperature probes, at a single point in an object with one or more "hot spots" near, but not coincident with the probe tip. The temperature, as measured by the probe, will behave as follows: The temperature may not rise immediately after the RF irradiation of the test object, but after several seconds, the temperature, as monitored by the probe, begins to rise more quickly as heat is conducted from a nearby hot spot. When the irradiation ceases, the temperature continues to rise as heat is conducted away from the hot spots to cooler regions where the probe is located. Usually heat is diffused away from the measurement point as shown in Figure 14. The rate of temperature rise seen by the probe (apparent slope) could be falsely interpreted as the local SAR at the location of the probe tip, which is smaller than the initial slope. A third source of error arises from the dielectric heating of certain high-resistance leads of the temperature probe as they exit the object being irradiated. When the E-field is parallel to the leads, significant heating of the leads at the point where they enter the probe could result in an artificially exaggerated surface SAR. It is, therefore, better to obtain the SAR that exists at the surface of an object with the sensor tip of an embedded probe located at the measurement point and the leads exiting the object at a location remote from the sensor. There are obviously other sources of error in measurements of SAR using these techniques, but they can be minimized by a thorough knowledge of the capabilities and limitations of the temperature probe being used and by careful application of scientific methods [B42], [B125].

An additional consideration that warrants attention is the multiple measurements of SAR in a given preparation or model. In large models, for example, SAR is needed in many locations, but often there are not enough nonperturbing probes available to obtain all the data simultaneously during a single irradiation If one or only a few probes are used to map SAR in a large volume, ideally the pre-irradiation value of $\Delta T/\Delta t$ would be zero (no "ambient" drift of the phantom's temperature) for subsequent irradiation. However, after the first exposure, it is common to observe an exponential post-irradiation cooling curve that lasts for many minutes or hours if high values of ΔT had occurred during prior RF irradiation (more than several degrees

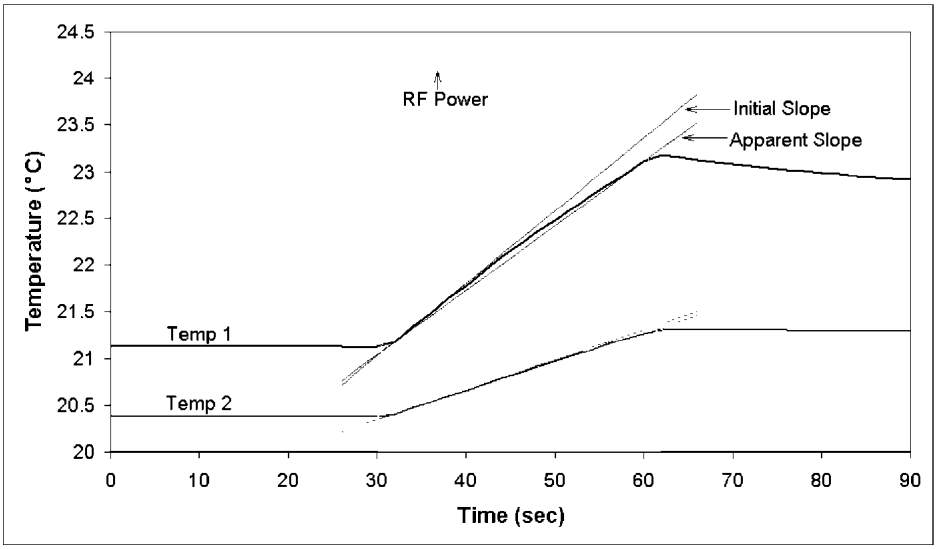

Figure 14—Typical thermal dosimetry data: temperature vs. time—before, after, and during irradiation

Celsius). For reasons of practicality and economy, it is important to obtain as much dosimetric data as possible during each day of laboratory experimentation. Therefore, a compromise should be made that provides good SAR data and also conserves time. A useful rule of thumb in deciding when to start another irradiation is to wait until the slope of the cooling curve is relatively constant (about 5% of the prior RF-induced rate of temperature rise over the period to be used for the next irradiation), and the decrease in temperature before irradiation is relatively small compared with the expected irradiation-induced $\Delta T/\Delta t$. Repeated experiments using consistent techniques are essential for obtaining accurate results in SAR studies utilizing temperature probes. Finally, after several RF irradiations of the same object, its temperature may have increased above acceptable limits, and the phantom or biological material may degrade.

The majority of SAR measurements are made using temperature probes. However, many researchers are not fully aware of the many factors that degrade accuracy of these measurements. For example, thermodynamic factors will always limit the accuracy and precision of SAR measurements, as will any uncertainty in the value of the heat capacity of the actual or simulated tissue being evaluated. The heat capacity is often mistakenly cited as that of water (about 15% higher than that of most high-water content tissue), which, even under optimal usage conditions, leads to uncertainties of at least ± 1–2 dB in the local SAR distribution in an object when measured by sampling the tissue volume with a temperature probe.

When using thermometers to measure SAR in electromagnetic fields, one must be aware of the possibility of RF interference in the thermometer's sensor, leads, or electronics. Several methods can be used to determine the magnitude of the interference. One method is to note changes at the instant that the RF power is switched on and off. If large, immediate changes are found, the probes should only be used to measure temperature prior to and just after RF exposure. Artifacts may also occur due to the interaction of the RF field with the electrical leads attached to the temperature-sensing element of the probe. This interaction can excite a thermally induced voltage at the junction of two dissimilar materials (thermoelectric effect), including high resistance (carbon-loaded Teflon) leads joined to metallic wires. Since this phenomenon is due to the heating of a junction, shielding of these areas should be used to minimize this source of measurement error. Metal foil or RF absorber can be used to shield these junctions. Details of these problems and additional solutions may be found in Crawford *et al*. [B62].

6.5.3 Calorimetric determination of whole-body-average SAR

Average whole body SAR may be measured using calorimetric methods. In the past, such methods have been used predominantly with small animals or animal models [B3], [B34], [B65], [B204]; recently, however, calorimetric twin-well methods have been successfully used to measure SAR in a full-size human model [B205]. The heart of the measurement system is the calorimeter device itself, and gradient-layer devices are commonly used. Gradient-layer calorimeters have a convenient voltage output signal that is proportional to the rate of heat energy flowing out of the device (positive voltage) or the rate of heat energy flowing inward (negative voltage). The signal generally has very low noise, and the sensitivity of a typical device is about 1.3 J/(mV-s).

In a laboratory setting, calorimetric SAR measurement begins with the thermal equilibration of the test object, usually a realistic animal model or a scaled human model. It is assumed that the laboratory temperature is ostensibly constant and is the same as that of the thermally stabilized test object and calorimeter. The test object is then irradiated for a measured period of time after which it is immediately placed inside the calorimeter. The calorimeter output voltage is then periodically monitored until all of the irradiation-induced heat energy has flowed from the object, and it is again at its initial temperature. This process may take hours or days depending on the size and mass of the object. By this time, the calorimeter voltage is zero, and the area under the curve described by the time-course of the calorimeter voltage is proportional to the energy deposited in the object. That area is then multiplied by the calibration constant of the device to obtain the total energy deposition in joules. Division of the energy deposition by the irradiation time in seconds yields the rate of energy deposition (power) in Watts; average SAR is obtained by dividing the resulting power by the mass (kilogram) of the test object.

If two matched calorimeters are used in conjunction with two identical test objects, these procedures can be used in the absence of strict temperature control, such as in an outdoor environment. However, twice the physical effort is required for outdoor SAR measurements, and all of the apparatus should be given some sort of protection from the effects of direct sunlight, rain, etc.

Although the calorimetric determination of the energy stored in the model once inside the calorimeter is quite accurate per se, the overall system accuracy in terms of SAR is limited by how closely the test object models the actual object and by the amount of irradiation-induced heat that escapes from the object without being measured. This method, moreover, requires sufficient time for the thermal equilibration processes and requires sufficient energy deposition in the test object to produce a calorimeter output signal that is enough above baseline to be measurable. However, the Dewar-flask method of calorimetry is a relatively simple, straightforward way of determining the whole-body-average SAR of small-bodied animals [B208]. The calorimetric technique of determining a whole-body-average temperature requires that the cadaver be immersed in a Dewar-flask containing a medium, such as water, at a known temperature; then the temperature of the cadaver, following irradiation, can be determined by noting the final temperature of the cadaver/medium mixture.

6.6 Estimation of SAR from external exposure-field measurement data

6.6.1 General

In practice, the fundamental problem confronted in assessing human exposure to nonuniform RF fields is selecting an appropriate protocol that will yield meaningful measures that can be related to whole-body-averaged and local SAR. A number of studies have been published that describe the measurement relationships between external exposure fields around an active, near-field radiator, and the resulting measured internal SAR in nearby simulated biological objects [B236]. Other studies report experimental data on the local internal SAR distribution relative to the spatial location of active radiators [B44], [B59], [B236]. Mathematical models useful for predicting internal SAR distributions in humans exposed to non-plane-wave

fields from various RF emitters have also been published [B44]. Similar data on the SAR induced by passive re-radiators is not generally available.

Contemporary MPEs are based on whole-body-averaged SAR thresholds for biological effects in RF-irradiated animals. The extrapolation of plane-wave exposures to whole-body-averaged SAR is supported by the many dosimetric studies, both experimental and mathematical, reported in the literature [B71]. For human exposure to plane-wave fields, the MPEs are often the maximum plane wave exposure that ensures that a given whole-body SAR will not be exceeded. The significance of exposure in close proximity to a near-field source, however, is difficult to estimate, especially when only external field strength data (obtained from radiation hazard survey meters) is available. (When both the individual electric and magnetic field vector components are known the computational techniques described in 7.5 may be used.)

The relationship between the spatial maximum field strength and the SAR is very complex and varies considerably as the orientation and spatial distribution of the fields change with respect to the exposed object. Consequently, induced SAR in an object or a person near a radiator or passive re-radiator is extremely difficult to estimate from measured external field strengths. These measured data can only provide the basis for crude estimates of the SAR spatial distribution maxima useful for establishing temporary personnel protection guides corresponding to a measured exposure situation (see also 6.6.2.4).

6.6.2 Enhanced or reduced SAR in personnel in close proximity to passive re-radiators or active radiators

Absorption in personnel exposed to reactive near fields may be either enhanced or reduced when compared with exposure in plane-wave fields. The reactive near-field region, for both active and passive radiators, i.e., where the reactive fields dominate over radiating fields, is limited to distances much smaller than a wavelength. Most MPEs are expressed in terms of those values of E^2, H^2, or S for plane-wave exposures that ensure that the *whole-body-averaged* SAR is below some nominal value. In many cases, where or how these parameters are to be measured, e.g., spatial averaging, is not specified. In some cases, a localized spatially averaged peak SAR may be specified. This local SAR defines the maximum SAR that is allowed to exist in any small amount of tissue, e.g., 1 g or 10 g. In many cases, the shape of the volume is also specified, e.g., any 1 g of tissue in the shape of a cube. During RF hazard surveys, the exposure field strengths are measured, not the internal SAR. When a surveyor measures the field strength in a region that may be occupied by a person, and the field strength exceeds the applicable MPE at one or more points in that region, noncompliance with the MPE is implied. However, since exposure to nonuniform fields produces a nonuniform SAR distribution throughout the object occupying the region, the maximum induced SAR may or may not exceed the peak or the whole-body-averaged SAR limits of the MPE depending on whether an "enhanced" or "reduced" absorption situation exists.[13]

Although the degree of induced SAR in a person exposed to a near-field source is difficult to relate to the maximum value of the local field strength (E or H), it can be normalized with respect to a standard plane-wave-exposure situation. The term normalized plane-wave absorption is defined as the SAR induced by a plane wave whose field strength is equal to the maximum field strength (E or H) measured in the near-field exposure situation in question at the site that a person would occupy. The maxima of the SAR spatial distribution induced by this normalized plane wave can then serve as a reference level for evaluation of the near-field exposure. If the corresponding SAR maxima induced in a person's body by the near-field source exceed the normalized plane-wave SAR, an enhanced absorption case exists; otherwise, a reduced absorption case exists.

The interpretation of field strength measurements near a passive re-radiator or active radiator should be performed carefully to determine if an enhanced absorption case actually exists. If the guidelines in 6.3.6 are followed during the measurement procedure and a typical, modern isotropic hazard survey meter is placed

[13]Many contemporary exposure guidelines and standards, e.g., [B132], allow the MPEs for E^2, H^2, and S to be exceeded provided the whole-body-averaged and spatial peak SARs are not.

near a passive re-radiator or an active radiator, the meter should accurately measure the field strengths. In many cases, the corresponding measured values may exceed the plane-wave limits of the MPE. However, the maximum RF energy that is actually absorbed in any part of a person's body and, hence, the maximum peak SAR, might not exceed the corresponding local SAR provisions of the same MPE. Conversely, some situations exist where the local SAR in a part of the body may indeed exceed the limits of the MPE [B87]. These two extreme cases (enhanced or reduced absorption) and their physical basis are examined in 6.6.2.1 and 6.6.2.2.

6.6.2.1 The reduced absorption case

In any situations involving the exposure of a person to near fields from a passive re-radiator or active radiator, the spatial maximum (local) SAR is relatively "low" with respect to the maximum local SAR that would be induced by a normalized plane-wave exposure, as discussed above. In virtually all cases, the whole-body-averaged SAR induced in a person under near-field exposure conditions is much less than the whole-body-averaged SAR associated with plane-wave exposure [B45], [B236]. Very high field strengths can be measured (with respect to the MPE) when a survey meter is placed close to a resonant (at the frequency of irradiation) passive re-radiator. Also, high field strengths may occur in the near field of active radiators. The field strengths that are indicated by a survey meter, in close proximity to a passive re-radiator or active radiator, may be much greater than the ambient field strengths existing only a fraction of a meter away, i.e., large field strength gradients exist.

Thorough experimental and theoretical studies of near-field exposure from active radiators indicate that in many cases reduced absorption results. Few such studies, however, have been carried out for passive re-radiators (6.6.2.3), but an example of the reduced potentially hazardous situation for a passive re-radiator easily can be envisioned. For example, high field strengths (relative to the ambient field strength) are generally measured in the immediate vicinity of small, resonant, passive re-radiators. These passive re-radiators include automobile steering wheels [B2], [B164] and/or short linear metal objects. If a person is near, but not touching the resonant object, little energy coupling exists between the re-radiator and the person. It would be expected, but has not been confirmed, that the SAR induced in the person's body, is small relative to the local SAR limits of most MPEs.

6.6.2.2 Enhanced absorption

Enhanced absorption is defined as the case where the spatial maximum SAR that is induced in a person's body by a reactive near-field source is not significantly less than the spatial-maximum SAR induced by a normalized plane-wave field. An example of the enhanced absorption involves personnel close to, or in contact with, an active radiator, or a large, passive re-radiator, e.g., a large linear object equal in length to a multiple number of half wavelengths at the frequency of irradiation. In this case, high SARs, relative to normalized plane-wave SAR, can be induced in certain areas of the person's body. This has been demonstrated for the case of a full-size model of a person in very close proximity to, or in contact with a re-radiator [B203]. This scenario can, perhaps, be illustrated by the situation of an individual standing near a low-frequency induction heater. While induction heaters primarily create magnetic fields for heating conducting materials such as metals, high electric fields can be produced by the electrical cables that connect the RF generator to the induction coils. These electric fields, when measured in the absence of the person, may imply relatively low induced body currents with relatively low peak SARs in the ankles. However, with the person present, substantial coupling between the body and the electric field source may exist, leading to substantially greater induced body currents, and local SARs, than would have been predicted on the basis of the nonperturbed electric fields. This is a case in which capacitive coupling between the individual and the source leads to considerably greater electric field intensity on the body surface with a concomitant increase in body current.

6.6.2.3 Studies of induced SAR by passive near-field radiators

Very little research has been performed to quantify the induced SAR associated with exposure to the near field of a passive re-radiator. A preliminary series of experiments has, however, indicated that both reduced and enhanced absorption situations are encountered, depending on the spatial relationship of the re-radiator to the model [B203].

6.6.2.4 Studies of induced SAR from nearby active radiators

Exposure of personnel to fields from nearby active radiators produces complex internal SAR distributions [B106]. Subclause 6.6.3 briefly describes several experimental and mathematical studies of a few common exposure situations and the resulting induced SAR distribution in nearby personnel.

6.6.3 Using near-field survey data to assess potentially excessive SAR in exposed personnel

6.6.3.1 Field measurements

MPEs of contemporary standards and guidelines are expressed in terms of E^2, H^2, and S are based on whole-body-averaged SARs, below which adverse effects are not expected to occur. For most exposure situations, however, it is necessary to estimate the potential RF hazard that may exist by measuring the incident fields, i.e., the induced SAR in exposed personnel cannot be measured directly; only the external exposure-field parameters can. For uniform plane-wave, whole-body exposure, however, the whole-body-averaged SAR can be determined with reasonable accuracy using exposure field data since most MPEs are based on mathematical models and calculations of the whole-body SAR associated with exposure to plane-wave fields.

For specific non-plane-wave RF exposure environments, coarse, order-of-magnitude estimates can be made of the regional or local SAR in various areas of an exposed person's body for the far-field case and for certain near-field exposure situations. In certain instances, it may be possible to obtain these estimates, without actually performing invasive SAR measurements, e.g., thorough measurements of the exposure field-strengths in the particular RF environment in question could be compared with these values with published SAR data. (References to the results of several comprehensive research studies of local SAR for various exposure conditions can be found in 6.6.1.) These measurements and comparisons will allow rough estimates to be made of the expected local SAR distribution in personnel exposed to fields similar to those of the RF environment surveyed. Under certain near-field exposure conditions, field strength data do not provide an adequate means for assessing potential RF hazards to personnel. When an RF radiator or re-radiator illuminates a small portion of a person's body, and the spatial distribution of the fields is highly nonuniform over the volume in question, measurement of the local SAR distribution may be the most appropriate means for hazard assessment [B21], [B219], [B220]. Therefore, under these circumstances, measurements of E and/or H may not be sufficient. This is especially true when the distance from the RF source to the exposed object is less than approximately three probe antenna lengths (see 6.3.6.4).

6.6.3.2 Induced current measurements

Noninvasive techniques have been developed to estimate SAR from the measurement of induced body current. These measurements are made with devices that are located very close to or in contact with the body. For example, in exposure situations involving RF fields at frequencies below a few hundred megahertz, the measurement of the total RF current flowing through the body, to ground, can be used to estimate the local SAR due to near-field coupling in various anatomical regions. This noninvasive technique is described in Annex C.2. Several techniques for the measurement of RF currents flowing in human extremities have been proposed. One technique, applicable over a wide range of frequencies, consists of a nonmetallic equivalent of a clamp-on ammeter. This technique was designed and studied via mathematical modeling, and its feasibility has been demonstrated experimentally [B103], [B111], [B113].

7. Theoretical calculations of SAR

7.1 General

Experimental methods for determining SAR are discussed in 6.5. The derivation of the term "SAR" is discussed in Chou *et al*. [B55] and NCRP [B195]. Both "dose rate" and "density of absorbed power" (sometimes called absorbed power density) are equivalent to SAR. Each term refers to the amount of energy absorbed per unit time, in a unit mass.

For steady-state sinusoidal fields, SAR is given by

$$SAR = \frac{1}{\rho}\omega\varepsilon_0\varepsilon'' E_{int}^2 \text{ W/kg}$$

$$SAR = \frac{\sigma}{\rho}E_{int}^2 \text{ W/kg} \tag{25}$$

Where

- ρ is the mass density of the body (kg/m^3),
- ε_0 is the permittivity of free space (F/m),
- ε'' is the imaginary part of the complex relative permittivity,
- ω is the angular frequency—($\omega = 2\pi f$ radians),
- σ is the conductivity (S/m),
- E_{int} is the rms electric field strength in V/m at a point in the body. (The subscript "int" used to emphasize the fact that the field inside the body is not the same as the external field strength surrounding an exposed object.)

There are three principal ways in which energy is transferred from an electric field to an absorbing object. One is the transfer of kinetic energy to electrons that are not tightly bound to any one atom and, hence, are called free electrons. The dc conductivity of a material is associated with the free electrons. The other two forms of energy transfer are friction associated with the alignment of electric dipoles with E_{int} and friction associated with ionic and molecular vibrational and rotational motion associated with E_{int}. Since ε'' represents the loss of energy in the E-field, a substance is considered "lossy" if ε'' is relatively large compared with ε'; thus, a lossy substance that is exposed to RF energy absorbs a relatively greater amount of electromagnetic energy. In most cases, the more water or other "polar" molecules a substance contains, per unit volume, the more lossy it is; and the drier a substance is, the less lossy. For example, a dry piece of paper placed in a microwave oven will not get hot; but a wet piece of paper will heat until the paper is dry, and then will heat no further. Fat has a lower water content than muscle tissue, so fat is less absorbing. It is important to remember that these relative statements are true only if E_{int} within the various materials is the same in each case. However, as explained below, the permittivity of the material also affects the coupling of external fields, thus influencing the magnitude of E_{int}.

The dielectric properties of materials are usually listed as dielectric constant and either loss tangent or conductivity. However, use of the term dielectric constant for material exhibiting the frequency-dependence of a material containing water is not accurate since the dielectric properties of water and biomaterials are not "constant" with frequency. The complex permittivity is defined as

$$\varepsilon = \varepsilon_0(\varepsilon' - j\varepsilon'') \tag{26}$$

Where $\varepsilon_0 = 8.854 \times 10^{-12}$ farads per meter and is the permittivity of free space, ε' is the dielectric constant or real part of the complex relative permittivity, and ε'' is the imaginary part of the complex relative permittivity. The loss tangent is defined as

$$\tan\delta = \frac{\varepsilon''}{\varepsilon'} \tag{27}$$

which is a measure of how "lossy" or energy-absorbing a material is. The conductivity σ is related to ε'' by

$$\varepsilon'' = \sigma/(\omega\varepsilon_0) \tag{28}$$

It is very important to note that the SAR is not a measure of temperature rise; it is a measure only of the rate of energy absorption per unit mass that depends upon the conductivity of the material [B131]. The temperature rise is a function of the SAR, but it is also a function of the thermal characteristics of the absorber, i.e., the size, shape, and thermal conductivity to the surroundings. The term "hot spots" is often used to refer to areas of locally high SAR, but this term is not meant to describe areas of localized high temperature since biological systems have various thermo-regulatory mechanisms that can automatically adjust the temperature in various regions of the system. More work needs to be done in the calculation of temperature distribution in living biological systems.

7.2 Factors affecting the internal fields

At each location inside a body, E and H should also satisfy Maxwell's equations. In addition, at any boundary between different dielectric media (such as bone and muscle tissue), E and H should satisfy certain boundary conditions; that is, at the boundary, the fields in the one medium should be specifically related to the fields in the other medium. The boundary conditions are usually expressed in terms of two vector field components; one component parallel to the boundary, and one normal to the boundary. The boundary conditions for the electric field in dielectrics are

$$\varepsilon_1 E_{1n} = \varepsilon_2 E_{2n} \tag{29}$$

$$E_{1p} = E_{2p} \tag{30}$$

Where subscript 1 represents quantities in one medium, and subscript 2 represents quantities in the other medium. Also, E_n is the component of the electric field normal to the boundary, and E_p is the component parallel to the boundary. Similar relations hold for the magnetic fields.

$$\mu_1 H_{1n} = \mu_2 H_{2n} \tag{31}$$

$$H_{1p} = H_{2p} \tag{32}$$

Where μ is the permeability of the medium. For nonmagnetic materials, $\mu_1 = \mu_2 = \mu_0$ and both components of H are continuous across a boundary. (It should be noted that the magnetic permeability of biological tissue is equal to that of free space.) The boundary conditions are important because they allow us to make significant qualitative statements about the internal fields.

7.3 Low-frequency internal fields

At very low frequencies, where the wavelength is very long compared with that of a biological system, most exposures are in the near field [B170]. At these frequencies the electric and magnetic near fields are approximately independent of each other and, therefore, are similar to static fields. Such fields are called

quasi-static fields. The characteristics of quasi-static electric fields can be demonstrated by considering the following example. Suppose a dielectric object is placed in a quasi-static field, E_{inc}, as shown in Figure 15. E_{inc} will cause the dielectric to polarize and produce a secondary field E_S both inside and outside the dielectric. The combination of the secondary and the incident fields inside the dielectric is called the internal field. At the boundary, the sum of the incident and secondary fields should satisfy the boundary conditions with the internal field. Often, the secondary field is less important in a qualitative interpretation; in which case, we can talk about the boundary conditions in terms of the incident field and the internal field. Near the ends of the object, the incident field in Figure 15(a) is primarily normal to the boundary. Therefore, the boundary conditions require that the internal field be very weak at the ends because it will be almost equal to $(\varepsilon_0/\varepsilon_1)(E_{inc} + E_S)$ and $\varepsilon_1 > \varepsilon_0$. On the other hand, at the sides of the object, the incident field is primarily parallel to the boundary, and the internal field will be almost equal to $E_{inc} + E_S$. Since is essentially parallel to the boundary over a much greater region than the region where it is mostly normal to the boundary, the internal field will be determined more by the boundary conditions on the parallel field components; hence, we say that the electric-field coupling in Figure 15(a) is strong. The electric-field coupling is weaker in Figure 15(b), because E_{inc} is mostly parallel to the boundary over a much smaller percentage of the object than in Figure 15(a). Thus, in Figure 15(a), where E_{inc} is aligned with the long axis of the object, strong electric fields are coupled into the object; if the object is lossy, it will absorb a proportionally large amount of energy. Conversely, in Figure 15(b), where E_{inc} is normal to the long axis of the object, weaker electric fields are coupled into the object, and it will, thus, absorb a proportionally smaller amount of energy.

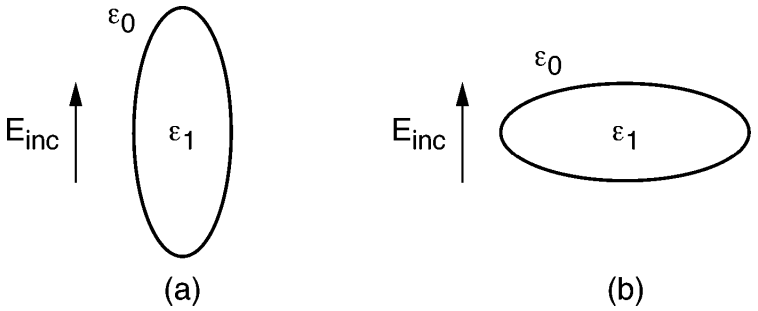

Figure 15—Dielectric object placed in a quasi-static electric field, E_{inc}

In a lossy object at low frequencies, the magnetic-field coupling can be thought of in terms of induced eddy currents that circulate in closed paths around the incident magnetic-field vector. The circulating currents represent energy transfer from the incident magnetic field to the object. In some sense, the magnitude of the energy transferred is proportional to the cross-sectional area intercepting H_{inc}. In Figure 16, the magnitude of the energy transferred is greater in (b) than in (a) because the cross-sectional area perpendicular to H_{inc} is greater in (b) than in (a). Consequently, the magnetic field coupling is stronger in Figure 16(b) than in Figure 16(a). Thus, for low frequencies, we can explain the relative differences in SAR for E-, H-, and K-polarizations, as shown by the dosimetric data. (The K vector defines the direction of propagation of a plane wave.) For E-polarization (where E is parallel to the long axis of the object), both E and H coupling are strong. For H-polarization (where H is parallel to the long axis of the object), both E and H coupling are weak. For K-polarization (where the wave propagation vector, k, is parallel to the long axis of the object), E coupling is weak, but H coupling is strong. Thus, for frequencies below resonance, the SAR is greatest for E-polarization, least for H-polarization, and intermediate for K-polarization.

Another important characteristic is related to interdependence of the fields in different parts of an absorber. At low frequencies (long wavelength with respect to the irradiated object), the fields in one part of a body are strongly affected by the other parts of the body, and field concentrations can be produced by combinations of size, shape, and orientation of the body in the incident field. At intermediate frequencies, the fields inside can be thought of as propagating waves that are partially transmitted and partially reflected at the boundaries, with constructive and destructive interference causing significant variations in field strength inside the body. Also, at these intermediate frequencies, E and H cannot exist separately and are strongly coupled together.

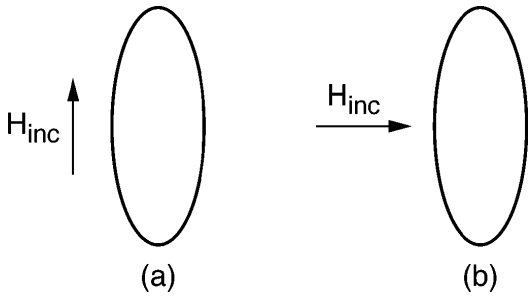

Figure 16—Prolate spheroid placed in a quasi-static magnetic field, H_{inc}

At very high frequencies, however, the internal fields in different parts of an absorber can be essentially uncoupled, as explained below.

7.4 High-frequency behavior

At very high frequencies, where the wavelength of the incident wave is very small compared with the size of the object, geometrical optics concepts apply. That is, the EM waves can be thought of as rays. In this case, for lossy objects, the effects are mostly surface effects because the depth of penetration decreases rapidly as frequency increases. This is the so-called skin effect. The penetration depth depends on both conductivity and frequency. At 10 GHz, for example, the skin depth in tissue is less than 5 mm. At these very high frequencies, the fields in one part of the body are affected only very slightly by other parts of the body.

7.5 Methods of calculation

In principle, the internal fields in any object irradiated by EM fields can be calculated by solving Maxwell's equations. In practice, this is very difficult and, until recently, could be done only for a few very special cases (idealized models), such as spheres or infinitely long cylinders. Because of the mathematical complexities involved in calculating SAR, a combination of techniques has been used to obtain SAR for various models as functions of frequency. Each of these techniques provides information over a limited range of parameters. Combining the information thus obtained, gives a reasonably good description of SAR as a function of frequency over a wide range of frequencies for a number of useful models.

Up to frequencies of about 30 MHz, a method called the long-wavelength approximation has been used with spheroidal models of human-sized objects. The extended-boundary-condition method (EBCM) has been used to make calculations for spheroidal models of humans up to approximately resonance (80 MHz). The iterative extended-boundary-condition method (IEBCM), an extension of the EBCM, has been used for calculation up to 400 MHz for spheroidal models. The classical solution of Maxwell's equations for cylindrical models (for human-sized objects or limbs) has been used to obtain useful average SAR data for E-polarization from about 500 MHz–7 GHz, and for H-polarization from about 100 MHz to about 7 GHz. An approximation based on geometrical optics is used to obtain useful SAR information above approximately 7 GHz. The moment-method solution of a Green's-function integral equation for the electric field is used up to about 400 MHz (for human-sized models). For K-polarization, a technique called the surface-integral-equation technique (SIE) is used up to about 400 MHz with a model consisting of a truncated cylinder capped on each end by hemispheres.

Numerical simulation techniques are now available for determining SAR and current distributions in highly sophisticated millimeter-resolution anatomically based models exposed to a wide variety of far-field and near-field sources [B84], [B90]. From a wide array of methods, including the moment method (MM) [B51], [B114], [B171], [B232], finite element method (FEM) [B54], [B178], [B191], [B267], finite-element time-domain method (FETD) [B38], [B52], generalized multipole technique (GMT) [B109] [B110], [B168], volume-surface integral equation method (VSIE) [B225] admittance [B10] and impedance [B94] methods, the finite-difference time-domain (FDTD) method [B50], [B97], [B84], [B169], [B227] has become the

most widely used method of choice for bioelectromagnetic applications in the range of a few megahertz to several gigahertz. An extension of the FDTD method, the frequency-dependent finite-difference time-domain method ($(FD)^2TD$) [B40], [B79], [B96], [B144], [B159], [B166], [B177], [B241], [B242], [B244], enables broad-band bioelectromagnetic simulations by including the effect of the frequency dispersion of the tissues. This method has been used to calculate SAR and current distributions in the body from ultra-short plane wave pulses with bandwidths of the order of 1 GHz [B79], [B96], [B242]. Several of these techniques are briefly described below.

7.5.1 Long-wavelength approximation

In the frequency range where the length of the irradiated object is approximately two-tenths or less of a free-space wavelength, SAR calculations are made by an approximation based on the first-order term of a power series expansion in γ of the electric and magnetic fields, where γ is the free-space propagation coefficient [B70]. This is called a perturbation method because it is based on the fact that the resulting fields are only a small change from the static fields. Equations for SAR have been derived for homogeneous spheroidal and ellipsoidal models of humans and animals [B142], [B182].

7.5.2 Extended-boundary-condition method (EBCM)

The EBCM is a matrix formulation based on an integral equation and expansion of the EM-fields in spherical harmonics. This method was developed by Waterman [B261] and has subsequently been used to calculate the SAR in prolate spheroidal models of humans and animals [B25]. The EBCM is exact within the limits of numerical computation capabilities, but numerical problems presently limit the method to frequencies below about 80 MHz for prolate spheroidal models of humans. In SAR calculations for prolate spheroidal models of humans, the long-wavelength approximation and the EBCM give identical results up to about 30 MHz, where the long-wavelength approximation begins to become inaccurate.

7.5.3 Iterative extended-boundary-condition method (IEBCM)

The EBCM has been extended [B163] to a technique called IEBCM that is capable of SAR calculations in prolate spheroidal models of humans up to at least 400 MHz. The IEBCM is different from the EBCM in two main respects. It makes use of more than one spheroidal harmonic expansion, which allows better convergence for elongated bodies at higher frequencies, and it uses iteration, beginning with an approximate solution, to converge to the solution. These two features of the IEBCM have significantly extended the range of calculations over that of the EBCM.

7.5.4 The cylindrical approximation

The SAR calculated for an appropriately long section of an infinitely long cylinder is a good approximation to the SAR of spheroids in the frequency range where the wavelength is very short compared with the length of the spheroid. The lowest frequency at which the approximation is useful depends both on the length of the spheroid and on the ratio of the major axis to the minor axis. For human-sized spheroids, the lower frequency limit occurs for E-polarization when the wavelength is about four-tenths of the length of the spheroid [B183].

7.5.5 Moment-method solution

A moment-method solution of a Green's-function integral equation for the electric field has been used to calculate the internal electric field in block models, so-called because the mathematical cells of which the model is composed are cubes [B51], [B114]. Whole-body-average SARs calculated by this method are very close to those calculated for spheroidal models. Although the block model has the advantage that it resembles the human body better than a spheroid because it has simulated arms, legs, and head, the calculations of the spatial distribution of the internal fields calculated using this method have been found to be of varying accuracy depending on the location of the cell in question [B183]. Apparently, the calculations

are of limited accuracy because the electric field in each mathematical cell is approximated by a constant, and this approximate field cannot satisfy the boundary conditions for cells that touch the curved surface of interfaces between two dissimilar dielectric materials, or the surface of the body (air-tissue boundary). An improved moment-method uses tetrahedra as mathematical cells [B222]. Special basis functions are defined within the tetrahedral volume elements to ensure that the normal electric field satisfies the correct conditions at interfaces between different dielectric media.

Hagmann [B115] has developed improved means for predicting regionally averaged SAR using the block model of man, with the moment-method technique. Since individual humans vary significantly in their physical size and configuration, regional averaging may be more meaningful than detailed values of SAR for individuals "blocks" within an idealized human model. These techniques insure convergence with no numerical instabilities, and also increase modeling flexibility.

7.5.6 Surface-integral-equation (SIE) technique

An SIE method based on a formulation of the EM-field equations in terms of integrals over induced currents on the surface of an object [B117], [B265] is used to calculate average SAR, principally for K-polarization, and mostly for models consisting of a truncated cylinder capped on each end by hemispheres. Average SAR for this model are close to those for a spheroid, depending on how the dimensions of the cylinder-hemispheres model are chosen relative to the spheroid.

7.5.7 Finite difference time-domain method (FDTD)

FDTD [B159], [B244], [B268] is a numerical method for solving electromagnetic field interaction problems. It uses a geometry mesh, usually of rectangular box-shaped cells (voxels), which is readily developed from CT or MRI scans of real human beings or animals. The constitutive parameters for each cell edge may be set independently so that objects having irregular geometries and inhomogeneous dielectric composition can be analyzed. The FDTD method has been used for a myriad of applications, including SAR and induced current calculations in the human body for plane-wave exposures [B97], exposure to leakage fields of parallel-plate dielectric heaters [B50], exposure to EMP [B48], annular phased arrays of aperture and dipole antennas for hyperthermia [B49], coupling of cellular telephones to the head [B68], [B90], [B98], [B139], [B176], exposure to RF magnetic fields in magnetic resonance imaging (MRI) machines [B92], and exposure to powerline fields [B97].

FDTD calculations have been extensively validated for both far- and near-field sources. For far-field sources, simulation results have been compared with analytical results for square [B257] and circular cylinders [B35], [B80], [B245], [B257], spheres [B89], [B99], [B126], plates [B246], layered half-spaces [B207], and even complicated geometries such as airplanes [B158]. Calculations of currents induced in a standing human have compared well with measurements [B47], [B81], [B89]. In the example shown in Figure 17, E_{inc} = 10 kV/m (vertically polarized, frontally incident) and B_{inc} = 33.42 μT from side to side of the model. The data are in excellent agreement with the data of Deno [B67] shown as a dot at the bottom of the curve.

For near-field sources, simulation results have been compared with analytical, measured, or method of moment results for dipole antennas in front of layered half-spaces, layered boxes, and homogeneous spheres [B78]. In addition, the FDTD method has been validated for near-field testing of realistic cellular telephones next to the human head [B68], [B90], [B139], [B176]. The analytical results are in excellent agreement with corresponding experimental results.

Depending on the application, human body models may be crude approximations or detailed meshes based on actual anatomy. Several suitable models have been developed from CT and MRI scans of humans. One of the first, which was taken from published anatomical cross sections, had a resolution of 6.55 mm [B93]. Models with resolutions of $2 \times 2 \times 2$ mm [B68], $1.974 \times 1.974 \times 3$ mm [B85], [B95], $0.9 \times 0.9 \times 1.5$ mm [B202], $1.1 \times 1.1 \times 1.4$ mm using subgridding in some regions [B201], and $3 \times 3 \times 3$ mm, based on MRI

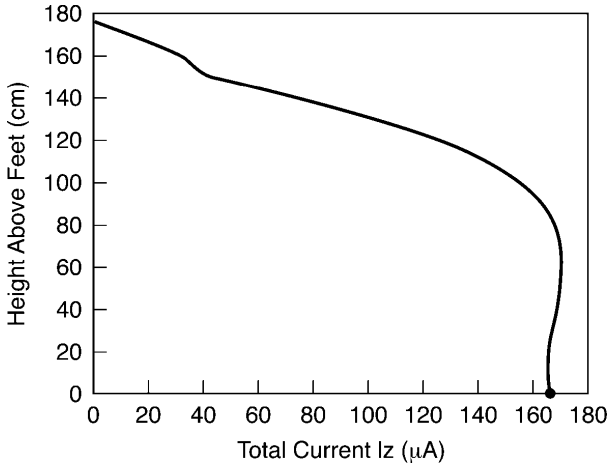

Figure 17—The calculated vertical currents passing through the various sections of a 6 × 6 × 6 mm MRI-based grounded model of the human body exposed to a 60 Hz electromagnetic field

scans [B139], [B175] have been reported. A popular source of anatomical data suitable as the basis of an FDTD biological mesh is the Visible Human Project [B259] of the National Library of Medicine. Various types of data are available, with the most useful perhaps being the cross sections. These are 1 mm slices for the male and 0.33 mm slices for the female. Both have a cross-sectional resolution of 0.33 mm. FDTD meshing of these data still requires considerable effort, especially in assigning the colors to particular tissue types of the slices.

Development of models suitable for FDTD dosimetric calculations, while straightforward, is not trivial. MRI and CT scans provide voxel maps of density, but many of the tissues have the same or similar densities, and many of the regions outside of the major organs require a detailed understanding of anatomy to determine what tissues are present, e.g., fat, fluid, air. Even when some automatic tissue definition can be used, the bulk of the task falls on manual tissue recognition by a trained anatomist. Moreover, since FDTD calculations use the tissue dielectric properties, i.e., dielectric constant and conductivity, and mass density at each voxel location, knowledge of these properties for each voxel is also required. Properties of many of the tissues have been measured over a wide frequency range [B71], [B82], [B83], [B100], [B238]. All tissues are highly frequency dispersive, and some tissues, e.g., bone, heart, skeletal muscle, demonstrate anisotropic properties at frequencies below 1 MHz [B75]. Additional measurements of tissue properties are on-going as there remains questions about variations in the properties with the individual's, age, health status, temperature, *in vivo* versus *in vitro*, etc.

The FDTD method solves Maxwell's differential equations at each cell edge at discrete time steps. Since no matrix solution is involved, electrically large geometries can be analyzed. FDTD solutions for three-dimensional complex biological geometries involving millions of cells have become routine, e.g., studies of SAR distributions associated with exposure to hand-held radio transceivers [B68], [B98], [B90], [B139], [B176]. FDTD may be used for both open region calculations, e.g., SAR and current distributions induced in the human body under plane-wave exposure conditions [B97], or closed regions, such as within a TEM cell. Commercial FDTD software is available from several sources, with some of these also offering FDTD meshes for human heads and bodies. These commercial packages provide a graphical user interface for viewing the FDTD mesh. Some provide interactive mesh editing, while others allow for import of objects from CAD programs.

The actual FDTD calculations may be excited in different ways. Most commonly, the electric fields on one or more mesh edges are determined by an analytical function of time, such as a gaussian pulse or sine wave. This then acts as a driven voltage source, which, for example, may be used to excite an antenna such as a

short monopole on a metal box to approximate a hand-held radio transceiver. This monopole antenna could be driven by a voltage source located on the mesh edge at the monopole base next to the top of the box. Both Kunz and Luebbers [B159] and Taflove [B244] describe methods for modeling RF sources. A variety of FDTD sources, including current sources, are described in Picket-May *et al*. [B211]. Alternatively, a plane wave may be incident on the object as the excitation source.

The time variation of the excitation may be either pulsed or sinusoidal. The advantage of the pulse is that the response for a wide frequency range can be obtained. For accurate results, however, the frequency dependent behavior of the biological materials must be included in the calculations. Methods for doing this are well known [B159], [B244] so that transient electromagnetic field amplitudes for pulse excitation can be calculated, e.g., $(FD)^2TD$ [B79]. When the results at a single frequency or at a few frequencies are all that is desired, sine wave excitation is preferred. This is especially true if results for the entire body are needed, such as the SAR distribution, since storing the transient results for the entire body mesh and applying Fast Fourier Transformations (FFT) to calculate the SAR versus frequency requires extremely large amounts of computer storage. (See Annex D for computer resource requirements for the FDTD method.)

7.5.8 Generalized multipole technique (GMT)

During the 1980s, several groups developed what were later unified under the name generalized multipole technique (GMT) [B174]. GMT refers to methods that approximate the unknown field in each domain by several sets of functions, which in contrast to the method of moments do not have singularities within their respective domains or their boundaries.

The expansions are matched at discrete points on the boundary of the domains, resulting in an overdetermined system of equations with a dense matrix. The overdetermination factor is typically between 2 and 10. The system is solved in the least squares sense, usually with QR-factorization methods [B102].

Since the global expansion functions of the GMT are very smooth at the boundaries, the accuracy close to the boundaries is very high, which is important for dosimetry applications. The greatest advantage of the GMT, however, lies in the fact that the residual errors resulting from the least squares technique can be employed to validate the quality of the results [B160]. Since the largest errors usually occur at the boundaries, the accuracy of the entire solution can be precisely determined [B215]. The GMT, therefore, leads to very reliable dosimetric assessments. Since the method is closely related to other analytical methods, accurate simulation of scattering problems ranging over many orders of magnitude in field strengths are possible.

The severe limitation of the GMT is the difficulty involved in simulating real-world applications. In contrast to the method of moments, in which sequential basis functions are equivalent to a compact current, a GMT expansion is equivalent to a current distribution over the whole boundary of the domain. For geometrically complex bodies, the selection and location of the origin of the expansion functions is not quite obvious and requires considerable expertise.

The method is described in detail in Hafner [B109]. Commercial software based on the GMT is available, including a graphic interface for the PC. The code has been successfully applied to dosimetric studies [B160] and [B161], and to antenna design [B247].

7.5.9 Impedance method

To obtain a detailed view of the power deposition pattern resulting from time-varying magnetic fields used in hyperthermia applications, a method for modeling portions of the human body using an impedance network has been developed [B94]. The region of interest is subdivided into a number of cells, each of which is then replaced by an equivalent impedance, and currents induced in the resulting network due to the prescribed magnetic field are found by the application of circuit theory. This approach allows very fine modeling of

inhomogeneities in the human body with cell sizes of 0.5 cm or smaller possible. In addition, the individual cells are assumed to have anisotropic electrical properties, which allows accurate modeling of interfaces.

7.6 Theoretical considerations for the determination of SAR associated with near-field exposures

The results of detailed mathematical analyses of the SAR distribution at different points within a person's body, due to exposure to near-field sources, aid in estimating the order of magnitude of the corresponding induced SAR. The corresponding exposure may or may not be in the reactive near field of a radiator. The following considerations can aid estimating the type of exposure (near or far field), and in the subsequent assessment of the feasibility of estimating the internal SAR distributions in exposed personnel.

7.6.1 Theoretical considerations for estimating RF coupling and SAR associated with reactive near-field exposure

Either reduced or enhanced absorption situations could exist (see 6.6) for personnel exposed to nonradiating, reactive near fields of a nearby source. One principal factor that determines the relative magnitude of the induced SAR is the type and degree of coupling between the RF source (an active radiator or passive radiator) and the exposed object. For the case where the distance between the object (person) and the source is much less than one wavelength, E and H exhibit a rapid decrease in amplitude with increasing separation distance. [See 4.1.4 and 6.3.6.2—Equation (23).]

The characteristics of the reactive near-field region are described in 4.1.4, and a mathematical expression for the fields at a point d from an electric dipole is shown in Equation (23). When the distance d is much smaller than λ, the term $(1/d^3)$ is dominant. Here, reactive near-field conditions produce a majority of the energy deposition in lossy dielectric objects. The coupling in a reactive near-field situation may be analyzed as a quasi-static, electromagnetic field problem. Capacitive (electric field) coupling provides the primary means of inducing energy from the electric fields surrounding the radiator into the exposed object. Magnetic fields can also induce RF energy (via internal currents), thereby producing additional RF absorption.

7.6.2 Theoretical studies of induced SAR: near-field vs plane-wave exposure

For the near-field exposure situation, the induced spatially averaged or whole-body-averaged SAR is almost always much less than the whole-body-average SAR induced by a normalized plane-wave exposure. (See 6.6.2 for a discussion of the normalized exposure field concept.) The only exception is when direct contact with a radiator or re-radiator induces a large RF current in the body that subsequently flows through the body to RF ground. The degree of coupling between the object (person) and the passive re-radiator will dictate whether an enhanced or a reduced absorption situation occurs with respect to spatially localized SAR.

The induced SAR associated with a generalized model of an active, near-field radiation source has been determined [B44]. Here, human exposure to a near-field source is compared with exposure to a plane-wave field. Both exposure situations were normalized to their respective spatial-maximum external E-fields for the reduced absorption case. In particular, mathematical analyses were performed using a block model of a person, and experimental verification was accomplished with human "phantom" models using implantable, E-field probes. The study involved a standing person immersed in a vertically polarized, spatially nonuniform E-field. The E-field distribution was defined as a half-cosine shape along both the vertical and horizontal axes. The field was further defined as existing in a lateral plane located just in front of the person's feet, simulating exposure to the emission from an RF heat-sealer. The plane containing the field was normal to an imaginary line drawn between the center of the radiator and the center of the person. Finally, the near field was assumed to decay rapidly with increasing distance from the source, so that a two-dimensional analysis was feasible.

The resulting induced, whole-body-averaged SAR in the above studies was shown to be significantly lower than the whole-body SAR induced by a plane wave. The general relationship between the SAR induced by near-field exposures and far-field exposures is [B236]

$$SAR_n = \frac{SAR_f}{\left[1 + \left(\frac{A_v}{d_v}\right)^2\right]\left[1 + \left(\frac{A_h}{d_h}\right)^2\right]} \tag{33}$$

Where

A_v is the constant,
A_h is the constant,
d_v is the dimension (in wavelengths) of the vertical extent of the field in the plane containing the object,
d_h is the dimension (in wavelengths) of the horizontal extent of the field in the plane containing the object.

The E-field in the abdominal region of the body was one-third, or less, than the corresponding abdominal E-field induced by a plane-wave. This implies a decrease in local SAR by a factor of at least 9 times, for the near-field case. However, near-field exposure situations are capable of inducing high values of SAR in some parts of the body. At 27 MHz, the above study found an SAR in the legs that was 3 times higher than the whole-body-averaged SAR. It should be noted that the above studies were clearly reduced absorption cases, with weak coupling to the RF source.

Annex A

(informative)

Additional calibration techniques for external field measuring instruments

A.1 General

Instead of a TEM cell, it is sometimes advantageous to use open parallel plates or transmission lines having a characteristic impedance other than 50 Ω. The major limitations of TEM cells and parallel plate lines are the inverse proportionality between the size and upper frequency limit. For proper operation, the spacing between the cell conductors, i.e., the width of the septum, and the length of the uniform line (non-tapered section), should all be less than $\lambda/2$. Another limitation is that a relatively large amount of power is required to produce desirable field intensities, for the usual case, where the characteristic impedance Z_0 and load resistance are 50 Ω. Some alternative methods are mentioned below.

A.2 Open parallel plates

Figure A.1 is a sketch of a system using open parallel plates to generate a known electric field at frequencies up to about 30 MHz. The expression for calculating the E-field existing between two flat conducting plates is the same as that for a TEM cell, namely

$$E = Vb \text{ (V/m)} \tag{34}$$

Where E is the electric field strength, V is the voltage difference between plates, and b is the plate spacing. The uncertainty of the field level is the same as that for a TEM cell. The wave impedance is greater than 120π Ω, similar to that of an unterminated TEM cell, and therefore, a larger E-field can be produced for a given RF input. If the line is made resonant by means of an inductor, larger field strengths can be produced, but more care must be taken to ensure the accuracy of calibration. In the example of Figure A.1, an E-field of 1000 V/m can generally be achieved with a 1 W power source.

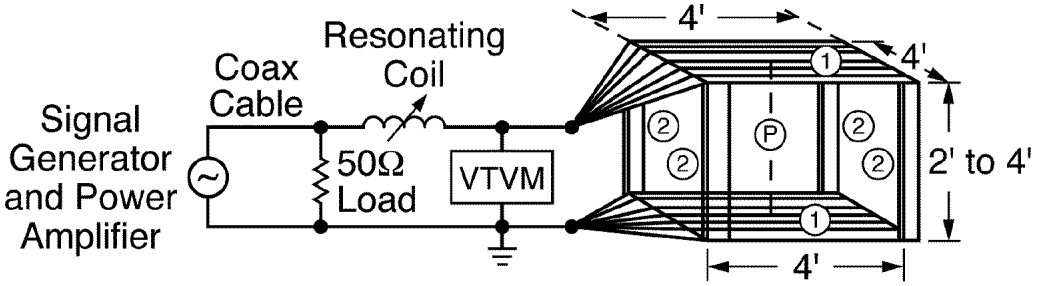

Notes:
(1) Top and bottom are metal clad plywood
(2) Vertical supports are wood 2x4s
(P) Location P is the optimum calibrating point

Figure A.1—Open parallel plate calibration system

A.3 Parallel-plate transmission line

Figure A.2 is a sketch of a parallel-plate line that is useful for generating known E- and H-fields at frequencies up to 30 MHz. This type of TEM calibrating line is specified in MIL-STD-462 [B187] and SAE Standard ARP-958 [B221]. The required value of load resistance for terminating the line with a minimum VSWR depends mainly on the plate spacing and width. The characteristic impedance of the line Z_0 is also affected by its surroundings, especially if the line is located in a shielded enclosure, such as a screen room. Therefore, the optimum value of terminating resistor should be verified experimentally from measurements of the E-field uniformity. The value of Z_0 for the parallel-plate line of Figure A.2 is 80–100 Ω. The E-and H-fields are again given by Equation (11) in 5.5.1.3.1.

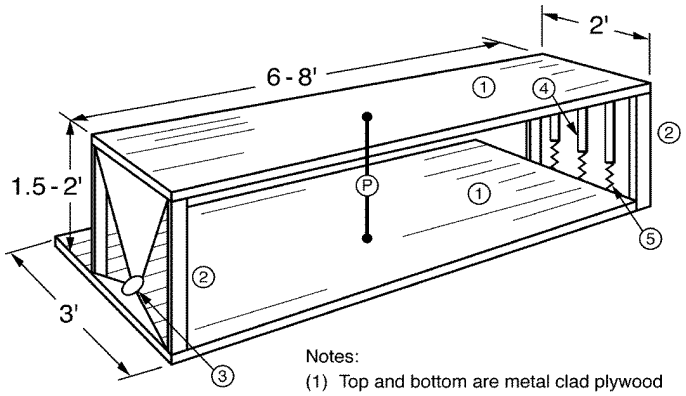

Figure A.2—Parallel plate transmission line for generating E- and H-fields at frequencies between 0.3 and 30 MHz

At frequencies approaching self-resonance of the system (similar to open-parallel plates), it is difficult to calculate the field level accurately, and it is then necessary to measure the field strength at the "calibrating point" with a small transfer probe, such as a 5 cm dipole that has been previously calibrated in another type of reference system.

A.4 Parallel-wire transmission line

A two-conductor TEM line using two balanced thin wires can also be used to generate calculable values of *E* and *H*. This transmission line has a relatively high characteristic impedance (Z_0 = 300–1000 Ω) so the E-field midway between the two wires is relatively high, but the field uniformity is not as good as that produced by flat plates. For example, a field strength of 200 V/m can be produced by a 10 W source when using a two-wire line with a spacing of 30 cm. Since the *E*/*H* ratio is 120π Ω, the H-field level is calculable and also is relatively high.

Figure A.3 shows the E-and H-field distribution in the vicinity of a two-wire line. The direction of the electric field vector at point P is also shown in the figure. *H* is perpendicular to *E*. If the length of the transmission line is greater than five times the distance between the wires, the equation for calculating the magnitude of *E* and *H* midway between the two wires is

$$E = \frac{2V}{Z_0(d + \sqrt{d^2 - r^2})} \tag{35}$$

and

$$H = E/(120\pi)$$

Where

E is the electric field strength midway between the two wires (V/m),
H is the magnetic field strength midway between the two wires (A/m),
V is the rms voltage on each line with respect to the neutral plane midway between the wires (V),
Z_0 is the characteristic impedance of the transmission line (Ω),
is the 120 $\cosh^{-1}$ (d/r),
d is the distance from the field point P (midpoint of line) to the center of each wire (m),
r is the radius of each wire (m).

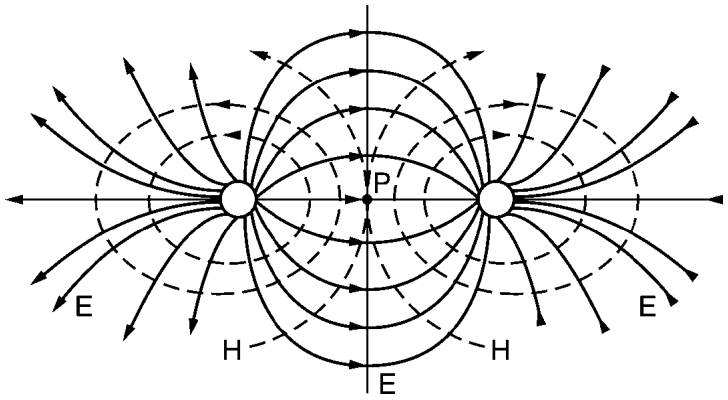

Figure A.3—Parallel wire transmission line for generating E- and H-fields

A.5 Long-wire antenna chamber

A standard screen room can be converted into a chamber with calculable E- and H-fields. This provides a large volume with a moderately uniform field distribution for the exposure of objects or for antenna calibrations at frequencies up to about 30 MHz. As shown in Figure A.4, a single wire is stretched horizontally between two insulators that are attached at opposite ends of the screen room. For a typical room with a height of 8 ft, the wire height is usually about 6 ft above the floor. This TEM transmission line is usually fed via a coaxial transmission line at one end of the room, using a shunt resistor R_1 to help terminate the coaxial line in its characteristic impedance. Resistor R_2 is used to terminate the single wire line in its characteristic impedance (usually 300–600 ohms).

Theoretical investigations of the fields in a screen room, when energized by a single-wire transmission line, indicate that the field uniformity is quite poor. The distribution of the E- and H-fields below the line depends on optimization of the line-terminating impedance. Equations to determine the values of E and H, and the approximate values of R_1 and R_2, are given in the literature [B5], [B6], [B7], [B187]. In the derivation of these equations, it is assumed that a pure resistance is an adequate termination for the wire transmission line. If the line height is greater than two-thirds the room height, the presence of the side-walls and floor of the screen room is generally ignored when calculating the characteristic impedance of the line. The field strength at point P, near the center of the screen room, is given approximately by

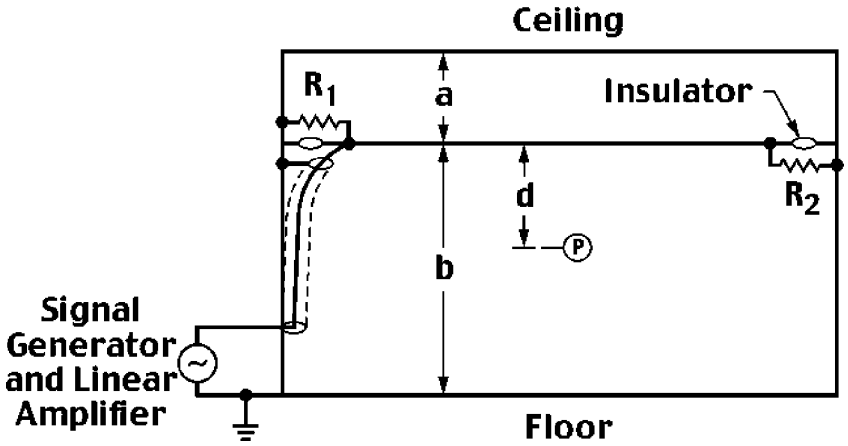

Figure A.4—Long-wire antenna chamber

$$E \approx \frac{60V}{(Z_0 + Z_g)}\left(\frac{1}{d} - \frac{1}{d+2a} - \frac{1}{d-2b} + \frac{1}{d-2a-2b} + \frac{1}{d+2a+2b} - \frac{1}{d-2a+4b} - \frac{1}{d+4a+2b} + \frac{1}{d-4a-4b}\right) \quad (36)$$

and

$$H \approx E/(120\pi)$$

Where

E is the electric field strength at point P midway between the ends of the screen room (V/m),
H is the magnetic field strength at the same point (A/m),
V is the voltage on the single wire transmission line (V),
Z_0 is the characteristic impedance of the line ([W]),
is the $\approx 60 \ln (2a/r)$,
Z_g is the impedance of the generator (Ω),
r is the radius of the wire (m),
a is the distance from the wire to the ceiling (m),
b is the distance from the wire to the floor (m),
d is the distance from the wire to field point P (m).

Annex B

(informative)

Theoretical calculations of exposure fields

B.1 Technical considerations of the RF source characteristics

Although the prediction of power-density levels in the vicinity of RF sources is complicated by many factors, useful estimates can be made. The quality of such calculations will depend on the analytical approach used, as well as on the accuracy of the values of the peak power, pulse duration, pulse repetition rate, antenna radiation patterns, antenna placement, and scanning rates that are used in the computations. Corrections for near-field effects may also be appropriate. The operating parameters listed below must be specified adequately so that the true average-radiated power from the antenna, and the resulting power density at a distant point, can be calculated.

For all sources (pulsed or CW), the antenna type and size, gain, antenna pattern including E- and H-plane beam widths and sidelobe distribution, antenna height above grade, operating frequency, antenna beam orientation (all possible cases), and the attenuation of the transmission line that connects the RF generator to the antenna should be known or estimated. For the calculation of the expected power density levels of pulse modulated sources, the maximum possible values of peak power, pulse duration, and pulse repetition rate that closely approximate, but do not exceed the maximum rated duty factor of a transmitter, should be used. In the case of multiple sources, the contribution of each source should be considered when estimating the combined effect.

B.2 Antennas—on axis

The field in front of an antenna can be characterized by the following three regions:

a) *Reactive near-field region*—This is the region of space immediately surrounding the antenna or leakage source where the reactive (nonradiating) components predominate and energy is stored in the field. The reactive near-field region extends to a distance of approximately one wavelength from the antenna, except for the case of electrically large antennas (whose physical size is greater, in any dimension, than several wavelengths).

b) *Radiating near-field region (Fresnel region)*—In this region, which starts at a distance from the antenna where the reactive field region has diminished to an insignificant amount, the antenna gain and the angular distribution of the radiated field vary proportionally with distance from the antenna. This is because the phase and amplitude relationships of the various waves arriving at the observation point from different areas of the antenna change with distance. For reflector-type antennas, such as parabolic dishes, the radiation is somewhat more complex in its distribution pattern.

c) *Far-field region (Fraunhofer region)*—This region is sufficiently far from the source that the phase and amplitude relationships of the waves arriving from different areas of the antenna do not change appreciably with distance. The antenna gain and angular pattern are essentially independent of distance, and the power density is inversely proportional to the square of the distance from the source. Although the transition from the nonradiating near field is a gradual one, the far-field region is commonly assumed to begin at a distance of about $2a^2/\lambda$ for antennas with equiphase excitation and extends to infinity (a is the largest linear aperture dimension and λ is the wavelength at the frequency of interest). This criterion is not adequate for all types of antennas and should not be applied indiscriminately.

Equation (37) can be used to compute an approximate value for the maximum power density S in the Fresnel and far-field regions of an antenna

$$S = \frac{GP_T}{4\pi d^2} = \frac{A_e P_T}{\lambda^2 d^2} \tag{37}$$

Where G is the far-field antenna gain (power ratio), P_T is the net power delivered to the antenna, d is the distance to the antenna, λ is the wavelength, and A_e is the effective area of the antenna. If G is not known, a useful approximation for S can be obtained by substituting A, the physical aperture area, for A_e in Equation (37). Since A is generally larger than A_e, the estimated value of S will be somewhat larger than the actual value.

Equation (37) can be used to estimate S at distances greater than about 0.5, $a^2/\lambda$where a is the largest aperture dimension. At closer distances, the values predicted by Equation (37) are too large and near-field estimates must be used. For commonly used horn and reflector antennas, the maximum power density S_m expected in the radiating near-field can be estimated by [B33], [B192]

$$S_m = \frac{4P_T}{A} \tag{38}$$

The values predicted by Equation (38) will be within ± dB of the correct value (in the absence of reflections) for square apertures with uniform, cosine, and cosine^2 amplitude tapers, and for circular apertures with tapers ranging from uniform up to $(1\text{-}q^2)^3$ [B192]. (See Annex E.)

If a computation indicates that the approximate power density is substantially less than the MPE, there is usually no need for further calculation since Equation (38) provides the maximum power density that can exist on the axis of the beam of an antenna that is focused at infinity, in the absence of reflections. (An antenna focused at a lesser distance could produce a higher power density in the region of its focal point, but this condition is unusual.)

If the computation from Equation (38) reveals a power density value that is equal to or greater than the MPE, it must be assumed that this value may exist at any point in the radiating near-field region and attention should be directed to the exposure fields in the far-field region.

Equation (37) and Equation (38) do not include the effect of ground reflections. Values of power density that exceed the free-space value by a factor of four times can result when the main beam is directed toward a planar ground or reflecting surface. If the shape of the reflecting surface is such that it produces focusing effects, even greater values may result. After considering the sources of error cited above one, may calculate the distance d_0 to the boundary of the potentially hazardous zone (in the presence of reflections) as follows:

$$d_0 = \sqrt{(GP)/(\pi S)}$$

The use of a cylindrical model has been found useful for evaluating the RF fields near vertical colinear dipole antennas similar to those used for cellular, personal communications services, paging, and two-way radio services [B251], [B253]. In this model, spatially averaged plane-wave equivalent power density (S) parallel to the antenna aperture may be estimated by dividing the net antenna input power P_{net} by the surface area of an imaginary cylinder surrounding the length h of the radiating aperture. Thus

$$S = \frac{P_{net}}{2\pi dh} \tag{39}$$

Where d is the radius of the cylinder (distance to the antenna).

While the actual power density will vary along the height of the antenna, the average value along its aperture will be close to the value predicted by Equation (40).

Tell [B253] found that this simple model compared very favorably with a more exact calculation based on the method of moments. Within the aperture of an element of a vertical colinear dipole array antenna operating at 881.5 MHz, Tell found that for distances closer than 16 ft. from the aperture, the cylindrical model predicted power densities within 20% of the actual spatially averaged power density.

For sector (directional) type antennas, power densities can be estimated by dividing the net antenna input power by that portion of the cylindrical surface corresponding to the angular beamwidth of the antenna. For example, in the case of a 120 degree azimuthal beamwidth, the surface area should correspond to one-third of that of a full cylinder; this will increase the power density near the antenna by three times that of an omnidirectional antenna. This is expressed as

$$S = \frac{P_{net}}{2\pi dh}\left(\frac{360}{\theta}\right) \tag{40}$$

Where θ_{bw} is the 3 dB beamwidth of the antenna (in degrees). Use of the 3 dB azimuthal beamwidth of the antenna will generally result in a conservative estimate of the power density for sector antennas since some of the power is radiated outside of the reported 3 dB beamwidth. Recently, Faraone *et al*. provided a rigorous proof that justifies use of the cylindrical model [B75]. The cylindrical model is also useful for estimating the power density adjacent to FM and TV broadcast antennas where workers may be located during tower work.

B.3 Antennas—off axis

It is more difficult to calculate the power density off the axis of the main beam of an antenna, and it requires the solution of complex mathematical equations. One approach reveals that the collimated beam in the radiating near field of a simple circular parabolic reflector antenna falls off with increasing distance approximately 12 dB per unit of antenna radius [192]. Many antennas, however, do not have simple shapes or illumination tapers. In such cases, the approximate formula above will not apply directly, and a more complex analysis is indicated. The U.S. Department of the Air Force Electromagnetic Radiation Hazards Technical Manual [B258] provides the results of such computations in the form of normalized curves. However, a high order of precision is not warranted when computing the expected power density because of the many physical parameters in the environment that create significant variations in the values predicted by idealized computations.

B.4 Scanning correction

In the case of scanning antennas, the average power density at a fixed point will be reduced by the value of the effective antenna-pattern beamwidth divided by the scanning angle (the number of degrees of antenna rotation during a scan). This assumes that a constant rotational velocity is used, and that the antenna rotates in one direction, rather than stopping after a scan, and reversing direction. Accordingly, the potentially hazardous distance is decreased by at least the square root of this ratio (if the period of rotation is less than the averaging time specified in the MPE). The antenna's effective beamwidth in the far field will, in general, be somewhat different from the 3 dB beamwidth. The exact value depends on the form factor of the radiation pattern and associated sidelobes.

In the Fresnel Zone, the effective angle of the beamwidth will vary with distance. Here, the average power density S of the scanning antenna is given approximately by the following relationship:

$$S = ((4P)/A)(a/(2\pi d))(360/\theta) \qquad (0 > 360(a/(2\pi d))) \tag{41}$$

and

$$S = (4P)/A) \qquad (0 > 360(a/(2\pi d))) \tag{42}$$

Where

- θ is the scanned angle, in degrees,
- P is the average power transmitted,
- A is the effective area of the antenna,
- a is the antenna diameter or width,
- d is the distance from the antenna.

B.5 Computational methods

Numerous computer software packages exist for analyzing antennas. These programs can often play a useful role in RF hazard assessments. Available software products include method of moment techniques for analyzing antennas composed of wire segments. This method is perhaps, for linear antennas, the most rigorous but can require considerable time to construct a model of the antenna being analyzed and requires experience for detecting when a given model result is inappropriate.

Other models have been developed to assist in the near-field assessment of RF compliance with various RF exposure standards, particularly at wireless telecommunications antenna sites. These models may make use of simplified calculation methods, similar to the those mentioned above, e.g., the cylindrical model method, for estimating the composite RF fields produced by multiple antennas located at an antenna site. Other programs make use of more calculation-intensive methods to achieve the same results by modeling the individual elements within each antenna.

Computational methods for analyzing large aperture antennas using the geometrical theory of diffraction (GTD) exist that can be used for near-field examination of earth station and radar antennas. More simplified methods are also available that perform estimates of near fields for large aperture antennas.

Users of such programs are cautioned to use care in selecting the appropriate model for the task at hand and to be aware of the many differences in how various computer programs provide output data on RF field levels. For example, most programs provide calculated values for electric or magnetic field strengths at a point in space, while others offer the ability to calculate spatially averaged estimates of power density.

Annex C

(informative)

Additional techniques for SAR measurement

C.1 Thermography

A method for rapid evaluation of the distribution of SAR throughout an entire planar surface of a biological object or a model that is composed of heterogeneous dielectric materials is described in Guy [B105] and Johnson and Guy [B141]. The method involves the use of a thermographic camera for recording the rate of temperature rise in a plane that bisects an entire model (phantom) or a cadaver of a biological subject under study. The temperature distribution before, and immediately after, brief, high-power irradiation is observed on the precut surface on each half of the bisected model. This is done to prevent cooling by evaporation or flow of the wet synthetic tissue out of its shell (usually composed of synthetic fat or rigid plastic foam).

The technique for using the phantom model to determine SAR distribution throughout a planar surface within a phantom is as follows [B42], [B106], [B125], [B141].

The model is first exposed to the same electromagnetic source that will be used to expose actual tissue. The power applied to the model will be considerably greater, however, in order to heat it in the shortest time possible. After a short exposure duration, the model is quickly disassembled and the temperature pattern over the surface of separation is observed and recorded by means of a thermographic camera. The exposure duration is typically 5–60 s, depending on the object size and source. After about a 5 s delay (for separating the two halves of the model), the recording is carried out within a 1 s period. Since the thermal conductivity of the model is low, the difference in the measured temperature distribution before and after heating will closely approximate the heating distribution over the planar surface, except in regions of high-temperature gradients where errors may occur due to appreciable diffusion of heat, e.g., at the bone-muscle or fat-muscle interface.

It should be noted that actual animal cadavers can be frozen, bisected (in a plane parallel to the E-field), and each half covered with a thin polyethylene sheet. Then the two halves can be placed tightly together so that the bisected surfaces are in tight contact (with no residual air gap). After the tissue temperature is equilibrated with the room, RF irradiation and subsequent thermographic measurements can proceed, but the precautions of thermodynamic degradation of heating patterns associated with excessive ΔT, etc. (see 6.5.2) should be considered.

As with temperature probes, thermodynamic factors and the imprecise knowledge of the value of the specific heat capacity of the tissue or phantom material tend to limit the accuracy and precision of SAR measurements made via thermography. In addition, a potentially large source of error exists unless the persons performing the measurements posses a great deal of experience. The preparation and use of bisected test subjects (particularly cadavers) for evaluation by thermography affects the accuracy of SAR measurements significantly. In particular, when attempting to provide a continuous, electrical path across the plane of bisection in the subject under test using a plastic or silkscreen membrane, air gaps at the interface frequently cause errors. Also, it is difficult to irradiate a subject, split it open, and observe the heating pattern in less than 5 s after irradiation ceases. This time delay creates large, thermodynamically induced errors, particularly at the boundaries of dissimilar tissues, and at the air/subject interface. Therefore, uncertainties of at least ± 1 dB–2 dB should always be expected and should be cited along with SAR data obtained via thermography.

C.2 Body current measurement

SAR may be assessed by measuring the RF current flowing in an exposed object; localized SAR can be derived from current measurements in the extremities. A simplified "effective cross-section" related to realistic anatomical features could be used to determine current density. For many years, a 9.5 cm^2 effective cross-section area for the human ankle was assumed. That value represents about 15% of the total area. However, recent experimental evidence points to an effective cross section of 60% of the total [B206].

In humans, measurement of the induced currents flowing in the legs to ground have been studied at RF frequencies below about 50 MHz [B87], [B108], [B254]. The induced current is determined by standing the individual on a conductive plate electrode and measuring either the current flowing to ground with a RF milliammeter or measuring the RF voltage drop across a known resistance connected between the plate electrode and ground. The value of the resistor should be small enough so as not to perturb the body current, i.e., small compared with the capacitive reactance of the plate and standing subject to ground. From the voltage drop V across the resistance R, the current I may be computed from the expression $I = V/R$. The SAR is then obtained by using the expression

$$SAR = (J^2/(\rho\sigma)) \quad \text{W/kg} \tag{43}$$

Where

J is the current density (A/m^2),
ρ is the mass density (kg/m^3),
σ is the tissue conductivity (S/m),

and J is determined by dividing the measured current by the cross-sectional area of the conductive tissues in the region of interest. Measurements of SAR derived from current measurements are most accurately related to anatomical areas where the effective conduction cross section and current are best known. At frequencies of 50 MHz and below, this is typically the legs and ankles, or arms and wrists.

As discussed in 5.6 and 6.4, flat plate, stand-on type body current meters potentially suffer from several sources of error. One error is related to loss of displacement current from the top electrode plate. Since this plate will have an RF potential on it due to its charge distribution, not all of the current will flow simply between the top plate, through whatever current sensing element exists between it and the bottom plate, and ground. Some current, in the form of displacement current can and will leave the top electrode and not flow through the sensing apparatus. This is not necessarily a large error, but it can affect measurement results. The escape of displacement currents can be reduced by placing a guard ring around the top plate in the form of a conductive lip that tends to capture the displacement current lines and return this current to the plate.

Another error is related to contact between the bottom plate and the surface that the subject is standing on. Since the bottom plate is normally flat and smooth, this may not make for the same quality of contact that would normally exist between the subject's feet and ground and, hence, result in a different current that actually flows between the body and the ground. In some cases, this could result in a lower current, but in other cases, a larger current due to enhanced coupling between the bottom plate and the ground than would occur between the bottom of the subject's feet and the ground.

C.3 Fabrication of simulated tissues

Phantom models are often used together with temperature probes, E-field probes, and thermographic cameras. They are composed of materials with dielectric, thermal, and geometric properties similar to the biological subject they represent. Phantom materials have been developed that simulate human fat, muscle, brain, and bone. The dielectric properties of the phantom can be varied over a wide range by varying the

percentage of constituent materials. In one formulation that was developed by Guy [B105], the relative amounts of polyethylene powder and the salinity of the water used for making the simulated muscle material can be varied to simulate specific tissues of high water content. This particular form of phantom material is very viscous, while pliable and putty-like, and is well suited for the construction of bisected phantoms for thermographic evaluation. Mixing techniques and the exact grain size of the polyethylene powder affect the homogeneity and dielectric properties significantly. Once poured into a mold, the gel has a tendency to entrap air pockets. (See Table 6 and Table 7 in Clause 6 for the conductivity of simulated tissues and biological tissues.) Formulas for preparing phantom muscle tissue-equivalent gels at various frequencies can be found in Chou *et al*. [B56].

A less viscous gel has been developed using hydroxethylcellulose (HEC) gelling agent and salt water (saline). Polyethylene powder or sugar should be added for use above 100 MHz [B118]. The HEC gel does not retain permanent voids and air bubbles as readily as the putty-like formulations [B4]. Visual inspection for air bubbles and the position of implanted probes can be performed simply in the optically transparent HEC gel.

Preservation with a bactericide is necessary when making either of these simulated soft-tissue gel or liquid formulations. Also, water evaporation should be prevented by proper sealing of the containers, or the molds or shells that contain the gel.

Annex D

(informative)

Finite difference time domain (FDTD) method

D.1 Cell-size and time-step size requirements

The choice of cell size is critical in applying FDTD. It must be small enough to provide accurate results at the highest frequency of interest, and yet be large enough to keep resource requirements manageable. Cell size is directly affected by the dielectric properties of the materials present. The greater the permittivity or conductivity, the shorter the wavelength at a given frequency and the smaller the cell size required. Once a cell size is selected, the maximum time step is determined by the Courant stability condition. After the cell size is determined, a problem space large enough to encompass the scattering object, plus space between the object and the outer absorbing boundary, is determined. From the number of Yee cells needed and the number of time steps required, resource requirements can be estimated (see D.2).

The fundamental constraint is that the cell size must be much less than the smallest wavelength for which accurate results are required. An often quoted constraint is "10 cells per wavelength," meaning that the side of each cell should be one-tenth of the wavelength at the highest frequency (shortest wavelength) of interest. For problems containing biological materials, this results in cells in the material that are much smaller than if only free space and perfect conductors were being considered. For example, consider a human body meshed with 5 mm cubical cells. At 10 cells per free-space wavelength, this would correspond to a maximum frequency of 6 GHz. However, since the relative dielectric constant of biological tissues is high, the wavelength in the tissue is reduced (by the square root of the relative dielectric constant). For example, if the maximum relative dielectric constant of the biological tissue in the model is 49, the wavelength in that tissue and, hence, the maximum frequency would be reduced to about 857 MHz, i.e., one-seventh of the free-space value. If results at higher frequencies are needed, the cell size must be reduced. (See Figure D.1 for the cell size requirement, as a function of frequency, for muscle tissue for $\lambda/4$ and $\lambda/10$ cell size criteria.)

Another cell size consideration is to have sufficient spatial resolution to model geometric features with reasonable accuracy. When calculating the whole-body-average SAR, it is sufficient to use the maximum cell size indicated by the Courant stability criterion. For determining the peak spatial SAR values, the cell grid spacing should be generally no larger than the size of the averaging cube. However, smaller FDTD cells may be needed for a region of relatively high dielectric material, or when considering fine geometric features such as the eyes. Smaller FDTD cells will substantially increase the problem size, however, if a uniform mesh is used throughout. One approach to reduce the total number of FDTD cells for these situations is to mesh local regions with smaller cells than in the main mesh [B153], [B270]. Some commercially available software has this local grid capability.

The other basic constraint on FDTD calculations is the time step size. For a three-dimensional grid with cell edges of length Δx, Δy, Δz, with v the maximum velocity of propagation in any medium in the problem, usually the speed of light in free space, the time step size Δt is limited by

$$v\Delta t \leq \frac{1}{\sqrt{\frac{1}{(\Delta x)^2 + (\Delta y)^2 + (\Delta z)^2}}} \tag{44}$$

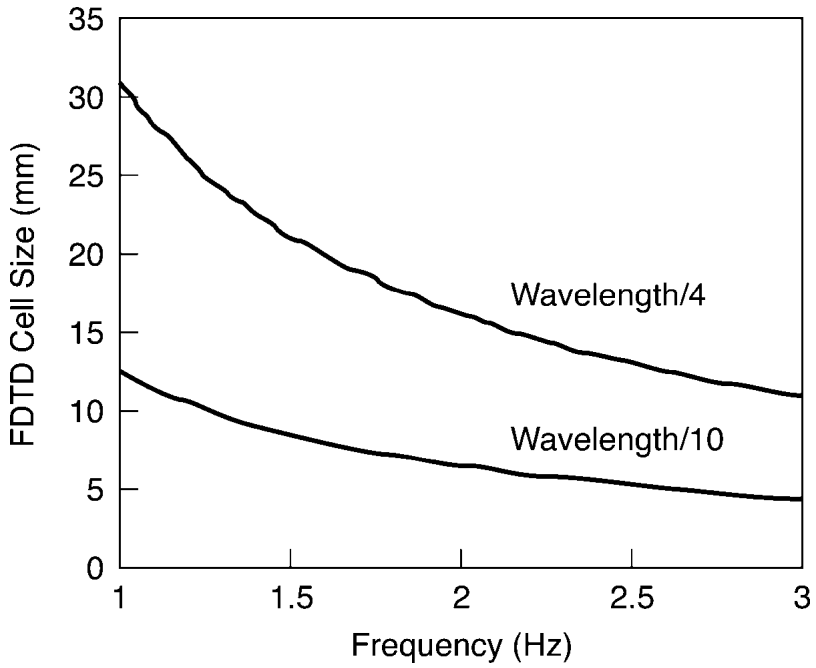

Figure D.1—FDTD cell-size requirements as a function of frequency for muscle, a high-water-content tissue

D.2 Estimation of the computer resources required

Given the shortest wavelength of interest, the cell dimensions are determined as one-tenth of this wavelength (or less if greater accuracy is required). From this and the physical size of the problem geometry, the total number of cells in the problem space (denoted as *NC*) can be determined. Assume that the material information for each cell edge is stored in 1 byte (INTEGER*1) arrays with only dielectric materials considered. An estimate of the computer storage required, in bytes (assuming single-precision field variables), can be obtained from

$$storage = NC \times \left(6\frac{components}{cell} \times 4\frac{bytes}{component} + 3\frac{edges}{cell} \times 1\frac{byte}{edge}\right) \tag{45}$$

Where components indicate the vector electric and magnetic field components. If magnetic materials are included, six edges must be considered for the material arrays. The relatively small number of auxiliary variables needed for the computation process have been ignored.

The computational cost in terms of the number of floating point operations required can be estimated from

$$Operations = 6 \times (components)/(cell) \times (15\ operations)/(component) \times N \tag{46}$$

Where 15 operations is the approximation based on experience and *N* is the total number of time steps. *N* is typically of the order of five to ten times the number of cells on one side of the problem space. *N* will be larger for resonant objects and smaller for lossy objects.

For a human body that fits into a box $63 \times 36 \times 183$ cm, with a 15 cell border around the body to separate it from the outer boundary, the problem space is about $160 \times 100 \times 400$ or 6.4 million cells. Using

Equation (45), the computer random access memory (RAM) necessary to do this calculation is approximately 172 MB. Since this does not allow for storage of instructions and other arrays, and since the operating system will take some computer memory, a machine with about 256 MB of RAM should be sufficient.

A conservative estimate of the number of time steps needed is 10 times the longest dimension in cells, or 4000 time steps. Using Equation (46), an estimate of 2.3×10^{12} operations results. In 2001, a typical MFLOPS (Million FLoating Point Operations per Second) rating for a Pentium 4 personal computer or a fast work station is about 1000. With this speed, our example calculation will require approximately 40 minutes. The calculation time can be reduced using multiprocessor computers or distributed computing.

While the high-frequency limitations of FDTD calculations are based on the size of the object in wavelengths, the low-frequency limitations are usually determined by a combination of the geometry features and time step. For example, consider applying FDTD for a 60 Hz calculation for a human body. Based on the wavelength, the FDTD cells could be huge, but then the body shape would be unrecognizable. If FDTD cells of 10 cm were chosen to make at least a crude body shape, the maximum time step would be 1.92×10^{-10} seconds. If calculations are to be made for at least one period of the sine wave in order to read some semblance of steady state, 86 million time steps would be required. To circumvent this problem, Gandhi *et al*. [B89] have used frequency scaling concepts that may be used in the quasi-static range of frequencies. Using this approach, the results obtained with FDTD for a model at 5–20 MHz are scaled to obtain the distribution of induced electric fields and current densities for a 1.31 cm resolution anatomically based model of a human body for exposure to E and H fields at 60 Hz [B89]. This frequency scaling helps to reduce the number of iterations by almost five orders of magnitude. Other methods, such as finite elements, may also be used for these very low frequencies.

Annex E

(informative)

Peak spatial-average SAR

E.1 Averaging volume

Millimeter resolution of experimental measurement systems and anatomically based computational models of the head and torso of humans has, in some cases, led to questions of interpretation of the appropriate volume over which spatial peak SARs should be averaged. Contemporary safety standards and guidelines specify time-averaged whole-body-averaged SARs and peak spatial-average SARs, neither of which should be exceeded. The spatial peak SAR is usually averaged over a specified volume, e.g., 1 g of tissue in the shape of a cube or 10 g of contiguous tissue [B132]. In some near-field exposure situations, e.g., hand-held cellular telephones, the peak SAR values are generally observed at or near the surface of the ear, which is irregular in shape and is made up of skin, fat, and cartilage with skull bone and brain behind this region. Finding a precise cube of tissue around the peak values is often not possible due to irregularities in shape. In addition, some tissues (particularly bone) are heavier than others, so even cubical subvolumes of the same size will have different mass, depending where in the head they are located.

Further complicating this issue in computational modeling is the fact that the FDTD voxel size is not always (in fact, rarely) divisible into exactly 1 g cubes. While it is possible to use interpolation or extrapolation of data to reduce the problem, the difficulties of handling surface structure and heterogeneous tissue masses remains. Since the fields from near-field sources decay rapidly away from the source, the size of the volume and the percentage of tissue encompassed can have a significant effect on the results. This was demonstrated by Gandhi *et al*. [B98] who calculated the spatial peak SARs associated with hand-held cellular and personal communication services (PCS) transceivers using the FDTD method with a resolution of $1.974 \times 1.974 \times 3$ mm. The results obtained using subvolumes of cells $5 \times 5 \times 4$ were significantly different from the results obtained using $6 \times 6 \times 3$ cells to obtain subvolumes of 1 cm^3, where each of the subvolumes selected were close to and around the regions of high SARs. One way to alleviate this problem is to take the tissue subvolume such that it does not extend beyond the exterior surfaces of the body; i.e., each of its faces must have some tissue. This cubical subvolume may have body-dictated pockets of air in it (e.g., the air in the crevices of the ear or the navel). Also the mass of the subvolume may not be smaller than 1.0 g but preferably as close to it as possible. This method has been used by Gandhi *et al*. [B98] to obtain the peak 1 g SARs for cellular telephones. The absorbed powers were divided by the mass calculated for the individual subvolumes to obtain the 1 g SARs.

It is important to note that this difficulty in interpreting spatial peak SAR criteria in the context of a shaped, possibly heterogeneous model is not unique to numerical simulation or to FDTD simulations in particular. Some measurement systems also provide a discrete set of values, at a given distance apart (resolution), and hence, the calculation of 1 g averaged SARs leads to the same difficulty, particularly if anatomically detailed phantoms are used. If regularly shaped models are used, the problem of calculating the 1 g SAR is lessened, but then the effects of the shape and properties of the ear and other features, which definitely affect the SAR distribution, are not considered.

When averaging SAR over a 1 g volume of tissue in the body, or over 10 g of tissues in an extremity, only SAR values from that tissue may be considered. If any cubic volume contains tissue from the body and from an extremity, each must be considered separately. Specifically, when determining the average SAR in a 1 g cube of tissue in the body, any tissue contained in the cube from an extremity should be treated as air, i.e., mass = 0 and SAR = 0. Similarly, when determining the average SAR in a 10 g cube of tissue in an extremity, any tissue contained in the cube from the body should also be treated as air. In addition, the

orientations of the cubes used for SAR averaging should align with the coordinate axes used in the experimental measurement or numerical computational procedures.

E.2 Peak spatial-average SAR in the body

For tissue in the body, the peak spatial-average SAR should be evaluated in cubical volumes that contain a mass that is within 5% of 1 g. The cubical volume centered at each location, as defined above, should be expanded in all directions until the desired value for the required mass is reached with no surface boundary of the averaging volume extending beyond the most exterior surface of the body (see Figure E.1). If the desired 1 g tissue mass is not obtained, the center of the cubical volume should be moved to the next location. During this process, reference should be kept of all locations used and those not used for averaging the SAR. Average SAR values are assigned to the centered location in each valid averaging volume. All locations included in an averaging volume should be flagged to indicate that they have been averaged at least once. Locations that are marked "used" and have never been in the center of an averaging volume should be assigned the highest 1 g averaged SAR value of the averaging volume in which they are enclosed (Figure E.2). Only those locations that are not part of any valid averaging volume should be marked as "unused." For the case of an "unused" location, a new averaging volume should be constructed with the unused location centered at one surface of the cube and the other five surfaces of the cube should be expanded evenly in all directions until the required 1 g of tissue in the body is enclosed within this volume, regardless of the amount of enclosed air (Figure E.3). Of the six possible cubes with a surface centered on the unused location, the smallest cube that contains the required mass should be used.

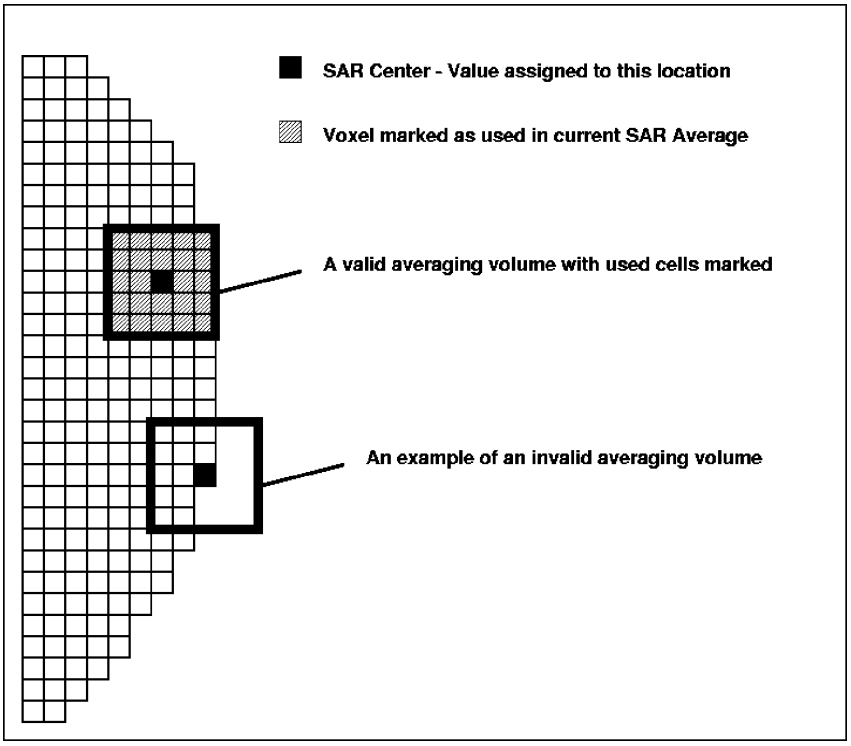

Figure E.1—The upper cube shows an averaging volume centered on the highlighted voxel. The averaging value will be formed from the enclosed cells and assigned to the highlighted location. The lower cube shows an invalid averaging volume. The right-most face of the averaging volume extends into air.

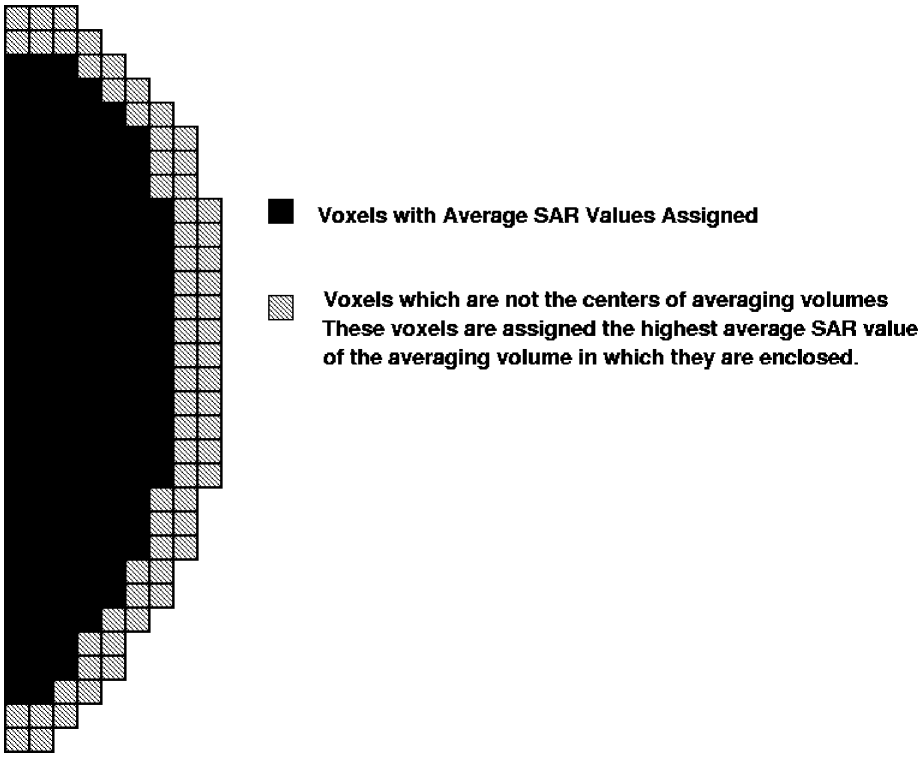

Figure E.2—The resulting plane of average values and "used" voxels

E.3 Peak spatial-average SAR in the extremities

For extremities, the peak spatial-average SAR should be evaluated in cubical volumes with a mass within 5% of 10 g. The cubical volume centered at each location, as defined above, should be expanded in all directions until the required mass of tissue of the extremity is reached, with no surface boundaries of the averaging volume extending beyond the most exterior surface of the extremity. If the desired 10 g tissue mass is not obtained, the center of the cubical volume should be moved to the next location (Figure E.4). The SAR assignment is the same as that used for determining the 1 g averaged SAR in tissue of the body, except a 10 g averaging volume is used. For extremities such as a child's pinna, where 10 g of tissue mass may not exist, the average SAR should be determined as the total SAR averaged over the total mass of the extremity of concern.

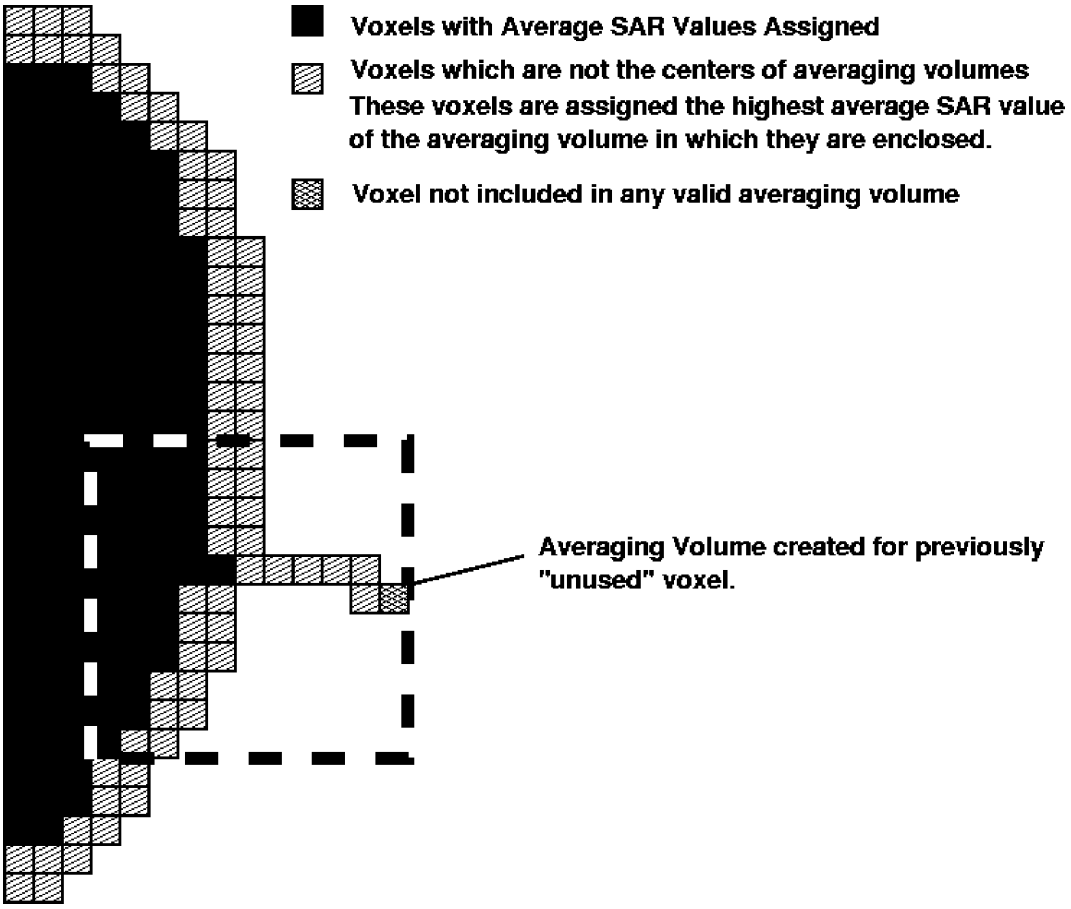

Figure E.3—A slice similar to the one shown in Figure E.2, except with a body protusion that shows a distal "unused voxel" remaining from the previous iterations of the averaging process. Also shown is the adjusted averaging volume created to include the previously unused voxel (centered at the exterior surface)

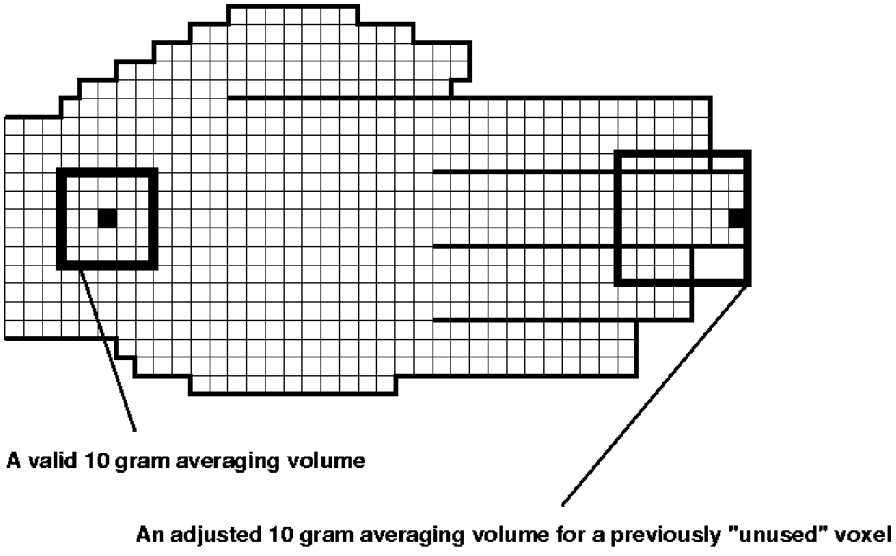

(a)

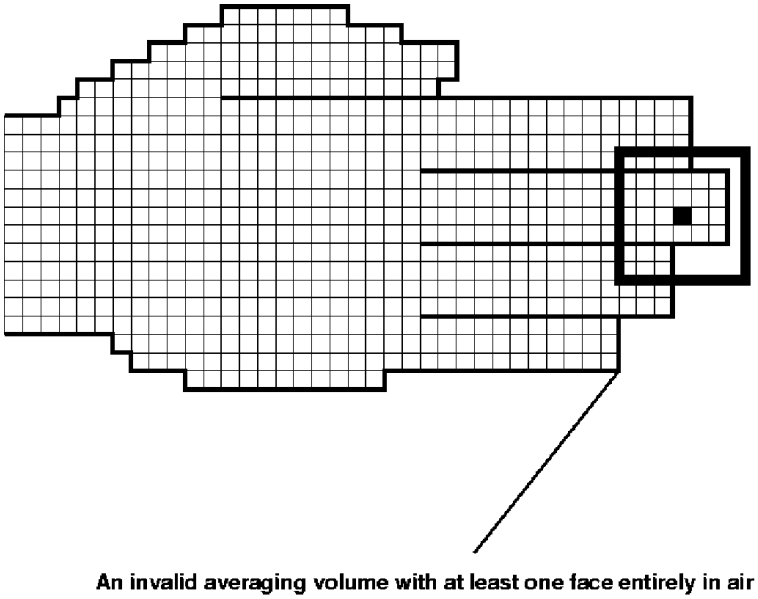

(b)

Figure E.4—Valid (a) and invalid (b) examples of averaging in extremities

Annex F

(informative)

Normalized on-axis power density: circular aperture

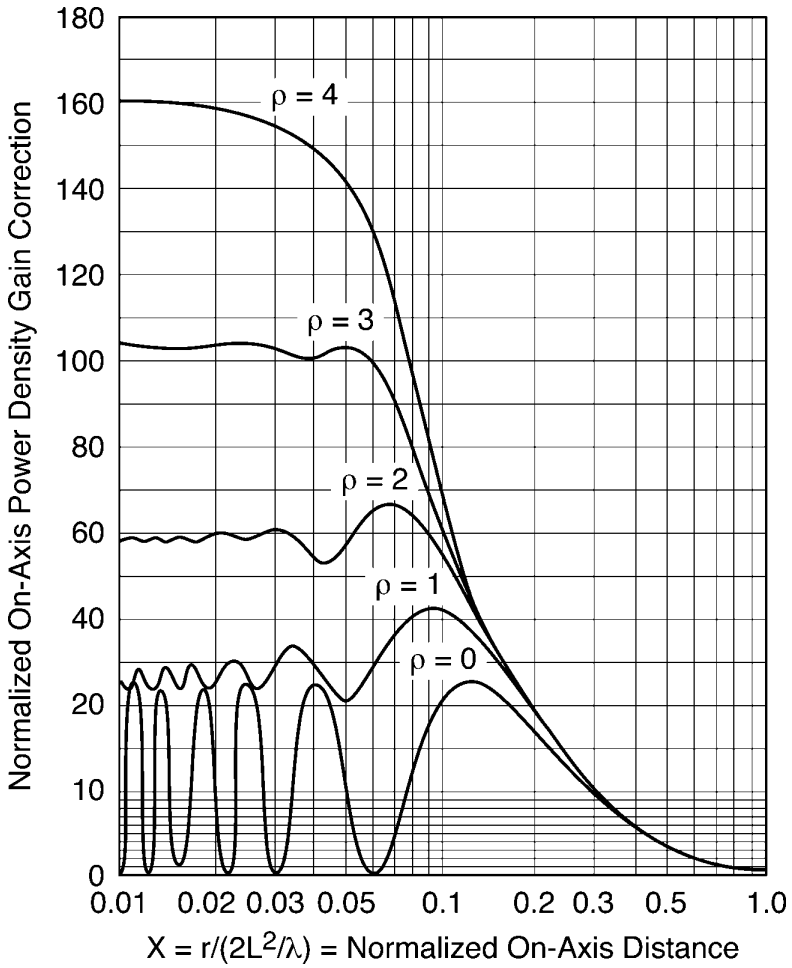

Where

X is the normalized distance from aperture,
r is the distance from aperture,
λ is the wavelength at frequency of interest,
L is the aperture diameter (same units as λ).

Figure F.1—Normalized on-axis power density curves for circular aperture $(1 - q)^p$ illumination tapers

Annex G

(informative)

Bibliography

[B1] ACGIH, "TLVs and BEIs: Threshold limit values for chemical substances and physical agents—Biological exposure indices," *American Conference of Governmental Industrial Hygienists*, Cincinnati, OH, 2000.

[B2] Adams, J., Kanda, M., and Shader, M., "Near field electric field strength levels of the EM environment applicable to automobile systems," *IEEE Electromagnetic Compatibility Symposium Record*, 1977.

[B3] Allen, S. J., and Hurt, W. D., "Calorimetric measurement of microwave energy absorption in mice after simultaneous exposure of 18 animals," *Radio Science*, vol. 14, no. 6S, pp.1–4, 1979.

[B4] Allen, S., Kantor, G., Bassen, H. I., and Ruggera, P. F., "CDRH RF phantom for hyperthermia systems evaluation," *International Journal of Hyperthermia*, vol. 4, pp. 17–23, 1988.

[B5] ANSI C63.2-1987, American National Standard for Specifications for Electromagnetic Noise and Field-Strength Instrumentation, 10 kHz–40 GHz.

[B6] ANSI C63.3-1964 (R1969), American National Standard for Specifications for Radio-Noise and Field-Strength Meters, 20 [E] 1000 Megacycles/Second.

[B7] ANSI C63.4-1991, American National Standard for Measurement of Radio-Noise Emissions from Low-Voltage Electrical and Electronic Equipment in the Range of 9 kHz–40 GHz.

[B8] IME Safety Library Publication 20, *Safety Guide for the Prevention of Radio Frequency Hazards in the Use of Commercial Electric Detonators (Blasting Caps)*, July 2001.[14]

[B9] ANSI/NCSL Z540-2-1997, American National Standard for Expressing Uncertainty—U.S. Guide to the Expression of Uncertainty in Measurement.

[B10] Armitage, D. W., Levine, H. H., and Pethig, R., "Radiofrequency induced hyperthermia computer simulation of specific absorption rate distributions using realistic anatomical models," *Physics in Medicine and Biology*, vol. 28. pp. 31–42, 1983.

[B11] Aslan, E., "Broad band isotropic electromagnetic radiation monitor," *IEEE Transactions on Instrumentation and Measurement*, vol. IM-21, no. 4, pp. 421–424, Nov. 1972.

[B12] Aslan, E., "Simplify leakage probe calibration," *Microwaves*, vol. 14, no. 12, pp. 52–57, Dec. 1975.

[B13] Aslan, E., "An ANSI radiation protection guide conformal probe," *Microwave Journal*, Apr. 1983.

[B14] Aslan, E., "A two MHz to forty GHz electromagnetic radiation probe," *International Microwave Power Institute Symposium Digest*, Minneapolis, MN, Sep. 17–19, 1984.

[14]ANSI/IME publications are available from the American National Standards Institute, Sales Department, 11 West 42 Street, New York, NY 10036, USA.

[B15] Aslan, E., "Non-ionizing radiation measurement methods and artifacts," *Proceedings of the National Association of Broadcasters Engineering Conference*, Las Vegas, NV, April 13–17, 1985.

[B16] Aslan, E., "A combined electric and magnetic field radiation monitor," *Journal of Microwave Power*, vol. 22, no. 2, 1987.

[B17] Aslan, E., and Boncore, J., "Time and spatial averaging for electromagnetic radiation monitors," *Presentation Summaries, 23, Microwave Power Symposium*, International Microwave Power Institute, Aug. 1988.

[B18] Athey, T. W., Stuchly, M. A., and Stuchly, S., "Measurement of radio frequency permittivity of biological tissues with an open-ended coaxial line: Part I," *IEEE Transactions on Microwave Theory and Techniques*, vol. MTT- 30, no. 1, pp. 82–86, Jan. 1982.

[B19] Babij, T. M., and Bassen, H., "Isotropic instruments for measurements of electric and magnetic fields in the 10–100 MHz range," *Abstracts of Papers of Second Annual Meeting, BEMS*, San Antonio, TX, Sept. 14–18, 1980.

[B20] Babij, T. M., and Bassen, H., *Broadband Isotropic Probe System for Simultaneous Measurement of Complex E- and H-Fields*, U.S. Patent 4,588,993, May 13, 1986.

[B21] Balzano, Q., Garay, O., and Steel, R. F., "Heating of biological tissue in the induction field of VHF portable radio transmitters," *IEEE Transactions on Vehicular Technology*, vol. VT-27, no. 2, pp. 51–56, May 1978.

[B22] Balzano, Q., Garay, O., and Steel, R. F., "Energy deposition in simulated human operators of 800 MHz portable transmitters," *IEEE Transactions on Vehicular Technology*, vol. VT-27, no. 4, pp. 172–181, Nov. 1978.

[B23] Balzano, Q., Garay, O., and Steel, R. F., "An attempt to evaluate the exposure of operators of portable radios at 30 MHz," *Proceeding of the 29th Vehicular Technology Conference*, Arlington Heights, IL, pp. 187–188, Mar. 1979.

[B24] Balzano, Q., Garay, O., and Manning, T., "Electromagnetic energy exposure of simulated users of portable telephones," *IEEE Transactions on Vehicular Technology*, vol. 44, no. 3, pp. 390–403, Aug. 1995.

[B25] Barber, P. W., "Electromagnetic power deposition in prolate spheroid models of man and animals at resonance," *IEEE Transactions on Biomedical Engineering*, vol. BME-24, no. 6, pp. 513–521, 1977.

[B26] Baron, D. A., "RF-induced body currents: Practical measurements," *Proceedings of an IRPA/ICNIRP Symposium*, Vienna, Austria, April 1996.

[B27] Bassen, H., "A broadband, miniature, isotropic electric field measurement system," *IEEE Electromagnetic Compatibility Symposium Record*, IEEE 75CH1002-5 EMC, Oct. 1975.

[B28] Bassen, H. I., Herchenroeder, P., Cheung, A., and Neuder, S. M., "Evaluation of implantable electric field probes within finite simulated tissues," *Radio Science*, vol. 12, no. 6(S), pp. 15–23, Nov./Dec. 1977.

[B29] Bassen, H., and Herman, W., "Precise calibration of plane-wave microwave power density using power equation techniques," *IEEE Transactions on Microwave Theory and Techniques*, vol. MTT-25, no. 8, pp. 701–706, Aug. 1977.

[B30] Bassen, H., and Hoss, R., "An optically linked telemetry system for use in electromagnetic field measurement probes," *IEEE Transactions on Electromagnetic Compatibility*, vol. EMC-20, no. 4, pp. 483–488, Nov. 1978.

[B31] Bassen, H., and Peterson, R., "Complete measurement of hazardous electromagnetic fields with electro optical crystals, biological effects of EM waves," vol. II, *Selected Papers of USNC/URSI Annual Meeting*, Boulder, CO, Oct. 1975; DHEW Publication (FDA) 77-8011, pp. 310–323, Dec. 1976.

[B32] Bassen, H., and Smith, S., "Electric field probes—A review," *IEEE Transactions on Antennas and Propagation*, vol. AP-31, no. 5, pp. 710–718, Sept. 1983.

[B33] Bickmore, R. W., and Hansen, R. C., "Antenna power densities in the Fresnel region," *IRE Proceedings*, no. 47, pp. 2119–2120, Dec. 1959.

[B34] Blackman, C. F., and Black, J. A., "Measurement of microwave radiation absorbed in biological systems, 2, analysis of Dewar-Flask calorimetry," *Radio Science*, vol. 12, no. 6S, pp. 9–14, 1977.

[B35] Borup, D. T., Sullivan, D. M., and Gandhi, O. P., "Comparison of the FFT conjugate gradient method and the finite-difference time-domain method for the 2D absorption problem," *IEEE Transactions on Microwave Theory and Techniques*, vol. MTT-35, no. 4, pp. 383–385, Apr. 1987

[B36] Bowman, R. R., "Calibration techniques for electromagnetic hazard meters: 500 MHz–20 GHz," National Bureau of Standards Report NBSIR 75-805, Apr. 1976.

[B37] Bramall, K. E., "Accurate microwave high power measurements using a cascaded coupler method," *Journal of Research, National Bureau of Standards (U.S.)*, vol. 75C, p. 185, July/Dec. 1971.

[B38] Brauer, J. R., *et al*., "Dynamic electric fields computed by finite elements," *IEEE Transactions on Industrial Applications*, vol. 25, no. 6, pp. 1088–1092, Nov./Dec. 1989.

[B39] Braun, E. H., "Gain of electromagnetic horns," *IRE Proceedings*, no. 41, pp. 109–115, Jan. 1953.

[B40] Bui, M. D., Stuchly, S. S., and Costache, G. I., "Propagation of transients in dispersive dielectric media," *IEEE Transactions on Microwave Theory and Techniques*, vol. MTT-39, pp. 1165–1172, Sept. 1991.

[B41] Cetas, T. C., "Thermometry," *An Introduction to the Practical Aspects of Clinical Hyperthermia*, Field, S. B., and Hand, J. W., editors. Bristol, PA: Taylor & Francis, 1990, pp. 423–477.

[B42] Cetas, T., and Connor, W. G., "Practical thermometry with a thermographic camera-calibration, transmission, and emittance measurements," *Rev-Sci Instrumentation*, vol. 49, no. 2, pp. 245–254, Feb. 1978.

[B43] Chang, D. C., Halbgewachs, R. D., and Harrison, Jr., C. W., "The electromagnetic field very near to a monopole," *IEEE Transactions on Electromagnetic Compatibility*, vol. EMC-17, pp. 97–105, May 1975.

[B44] Chatterjee, I., Gandhi, O. P., and Hagmann, M., "Numerical and experimental results for near field electromagnetic absorption in man," *IEEE Transactions on Microwave Theory and Techniques*, vol. MTT-30, no. 11, pp. 2000–2005, Nov. 1982.

[B45] Chatterjee, I., Hagmann, M. J., and Gandhi, O. P., "An empirical relationship for electromagnetic absorption in man for near-field exposure conditions," *IEEE Transactions on Microwave Theory and Techniques*, vol. MTT-29, pp. 1235–1238, Oct. 1981.

[B46] Chen, J-Y., and Gandhi, O. P., "Current meters for assessment of RF hazards to 100 MHz," *Eleventh Annual Meeting Abstracts*, Bioelectromagnetics Society, Tucson, AZ, p. 22, June 18–22, 1989.

[B47] Chen, J-Y., and Gandhi, O. P., "RF currents induced in an anatomically-based model of a human for plane-wave exposures 20-100 MHz," *Health Physics*, vol. 57, pp. 89–98, 1989.

[B48] Chen, J-Y., and Gandhi, O. P., "Currents induced in an anatomically based model of a human for exposure to vertically polarized electromagnetic pulses," *IEEE Transactions on Microwave Theory and Techniques*, vol. 39, no. 1, pp. 31–39, Jan. 1991.

[B49] Chen, J-Y., and Gandhi, O. P., "Numerical simulation of annular-phased arrays of dipoles for hyperthermia of deep-seated tumors," *IEEE Transactions on Biomedical Engineering*, vol. 39, no. 3, pp. 209–216, Mar. 1992.

[B50] Chen, J. Y., Gandhi, O. P., and Conover, D. L., "SAR and induced current distributions for operator exposure to RF dielectric sealers," *IEEE Transactions on Electromagnetic Compatibility*, vol. 33, no. 3, pp. 252–261, Mar. 1991.

[B51] Chen, K. M., and Guru, B. S., "Internal EM field and absorbed power density in human torsos induced by 1 [E] 500 MHz EM waves," *IEEE Transactions on Microwave Theory and Techniques*, vol. MTT-25, no. 9, pp. 746–755, Sept. 1977.

[B52] Chen, C. H., and Lien, C. D., "A finite element solution of the wave propagation problem for an inhomogeneous dielectric slab," *IEEE Transactions an Antennas and Propagation*, vol. 27, no. 6, pp. 887–880, Nov. 1989.

[B53] Cheung, A., Bassen, H., Swicord, M., and Witters, D., "Experimental calibration of a miniature electric field probe within simulated muscular tissues," *Selected papers of the USNC/URSI Annual Meeting*, vol. II, Boulder CO, October 20-23, 1975; DHEW Publication (FDA) 77-8011, pp. 324–327, Dec. 1976.

[B54] Chiba, *et al*., "Application of the Finite Element Method to Analysis of Induced Current Densities Inside Human Model Exposed to 60 Hz Electric Field," IEEE Transactions on Power Application Systems, vol. PAS-103, no. 7, pp. 1895–1902, 1984.

[B55] Chou, C. K., Bassen, H., Osepchuk, J., Balzano, Q., Petersen, R., Meltz, M., Cleveland, R., Lin, J. C., and Heynick, L., "Radio frequency electromagnetic exposure: Tutorial review on experimental dosimetry," *Bioelectromagnetics*, vol. 17, pp. 195–206, 1996.

[B56] Chou, C. K., Chen, G. W., Guy, A. W., and Luk, K. H., "Formulas for preparing phantom muscle tissue at various radiofrequencies," *Bioelectromagnetics*, vol. 5, pp. 435–441, 1984.

[B57] Chu, T. S., and Semplak, R. A., "Gain of electromagnetic horns," *Bell System Technical Journal*, pp. 527–537, Mar. 1965.

[B58] Cleveland, R., "Evaluating compliance with FCC-specified guidelines for human exposure to radiofrequency radiation," FCC-OST Bulletin No. 65, Federal Communications Commission, Washington, DC, Oct. 1985.

[B59] Cleveland, R., and Athey, T. W., "Specific absorption rate (SAR) in models of the human head Exposed to Hand Held UHF Portable Radios," *Bioelectromagnetics*, vol. 10, pp. 173–186, 1989.

[B60] *Conference of Radiation Control Program Directors, Instrumentation for Nonionizing Radiation Measurement*, FDA 84-8222, Food and Drug Administration, Rockville, MD 20857, 1984.

[B61] Crawford, M. L., "Generation of standard EM Fields Using TEM Transmission Cells," IEEE Transactions on Electromagnetic Compatibility, vol. EMC-16, pp. 189–195, Nov. 1974.

[B62] Crawford, M. L., Workman, J. L., and Thomas, C. L., "Expanding the bandwidth of TEM cells for EMC measurements," *IEEE Transactions on Electromagnetic Compatibility*, vol. EMC-20, no. 3, p. 368–375, Aug. 1978.

[B63] Crawford, M. L., and Workman, J. L., "Using a TEM cell for EMC measurements of electronics equipment," NBS Technical Note 1013, July 1981.

[B64] Damelin, J., "VHF-UHF Radiation Hazards and Safety Guidelines," Report no. 7104, Federal Communication Commission, Washington, DC, July 1974.

[B65] D'Andrea, J. A., Emmerson, R. Y., Bailey, C. M., Olsen, R. G., and Gandhi, O. P., "Microwave radiation absorption in the rate: Frequency-dependent SAR distribution in body and tail," *Bioelectromagnetics*, vol. 6, pp. 199–206, 1985.

[B66] Davidson, A. L., "Mobile antenna gain at 900 MHz," *IEEE Transactions on Vehicular Technology*, vol. VT-24, pp. 54–58, Nov. 1975.

[B67] Deno, D. W., "Current induced in the human body by voltage transmission line electric field-measurement and calculation of distribution and dose," *IEEE Transactions on Power Apparatus and Systems*, vol. PAS-96, no 5, pp. 1517–1527, Sept./Oct. 1977.

[B68] Dimbylow, P. J., and Mann, S. M., "SAR calculations in an anatomically based realistic model of the head for mobile communication transceivers at 900 MHz and 1.8 GHz," *Physics in Medicine and Biology*, vol. 39, pp. 1537–1553, 1994.

[B69] Driver, L. D., and Kanda, M., "An optically linked electric and magnetic field sensor for Poynting vector measurements in the near field of radiating source," *IEEE Transactions on Electromagnetic Compatibility*, vol EMC-26, no. 3, pp. 495–503, Aug. 1984.

[B70] Durney, C. H., *et al*., "Long-wavelength analysis of planewave irradiation of a prolate spheroid model of man," *IEEE Transactions on Microwave Theory and Techniques*, vol. MTT-23, no. 2, pp. 246–254, 1975.

[B71] Durney, C., Massoudi, H., and Iskander, M., R*adiofrequency Radiation Dosimetry Handbook (Fourth Edition)*, U.S. Air Force School of Aerospace Medicine, Report USAFSAM-TR-85-73, 1986.

[B72] Engen, G. F., "An improved method for microwave power calibration with application to the evaluation of connectors," *Journal of Research, National Bureau of Standards (U.S.)*, vol. 75C, p. 89, Apr./June 1971.

[B73] Engen, G. F., "Theory of UHF and microwave measurements uing the power equation concept," National Bureau of Standards Technical Note 637, Apr. 1973.

[B74] EPA, "Radiofrequency electromagnetic fields and induced currents in the Spokane, Washington area," Technical Report EPA/520/6-88/008, U.S. Environmental Protection Agency, Las Vegas, NV, June 1988.

[B75] Fraaone, A., Yew-Siow Tay, R., Joyner, K., and Balzano, Q., "Estimation of the average power density of cellular base-station collinear array antennas," *IEEE Tranactions on Vehicular Technology*, vol. 49, no. 3, May 2000.

[B76] Epstein, B. R., and Foster, K. R., "Anisotropy in dielectric properties of skeletal muscle," *Med. Biol. Eng. Comput*., vol. 21, pp. 51–55, 1983.

[B77] Fujimoto, K., and James, J., editors, *Mobile Antenna Systems Handbook*. Norwood, MA: Artech House, 1994, pp. 258–262.

[B78] Furse, C. M., and Gandhi, O. P., "Calculation of electric fields and currents induced in a millimeter-resolution human model at 60 Hz using the FDTD method," *Bioelectromagnetics*, vol. 19, pp. 293–299, 1998.

[B79] Furse, C. M., Chen, J. Y., and Gandhi, O. P., "The use of the frequency-dependent finite-difference time-domain method for induced currents and SAR calculations for a heterogeneous model of the human body," *IEEE Transactions on Electromagnetic Compatibility*, vol. 36, pp. 128–133, Jan. 1994.

[B80] Furse, C. M., Mathur, S. P., and Gandhi, O. P., "Improvements in the finite-difference time-domain method for calculating the radar cross section of a perfectly conducting target," *IEEE Transactions on Microwave Theory and Techniques*, vol. 38, no. 7, pp. 919–927, July 1990.

[B81] Furse, C. M., Yu, Q. S., and Gandhi, O. P., "Validation of the finite-difference time-domain method for near-field bioelectromagnetic simulations," *Microwave and Optical Technology Letters*, vol. 16, pp. 341–345, 1997.

[B82] Gabriel, C., "Compilation of the Dielectric Properties of Body Tissues at RF and Microwave Frequencies," AL/OE-TR-1996-0037, prepared for the U.S. Air Force Armstrong Laboratory, Brooks AFB, TX, June 1996.

[B83] Gabriel, S., Lau, R. W., and Gabriel, C., "The dielectric properties of biological tissues: III. Parametric models for the dielectric spectrum of tissues," *Phys. Med. Biol.*, vol. 41, pp. 2271–2293, 1996.

[B84] Gandhi, O. P., "Numerical methods for specific absorption rate calculations," *Biological Effects and Medical Applications of Electromagnetic Energy*, Gandhi, O. P., editor. Englewood Cliffs, NJ: Prentice-Hall, 1990, pp. 113–140.

[B85] Gandhi, O. P., "Some numerical methods for dosimetry: Extremely low frequencies to microwave frequencies," *Radio Science*, vol. 30, pp. 161–177, Jan./Feb. 1995.

[B86] Gandhi, O. P., and Aslan, E. E., *Human Equivalent Antenna for Electromagnetic Fields*, U.S. Patent No. 5,394,164, Feb. 28,1995.

[B87] Gandhi, O. P., Chatterjee, I., Wu, D., and Gu, Y. G., "Likelihood of high rates of energy deposition in the human legs at the ANSI recommended 3-30 MHz RF safety levels," *IEEE Proceedings*, vol. 73, pp. 1145–1147, 1985.

[B88] Gandhi, O. P., Chatterjee, I., Wu, D., D'Andrea, J. A., and Sakamoto, K., "Very low frequency (VLF) hazard study," USAFSAM-TR-84 submitted to USAF School of Aerospace Medicine (RZP), Aerospace Medical Division (AFSC), Brooks AFB, TX, Jan. 1985.

[B89] Gandhi, O. P., and Chen, J. Y., "Numerical dosimetry at power-line frequencies using anatomically based models," *Bioelectromagnetics Supplement*, vol. 1, pp. 43–60, 1992.

[B90] Gandhi, O. P., and Chen, J. Y., "Electromagnetic absorption in the human head from experimental 6 GHz hand-held transceivers," *IEEE Transactions on Electromagnetic Compatibility*, vol. 37, pp. 547–558, May 1995.

[B91] Gandhi, O. P., Chen, J. Y., and Riazi, A., "Currents induced in a human being for plane-wave exposure conditions 0-50 MHz and for RF sealers," *IEEE Transactions on Biomedical Engineering*, vol. BME-33, pp. 757–767, Sept. 1986.

[B92] Gandhi, O. P., Chen, S. B., Yuan, X., and Chen, J. Y., "Dosimetry for time-varying magnetic fields in MR imaging," *Abstracts of the Sixteenth Annual Meeting of the Bioelectromagnetics Society*, Copenhagen, Denmark, p. 16, June 12–17, 1994.

[B93] Gandhi, O. P., and DeFord, J. F., "Calculation of EM power deposition for operator exposure to RF induction heaters," *IEEE Transactions on Electromagnetic Compatibility*, vol. EMC-30, pp. 63–68, 1988.

[B94] Gandhi, O. P., DeFord, J., and Kanai, K., "Impedance method for calculation of power deposition Patterns in magnetically induced hyperthermia," *IEEE Transactions on Biomedical Engineering*, vol. BME-31, pp. 644–651, June 1984.

[B95] Gandhi, O. P., and Furse, C. M., "Millimeter-Resolution MRI-Based Models of the Human Body for electromagnetic Dosimetry from ELF to Microwave Frequencies," Voxel Phantom Development, Proceedings of an International Workshop held at the National Radiological Protection Board, Chilton, UK, P. J. Dimbylow, Ed., 1995.

[B96] Gandhi, O. P., Gao, B. Q., and Chen, J. Y., "A frequency-dependent finite-difference time-domain formulation for general dispersive media," *IEEE Transactions on Microwave Theory and Techniques*, vol. 41, no. 4, pp. 658–665, Apr. 1993.

[B97] Gandhi, O. P., Gu, Y. G., Chen, J. Y., and Bassen, H. I., "Specific absorption rates and induced current distributions in an anatomically based human model for plane-wave exposures," *Health Physics*, vol. 63, no. 3, pp. 281–290, 1992.

[B98] Gandhi, O. P., Lazzi, G., and Furse, C. M., "Electromagnetic absorption in the human head and neck for mobile telephones at 835 and 1900 MHz," *IEEE Transactions on Microwave Theory and Techniques*, vol. 44, no. 10, pp. 1884–1897, Oct. 1996.

[B99] Gao, B. Q., and Gandhi, O. P., "An expanding-grid algorithm for the finite-difference time-domain method," *IEEE Transactions on Electromagnetic Compatibility*, vol. 34, pp. 277–283, 1992.

[B100] Geddes, L. A., and Baker, L. E., "The specific resistance of biological material—A compendium of data for the biomedical engineer and physiologist," *Medical and Biological Engineering*, vol. 5. New York: Pergamon Press, 1993, pp. 271–293.

[B101] Giri, D. V., Baum, C. E., and Schilling, H., "Electromagnetic considerations of a spatial modal filter for suppression of non-TEM modes in the transmission line type EMP simulators," SSN 247, Dec. 1978.

[B102] Golub, G. H. and Van Loan, C. F., *Matrix Computations*, 2nd ed. Baltimore, MD: Johns Hopkins University Press, 1989.

[B103] Gronhaug, M. L., "Measurement of EMP induced currents in the human body," NDRE Report FFF 510-VM/136, Norwegian Defence Research Establishment, Kjeller, Norway, 1988.

[B104] Gruner, L., "Characteristics of crossed rectangular coaxial structures," *IEEE Transactions on Microwave Theory and Techniques*, vol. MTT-28, pp. 622–627, June 1980.

[B105] Guy, A. W., "Analyses of electromagnetic fields induced in biological tissues by thermographic studies on equivalent phantom models," *IEEE Transactions on Microwave Theory and Techniques*, vol. 19, pp. 205–214, 1971.

[B106] Guy, A. W. and Chou, C. K., "Specific absorption rates of energy in man models exposed to cellular UHF mobile-antenna fields," *IEEE Transactions on Microwave Theory and Techniques*, vol. MTT-3, no. 6, pp. 671–679, June 1986.

[B107] Guy, A. W., "Measurement and analysis of electromagnetic field emissions from 24 video display terminals in American Telephone and Telegraph Office, Washington, DC," NIOSH HETA 85-077, NIOSH, Cincinnati, OH, 1987.

[B108] Guy, A. W., and Chou, C. K., "Hazard analysis: Very low frequency through medium frequency range," Report for USAF School of Aerospace Medicine, Contract F 33615-78-D-0617, Brooks Air Force Base, TX, 1982.

[B109] Hafner, C., *The Generalized Multipole Technique for Computational Electromagnetics*. Boston: Artech House Books, 1990.

[B110] Hafner, C., and Kuster, N., "Computations of electromagnetic fields by the MMP method (GMT)," *Radio Science*, vol. 26, pp. 291–297, Feb. 1991.

[B111] Hagmann, M. J., and Babij, T., "Device for non-perturbing measurement of current as a dosimeter," *Proceedings of the 8th Annual Meeting of the North American Hypothermia Group*, Philadelphia, PA, April 16–21, 1988, p. 51.

[B112] Hagmann, M. J., and Babij, T. M., "Noninvasive measurement of current for dosimetry," USAF/AL Occupational and Environmental Health Directorate Report AL-TR-1991-0044, 1992.

[B113] agmann, M. J., and Babij, T. M., "Noninvasive measurement of current in the human body for electromagnetic dosimetry," *IEEE Trans. Biomed. Eng.*, vol. 40, no. 6, pp. 418–423, 1993.

[B114] Hagmann, M. J., Gandhi, O. P., and Durney, C. H., "Numerical calculation of electromagnetic energy deposition for a realistic model of man," *IEEE Transactions on Microwave Theory and Techniques*, vol. MTT-27, no. 9, pp. 804–809, 1979.

[B115] Hagmann, M. J., and Levin, R., "Accuracy of block models for evaluation of the deposition of energy by electromagnetic fields," *IEEE Transactions on Microwave Theory and Techniques*, vol. MTT-34, 653–659, June 1986.

[B116] Hankin, N. N., "An evaluation of selected satellite communication system as source of environmental microwave radiation," Report EPA-520/2-74-008, Environmental Protection Agency, Washington, DC, Dec. 1974.

[B117] Harrington, R. F., and Mautz, J. R., "Green's function for surfaces of revolution," *Radio Science*, vol. 7, no. 5, pp. 603–611, 1972.

[B118] Hartsgrove, G., Kraszewski, A., and Surowiec, A., "Simulated biological materials for electromagnetic radiation absorption studies," *Bioelectromagnetics*, vol.8, pp. 29–36, 1987.

[B119] Herman, W., and Witters, D., "Microwave Hazard Instruments, An Evaluation of Narda 8100, Holaday 1500, and Simpson 380 M," HHS Publication (FDA) 80-8122, June 1980.

[B120] Hill, D., "A waveguide technique for the calibration of miniature implantable electric field probes for use in microwave bioeffects studies," *IEEE Transactions on Microwave Theory and Techniques*, pp. 92–99, Jan. 1982.

[B121] Hill, D. A., "Bandwidth limitation of TEM cell due to resonances," *Journal of Microwave Power*, vol. 18, pp. 181–195, 1983.

[B122] Hill, D. A., Kanda, M., Larsen, E. B., Koepke, G. H., and Orr, R. D., "Generating Standard Reference Electromagnetic Fields in the NIST Anechoic Chamber, 0.2–40 GHz," NIST Technical Note 1335, Mar. 1990.

[B123] Hill, D. A., and Walsh, J. A., "Radiofrequency current through the feet of a grounded human," *IEEE Transactions on Electromagnetic Compatibility*, vol. EMC-27, pp. 18–23, 1985.

[B124] Ho, H., "Contrast of dose distribution in phantom heads due to aperture and plane wave sources," *Annals of the New York Academy of Science*, vol. 247, pp. 454–472, 1975.

[B125] Hochuli, C., "Procedures For Evaluating Nonperturbing Temperature Probes in Microwave Fields," FDA 81-8143 Food & Drug Administration, Rockville, MD, 1981.

[B126] Holland, R., Simpson, L., and Kunz, K. S., "Finite-difference analysis of EMP coupling to lossy dielectric structures," *IEEE Transactions on Electromagnetic Compatibility*, pp. 203–209, Aug. 1980.

[B127] Hopfer, S., "The design of broad-band resistive radiation probes," *IEEE Transactions on Instrumentation and Measurement*, vol. IM-21, no. 4, Nov. 1972.

[B128] Hopfer, S., "An ultra broad-band (200 kHz-26 GHz) high sensitivity probe," *IEEE Transactions on Instrumentation and Measurement*, vol. IM-29, no. 4, Dec. 1980.

[B129] Hudson, P. A., "A high directivity broadband coaxial coupler," *IEEE Transactions on Microwave Theory and Techniques*, vol. MTT-14, p. 293, June 1966.

[B130] Hudson, P. A., and Saulsbury, L. F., "An adjustable-slot-length UHF coaxial coupler with decade bandwidth," *IEEE Transactions on Microwave Theory and Techniques*, vol. MTT-19, p. 781, Sept. 1971.

[B131] Hurt, W. D., "Specific absorption rate measurement techniques," *Proceedings of the 22nd Midyear Topical Meeting on Instrumentation*, San Antonio, TX, pp. 139–151, Dec. 4–8, 1988.

[B132] International Commission on Non-Ionizing Radiation Protection, "Guidelines for limiting exposure to time-varying electric, magnetic and electromagnetic fields (Up to 300 GHz)," *Health Physics*, vol. 74, no. 4, pp. 494–522, 1998.

[B133] IEEE Std 1140™-1994, IEEE Standard for the Measurement of Electric and Magnetic Fields from Video Display Terminals (VDTs) from 5 Hz–400 kHz.[15]

[B134] IEEE Std 1309-1996, IEEE Standard for Calibration of Electromagnetic Field Sensors and Probes, Excluding Antennas, from 9 kHz–40 GHz.

[B135] IEEE Std 1460-1996, IEEE Guide for the Measurement of Quasi-Static Magnetic and Electric Fields.

[B136] IEEE Std. C95.3™-1991, IEEE Recommended Practice for the Measurement of Potentially Hazardous Electromagnetic Fields-RF and Microwave.

[B137] IEEE Std C95.4™-2002, IEEE Recommended Practice for Determining Safe Distances from Radio Frequency Transmitting Antennas When Using Electric Blasting Caps During Explosive Operations.

[B138] Jakes, W. C., Jr., "Gain of electromagnetic horns," *IRE Proceedings*, no. 39, p. 161, Feb. 1951.

[15]The IEEE standards or products referred to in Annex G are trademarks owned by the Institute of Electrical and Electronics Engineers, Incorporated.

[B139] Jensen, M. A., and Rahmat-Samii, Y., "EM interaction of handset antennas and humans in personal communications," *Proceedings of the IEEE*, vol. 83, pp. 7–17, 1995.

[B140] John, W., "The calibration problem of dipole probes for unraveled measurement at microwave radiators," *Nachrichtentechn*, vol. Z28, no. 3, pp. 89–92, 1975.

[B141] Johnson, C. C., and Guy, A. W., "Nonionizing electromagnetic wave effects in biological material and systems," *IEEE Proceedings*, vol. 60, pp. 692–718, 1972.

[B142] Johnson, C. C., *et al*., "Long-wavelength electromagnetic power absorption in prolate spheroidal models of man and animals," *IEEE Transactions on Microwave Theory and Techniques*, vol. MTT-23, no. 9, pp. 739–747, 1975.

[B143] Jordan, E. E., *Electromagnetic Waves and Radiating Systems*. New York: Prentice-Hall, 1950.

[B144] Joseph, R. M., Hagness, S. C., and Taflove, A., "Direct time integration of Maxwell's equations in linear dispersive media with absorption for scattering and propagation of femtosecond electromagnetic pulses," *Optics Letters*, vol. 16, no. 18, pp. 1412–1414, Sept. 1991.

[B145] Jull, E. V., "Finite-range gain of sectorial and pyramidal horns," *Electronics Letters*, no. 6, pp. 680–681, Oct. 15, 1970.

[B146] Jull, E. V., "Errors in the predicted gain of pyramidal horns," *IEEE Transactions on Antennas and Propagation*, vol. AP-21, no. 1, pp. 25–31, Jan. 1973.

[B147] Kanda, M., "Analytical and numerical techniques for analyzing an electrically short dipole with a nonlinear load," *IEEE Transactions on Antennas and Propagation*, vol. AP-28, no. 1, pp. 71–78, Jan. 1980.

[B148] Kanda, M., "An electromagnetic near-field sensor for simultaneous electric and magnetic-field measurements," *IEEE Transactions on Electromagnetic Compatibility*, vol. EMC-26, no. 3, pp. 102–110, Aug. 1984.

[B149] Kanda, M., *et al*., "Standards for electromagnetic-field measurements," *IEEE Proceedings*, vol. 74, no. 1, pp. 120–128, Jan. 1986.

[B150] Kanda, M., and Driver, L. D., "An isotropic electric-field probe with tapered resistive dipoles for broad-band use, 100 kHz–18 GHz," *IEEE Transactions on Microwave Theory and Techniques*, vol. MTT-35, no. 2, pp. 124–130, Feb. 1987.

[B151] Kanda, M., and Orr, D., "Near-field gain of a horn and open-ended waveguide: Comparison between theory and experiment," *IEEE Transactions on Antennas and Propagation*, vol. AP-35, no. 1, Jan. 1987.

[B152] Kanai, H., Chatterjee, I., and Gandhi, O. P., "Human body impedance for electromagnetic hazard analysis in the VLF to MF band," *IEEE Transactions on Microwave Theory and Techniques*, vol. MTT-32, pp. 763–772, Aug. 1984.

[B153] Kim, I. S., and Hoefer, W. J. R., "A local mesh refinement algorithm for the time-domain finite-difference method using Maxwell's equations," *IEEE Transactions on Microwave Theory and Techniques*, vol. 38, pp. 812–815, 1990.

[B154] Kinber, B. Y., and Tseytlin, V. B., "Measurement error of the directive gain and of the radiation pattern of antennas at short range," *Radio Engineering and Electronic Physics*, no. 9, pp. 1304–1314, Sept. 1964.

[B155] King, R. W. P., *Electromagnetic Engineering*, vol. I. New York: McGraw-Hill, 1945.

[B156] Königstein, D., "A new family of TEM cells with enlarged bandwidth and optimized working volume," *Proceedings of the International Electromagnetic Compatibility Symposium*, Zurich Switzerland, pp. 127–132, 1987.

[B157] Köenigstein, D., and Hansen, D., "A new family of TEM-cells with enlarged bandwidth and optimized working volume," *7th International Zurich Symposium and Technical Exhibition on Electromagnetic Compatibility*, March 3–5, 1987.

[B158] Kunz, K. S., and Lee, K.-M., "A three-dimensional finite-difference solution of the external response on an aircraft to a complex transient EM environment: Part II—Comparisons of predictions and measurements," *IEEE Transactions on Electromagnetic Compatibility*, pp. 333–341, May 1978.

[B159] Kunz, K. S., and Luebbers, R. J., *The Finite-Difference Time-Domain Method for Electromagnetics*. Boca Raton, FL: CRC Press, 1993.

[B160] Kuster, N., "Multiple multipole method applied to an exposure safety study," *ACES Special Issue on Bioelectromagnetic Computations*, A. H. J. Fleming and K. H. Joyner, Eds., vol. 7, no. 2, pp. 43–60, Applied Computational Electromagnetics Society, 1992.

[B161] Kuster, N., "Multiple multipole method for simulating EM problems involving biological bodies," *IEEE Transactions on Biomedical Engineering*, vol. 40 no. 7, pp. 611–620, July 1993.

[B162] Kuster, N., and Balzano, Q., "Energy absorption mechanisms by biological bodies in the near field of dipole antennas above 300 MHz, "*IEEE Transactions on Vehicular Technology*, vol. 41, no. 1, pp. 17–23, Feb. 1992.

[B163] Lakhtakia, A., *et al*., "An iterative extended boundary condition method for solving the absorption characteristic of lossy dielectric objects of larger aspect ratio," *IEEE Transactions on Microwave Theory and Techniques*, vol. MTT-31, pp. 640–647, 1983.

[B164] Lambdin, D., "An investigation of energy density in the vicinity of vehicles with mobile communication and near a hand-held walkie-talkie," Environmental Protection Agency ORP EAD 79-2, NTIS PB298251, 1979.

[B165] Larsen, E., "Techniques for producing standard EM fields from 10 kHz–10 GHz for evaluating radiation monitors," *Proceedings of the 1978 Symposium on Electromagnetic Fields in Biological Systems*, Ottawa, Canada, June 28–30, 1978.

[B166] Lee, C. F., Shin, R. T., and Kong, J. A., "Application of FD-TD technique to dispersive materials," *PIERS Proceedings*, 1991.

[B167] Leonard, J., Foster, K., and Athey, T. W., "Thermal properties of tissue equivalent phantom materials," *IEEE Transactions on Biomedical Engineering*, vol. 31, pp. 533–536, 1984.

[B168] Leuchtmann, P., and Bomholt, L., "Thin wire feature for the MMP-code," *6th Annual Review Progress in Applied Computational Electromagnetics, (AECS) Conference Proceedings*, Monterey, CA, Mar. 1990.

[B169] Lin, J. C., and Gandhi, O. P., "Computational models for predicting field intensity," *Handbook of Biological Effects of Electromagnetic Fields*, C. Polk and E. Postow, Eds. Boca Raton, FL: CRC Press, 1995, pp. 337–402.

[B170] Lin, J. C., Guy, A. W., and Johnson, C. C., "Power deposition in a spherical model of man exposed to 1-20 MHz EM fields," *IEEE Transactions on Microwave Theory and Techniques*, vol. MTT-21, no. 12, pp. 791–797, 1973.

[B171] Livesay, D. E., and Chen, K. M., "Electromagnetic fields induced inside arbitrary shaped biological bodies," *IEEE Transactions on Microwave Theory and Techniques*, vol. 22, no. 12, pp. 1273–1280, 1974.

[B172] Loeb, L. B., *Fundamentals of Electricity and Magnetism*, 3rd ed. New York: Dover, 1961, pp. 56–62.

[B173] Lubinas V., and Joyner, K. H., "Measurements of RF induced ankle currents," *Proceedings of the URSI International Symposium on Electromagnetic Theory*, Sydney, Australia, August 17–29, pp. 327–329, 1992.

[B174] Ludwig, A., "A new technique for numerical electromagnetics," *IEEE AP-S Newsletter*, vol. 31, pp. 40–41, Feb. 1989.

[B175] Luebbers, R., and Baurle, R., "FDTD predictions of electromagnetic field in and near human bodies using visible human project anatomical scans," *IEEE AP-S International Symposium and URSI Radio Science Meeting*, Baltimore, MD, July 21–26, 1996.

[B176] Luebbers, R., Chen, L., Uno, T., and Adachi, S., "FDTD calculation of radiation patterns, impedance and gain for a monopole antenna on a conducting box," *IEEE Transactions on Antennas and Propagation*, vol. AP-40, pp. 1577–1582, 1992.

[B177] Luebbers, R., Hunsberger, F. P., Kunz, K. S., Sandler, R. B., and Schneider, M., "A frequency-dependent finite-difference time-domain formulation for dispersive materials," *IEEE Transactions on Electromagnetic Compatibility*, vol. EMC-32, pp. 222–227, Aug. 1990.

[B178] Lynch, D. R., *et al*., "Finite element solution of Maxwell's equations for hyperthermia treatment planning," *Journal of Computational Physics*, vol. 58, pp. 246–269, 1985.

[B179] Ma, M. T., Kanda, M., Crawford, M. L., and Larsen, E. B., "A review of electromagnetic compatibility/interference measurement methodologies," *IEEE Proceedings*, vol. 73, no. 3, pp. 388–411, Mar. 1985.

[B180] Mantiply, E. D., "An automated TEM cell calibration system," Technical Report EPA 520/1-84-024, U.S. Environmental Protection Agency, Las Vegas, NV, Oct. 1985 (NTIS Order PB85-134377).

[B181] Mantiply, E. D., "Characteristics of broadband radiofrequency field strength meters," *IEEE Proceedings of Engineering in Medicine and Biology Society, 10th Annual International Conference*, New Orleans, LA, Nov. 4–7, 1988.

[B182] Massoudi, H., *et al*., "Long-wavelength electromagnetic power absorption in prolate spheroidal models of man and animals," *IEEE Transactions on Microwave Theory and Techniques*, vol. MTT-25, no. 1, pp. 41–46, 1977.

[B183] Massoudi, H., *et al*., "Geometrical-option and exact solutions for internal fields and SARs in a cylindrical model of man as irradiated by an electromagnetic planewave," *Abstract of Scientific Papers, URSI International Symposium on the Biological Effects of the Electromagnetic Waves*, Airlie, VA, Oct. 30–Nov. 4, 1977.

[B184] Massoudi, H., *et al*., "Limitation of the cubical block model of man in calculating SAR distributions," *IEEE Transactions on Microwave Theory and Techniques*, vol. MTT-32, pp. 746–752, Aug. 1984.

[B185] Masterson, K. D., and Driver, L. D., "Broadband, isotropic photonic electric field meter for measurements from 10 kHz to above 1 GHz," *Proceedings, SPIE*, vol. 987, 1989.

[B186] Masterson, K. D., Driver, L. D., and Kanda, M., "Photonic probes for measurement of electromagnetic fields over broad bandwidths," *1989 IEEE National Symposium on Electromagnetic Compatibility Digest*, Boulder, CO, May 23–25, 1989.

[B187] MIL STD-462 (1986), Measurement of Electromagnetic Interference Levels.

[B188] Misakian, M., *et al*., "Miniature ELF electric field probe," *Review of Scientific Instruments*, vol. 49, no. 7, July 1978.

[B189] Misakian, M., and Fennimore, C., "Distributions of measurement error for three-axis magnetic field meters during measurements near appliances, "*IEEE Transactions on Instrumentation and Measurements*, vol. 45, pp. 244–249, 1996.

[B190] Misakian, M., and Fennimore, C., "Distributions of measurement errors for single-axis magnetic meters during measurements near appliances," *Bioelectromagnetics*, vol. 18, pp. 273–276, 1997.

[B191] Morgan, M. A., "Finite element calculation of microwave absorption by the cranial structures," *IEEE Transactions on Biomedical Engineering*, vol. BME-28, no. 10, pp. 687–695, Oct. 1981.

[B192] Mumford, W. W., "Some technical aspects of microwave radiation hazards," *IRE Proceedings*, no. 49, pp. 427–447, Feb. 1961.

[B193] Naghski. D. H., Boyd, J. T., Jackson, H. E., Sriram, S., and Kingsley, S. A., "An integrated photonic Mach-Zehnder interferometer with no electrodes for sensing electric fields," *Journal of Light Technology*, vol. 12, no. 6., pp. 1092–1098, 1994.

[B194] Nahman, N. S., Kanda, M., Larsen, E. B., and Crawford, M. L., "Methodology for standard electromagnetic field measurements," *IEEE Transactions on Instrumentation and Measurement*, vol. IM-34, no. 4, pp. 490–503, 1985.

[B195] NCRP, "Radiofrequency electromagnetic fields—Properties, quantities and units, biophysical interaction, and measurements," NCRP Report 67, National Council on Radiation Protection and Measurements, Washington, DC, 1981.

[B196] NCRP, "A practical guide to determination of human exposure to radio frequency radiation," NCRP Report 119, National Council on Radiation Protection and Measurements, Bethesda, MD, 1993.

[B197] Nesmith, B., and Ruggera, P., "Performance evaluation of RF electric and magnetic field measuring instruments," Report FDA 81-8185, Food and Drug Administration, Rockville, MD, 1982.

[B198] Newell, A. C., Baird, R. C., and Wacker, P. F., "Accurate measurement of antenna gain and polarization at reduced distances by an extrapolation technique," *IEEE Transactions on Antennas and Propagation*, vol. AP-21, pp. 418–431, July 1973.

[B199] NIS, "The treatment of uncertainty in EMC measurements," NIS Report 81, The National Physical Laboratory of the United Kingdom, Teddington, Middlesex, England.

[B200] NIST, "Guidelines for evaluating and expressing the uncertainty of NIST measurement results," NIST Technical Note 1297 (TN1297), National Institute of Standards and Technology, Gaithersburg, MD.

[B201] Okoniewski, M., and Stuchly, M. A., "A study of the handset antenna and human body interaction," *IEEE Transanctions on Microwave Theory and Techniques*, vol. 44, no. 10, pp. 1855–1864, Oct. 1996.

[B202] Olley, P., and Excell, P. S., "Classification of a high resolution voxel image of a human head," *Voxel Phantom Development, Proceedings of an International Workshop*, National Radiological Protection Board, Chilton, UK, P. J. Dimbylow, Ed., 1995.

[B203] Olsen, R. G., "Localized specific absorption rate (SAR) in a full-size man model near a shipboard monopole antenna: Effects of near-field, re-radiating structures and of whole-body resonance," *Eighth Annual Meeting—Abstracts of the Bioelectromagnetics Society*, p. 34, June 1–5, 1986.

[B204] Olsen, R. G., and Grinner, T. A., "Partial-body resonances in a sitting Rhesus model at 1.29 GHz," *Radiation Environment Biophysiology*, vol. 21, pp. 33–43, 1982.

[B205] Olsen, R. G., and Griner, T. A., "Outdoor measurements of SAR in a full-size human model exposed to 29.2 MHz near-field irradiation," *Bioelectromagnetics*, vol. 10, pp. 162–171, 1989.

[B206] Olsen, R. G., Van Matre, B. J., and Lords, J. L., *RF-Induced Ankle Heating in a Rhesus Monkey at 100 MHz, in Electricity and Magnetism in Biology and Medicine*, F. Bersani, Ed. New York: Plenum Press, 1999.

[B207] Oristaglio, M. L., and Hohmann, G. W., "Diffusion of electromagnetic fields into a two dimensional earth: A finite-difference approach," *Geophysics*, pp. 870–894, July 1984.

[B208] Padilla, J. M., and Bixby, R. R., "Using Dewar-flask calorimetry and rectal temperatures to determine the specific absorption rates of small rodents, "USAF School of Aerospace Medicine, Report USAFSAM-TP-86-3, 1986.

[B209] Passour, J., Hagmann, M., Koves, L., Jabari, M., and Hurt, W. D., "Development of an RF current monitor to measure currents induced in the human body, "US Air Force Occupational and Environmental Health Directorate, Brooks AFB, TX, Report AL/OE-TR 1995-0158, 1995.

[B210] Phillips, R. D., Hunt, E. L., and King, N. W., "Field measurements of absorbed dose and biologic dosimetry of microwaves," *Ann NY Acad Sci*, vol. 247, pp. 162–171, 1975.

[B211] Picket-May, M. A., Taflove, A., and Baron, "FD-TD modeling of digital signal propagation in 3-D circuits with passive and active loads," *IEEE Transactions on Microwave Theory and Techniques*, vol. MTT-42, pp. 1514–1523, 1994.

[B212] Pokovic, K., Schmid, T., and Kuster, N., "E-field probes with improved isotropy in brain simulating liquids, "*ELMAR Proceedings*, Zadar (Croatia), June 23–25, 1996.

[B213] Ramo, S., Whinnery, J. R., and Van Duzer, T., *Fields and Waves in Communication Electronics*. New York: Wiley, 1965, pp. 375–395.

[B214] Randa, J. and Kanda, M., "Multiple-source, multiple-frequency error of an electric field meter," *IEEE Transactions on Antennas and Propagation*, vol. AP-33, no. 1, pp. 2–9, Jan. 1985.

[B215] Regli, P., "Estimating the far field accuracy of MMP results," *2nd International Conference and Workshop on Approximations and Numerical Methods for the Solution of the Maxwell Equations Workshop Proceedings*, The George Washington University, Oct. 1993.

[B216] Rogers, S. J., "Radiofrequency burn hazards in the MF/HF band," *Proceedings of a Workshop on the Protection of Personnel Against Radiofrequency Electromagnetic Radiation*, U.S. School of Aerospace Med-

icine Review 3-81, U.S. Air Force, Aerospace Medical Division, Brooks Air Force Base, TX, pp. 76–89, 1981.

[B217] Rudge, A., and Knox, R., "Near field instrumentation," U.S. Department of Health, Education, and Welfare Publication BRH/DEP 70-16, July 1970.

[B218] Ruggera, P. E., "H-field instrumentation and calibration below 500 MHz," *Biological Effects of EM Waves, vol. II: Selected Papers of USNC/URSI Annual Meeting*, Boulder, CO, Oct. 1975; DHEW Publication (FDA) 77-8011, pp. 281–296, Dec. 1976.

[B219] Ruggera, P. E., "Measurements of electromagnetic fields in the close proximity of CB antennas," Report FDA 79-8080, Food and Drug Administration, Rockville, MD, NTIS PB2924404/AS, 1979.

[B220] Ruggera, P. E., "Measurements of emission levels during microwave and shortwave diathermy treatments," HHS Report (FDA), 80-8019, Food and Drug Administration, Rockville, MD, NTIS PB80-1914772, 1980.

[B221] SAE Standard ARP-958 (1991), Electromagnetic Measurement Antennas; Standard Calibration Requirements and Methods.

[B222] Schaubert, D. H., *et al*., "A tetrahedral modeling method for electromagnetic scattering by arbitrarily shaped inhomogeneous dielectric bodies," *IEEE Transactions on Antenna and Propagation*, vol. AP-32, no. 1, pp. 77–85, 1984.

[B223] Schelkunoff, S. A., *Electromagnetic Waves*. New York: D. Van Nostrand, 1943, pp. 359–365.

[B224] Schmid, T., Egger, O., and Kuster, N., "Automated E-field scanning system for dosimetric assessments, "*IEEE Transactions on Microwave Theory and Techniques*, vol. 44, pp. 105–113, Jan. 1996.

[B225] Shankar, V., Hall, W. F., and Mohammadian, A. H., "A time-domain differential solver for electromagnetic scattering problems," *Proceedings of the IEEE*, vol. 77, pp. 709–721, 1989.

[B226] Silver, S., *Microwave Antenna Theory and Design*, M.I.T. Radiation Laboratory Series, no. 12. New York: McGraw-Hill, 1950.

[B227] Simunic, Ed., "Reference models for bioelectromagnetic test of mobile communication systems," *Proceedings of the COST 244 Meeting*, Rome, Italy, Nov.17–19, 1994.

[B228] Slayton, W. T., "Design and calibration of microwave antenna gain standards," NRL Report 4433, Naval Research Laboratory, Washington, DC, Nov. 1984.

[B229] Smith, G., "The electric-field probe near a material interface with application to probing of fields in biological bodies," *IEEE Transactions on Microwave Theory and Techniques*, vol. MTT-27, no. 3, pp. 270–278, Mar. 1979.

[B230] Soejima, T., "Fresnel gain of aperture aerials," *IEEE Proceedings*, no. 110, pp. 1021–1027, June 1963.

[B231] Sorenson, S., Strickland, R., Aslan, E., and Johnston, A., "Calibration of Narda probes at 94 GHz," *RF Radiation and Ultrawideband Measurements Symposium*, Brooks AFB, TX, Feb. 1995.

[B232] Spiegel, R. J., "A review of numerical models for predicting the energy deposition and resultant thermal response in humans exposed to electromagnetic fields," *IEEE Transactions on Microwave Theory and Techniques*, vol. 32, pp. 730–746, 1984.

[B233] Steinhart, I. S., and Hart, S. R., "Calibration curves for thermistors" *Deep Sea Research*, vol 15. J. Milliman, Ed. New York, Pergamon Press, 1968, p. 497.

[B234] Stuchly, S., "Specific absorption rate distribution in a heterogeneous model of the human body at radiofrequencies," Report PB87-201356, Ottawa University, Ontario, Canada, 1987.

[B235] Stuchly, S., Barski, M., Tam, B., Hartsgrove, G., and Symons, S., "Computer-Based Scanning System for Electromagnetic Scanning," Rev. Sci. Instrum., vol. 54, no. 11, pp. 1547–1550, Nov. 1983.

[B236] Stuchly, M., and Kraszewski, A., "Exposure of human models in the near field of and far field—A comparison," *IEEE Transactions on Biomedical Engineering*, vol. BME-32, no. 7, pp. 702–711, 1985.

[B237] Stuchly, S., Kraszewski, A., and Stuchly, M. A., "Uncertainties in radiofrequency dielectric measurements of biological substances, "*IEEE Transactions on Instruments and Measurements*, vol. IM-36, no. 1, pp. 67–70, March 1987.

[B238] Stuchly, M. A., and Stuchly, S. S., "Dielectric properties of biological substances—Tabulated," *Journal of Microwave Power*, vol. 15, no. 1, pp. 19–26, 1980.

[B239] Stuchly, M. A., Stuchly, S. S., and Kraszewski, A., "Implantable electric field probes, some performance characteristics," *IEEE Transactions on Biomedical Engineering*, vol. BME-31, no. 7, pp. 526–531, 1984.

[B240] Stuchly, S. S., Stuchly, M. A., Kraszewski, A., and Hartsgrove, G., "Energy deposition in a model of man: Frequency effects," *IEEE Transactions on Biomedical Engineering*, vol. BME-33, no. 7, pp. 702–711, July 1986.

[B241] Sullivan, D. M., "Frequency-dependent FDTD methods using Z transformations," *IEEE Transactions on Antennas and Propagation*, vol. AP-40, pp. 1232–1230, 1992.

[B242] Sullivan, D. M., "A frequency-dependent FDTD method for biological applications," *IEEE Transactions on Microwave Theory and Techniques*, vol. MTT-40, pp. 532–539, 1992a.

[B243] Swicord, M., "Problems of power measurement using non-square-law detectors," DHEW Publication (FDA) 72-8004, Food and Drug Administration, Rockville, MD, Aug. 1971.

[B244] Taflove, A., *Computational Electrodynamics: Finite-Difference Time-Domain Method*. Boston: Artech House, 1995.

[B245] Taflove, A., and Brodwin, M., "Numerical solutions of steady-state electromagnetic scattering problems using the time-dependent Maxwell's equations," *IEEE Transactions on Microwave Theory and Techniques*, pp. 623–630, Aug. 1975.

[B246] Taflove, A., Umashankar, K. R., and Jurgens, T. G., "Validation of FD-TD modeling of the radar cross section of three-dimensional structures spanning up to nine wavelengths," *IEEE Transactions on Antennas and Propagation*, pp. 662–666, June 1985.

[B247] Tay, R. Y., and Kuster, N., "Performance of the generalized multipole technique (GMT/MMP) for antenna design and optimization," *Applied Computational Electromagnetics (ACES) Journal*, vol. 9, no. 3, pp. 79–89, Dec. 1994.

[B248] Tell, R. A., "Near-field radiation properties of simple linear antennas with applications to radiofrequency hazards and broadcasting," Technical Report ORP/EAD 78-4, U.S. Environmental Protection Agency, Las Vegas, NV, NTIS Order PB 292647, June 1978.

[B249] Tell, R. A., "Real-time data averaging to determining human RF exposure," *Proceedings, 40th Annual Broadcast Engineering Conference*, National Association of Broadcasters, Dallas, TX, pp. 388–394, Apr. 12-16, 1986.

[B250] Tell, R. A., "An investigation of RF induced hot spots and their significance relative to determining compliance with ANSI radiofrequency protection guides," Technical Report prepared for the National Association Broadcasters, Washington, DC, by Richard A. Tell Associates, Inc., Las Vegas, NV, 1989.

[B251] Tell, R. A., "Engineering services for measurement and analysis of radiofrequency (RF) fields, "Federal Communications Commission Technical Report FCC/OET RTA 95-01, NTIS PB95-253829, 1995.

[B252] Tell, R. A., "A practical assessment of the variability associated with broadband RF survey instruments," *Proceedings of RF radiation and Ultra-Wideband Measurements Symposium*, U.S. Air Force, Armstrong Laboratory, Brooks Air Force Base, San Antonio, TX Feb. 13–16, 1995.

[B253] Tell, R. A., "CTIA's EME design and operations considerations for wireless antennas sites," Technical Report for the Cellular Telecommunications Industry Association, Washington, DC, prepared by Richard A. Tell Associates, Inc., Las Vegas, NV, 1996.

[B254] Tell, R. A., Mantiply, E. D., Durney, C. H., and Massoudi, H., "Electric and magnetic field intensities and associated induced currents in man in close proximity to a 50 kW AM standard broadcast station," *Program Abstracts, USNC/URSI and Bioelectromagnetics Symposium*, Seattle, WA, p. 360, June 18–22, 1979.

[B255] Tippet, J., and Chang, D., "Characteristic impedance of a coaxial line with offset inner conductor," *IEEE Transactions on Microwave Theory and Techniques*, vol. MTT-26, pp. 876–883, Nov. 1978.

[B256] Tseytlin, V. C., and Kinber, B. Y., "Measurement of the directive gain of horn antennas at a short distance," *Radio Engineering and Electronic Physics*, no. 10, pp. 10–16, Jan. 1965.

[B257] Umashankar, K., and Taflove, A., "A novel method to analyze electromagnetic scattering of complex objects," *IEEE Transactions on Electromagnetic Compatibility*, vol. EMC-24, pp. 397–405, Nov. 1982.

[B258] USAF, *Electromagnetic Radiation Hazards Technical Manual*, TO 31Z-10-4, Aug. 1966, U.S. Dept. of the Air Force, 1966.

[B259] Visible Human Project, National Library of Medicine, Bethesda, MD. Available online: http: www.nlm.nih.gov/research/visible/visible-human.

[B260] Wacker, P. F., and Bowman, R. R., "Quantifying hazardous electromagnetic fields: Scientific basis and practical considerations," *IEEE Transactions on Microwave Theory and Techniques*, vol. MTT-10, pp. 178–187, Feb. 1971.

[B261] Waterman, P. C., "Symmetry, unitarity and geometry in electromagnetic scattering," *Physics Review*, vol. 3, pp. 825–839, 1971.

[B262] Weil, C. M., Joines, W. T., and Kinn, J. B., "Frequency range of large-scale TEM mode rectangular strip lines," *Microwave Journal*, vol. 24, pp. 93–100, 1981.

[B263] Wilson, P., Chang, D., and Ma, M., "Excitation of a TEM cell by a vertical electric Hertzian dipole," NBS Tech Note 1037, National Bureau of Standards, Boulder, CO, Mar. 1981.

[B264] Woods, D., "Standard intensity electromagnetic field installation for calibration of radiation hazard monitors from 400 MHz–40 GHz," *Nonionizing Radiation*, pp. 9–17, June 1969.

[B265] Wu, T.-K., "Electromagnetic fields and power deposition in body-of-revolution models of man," *IEEE Transactions on Microwave Theory and Techniques*, vol. MTT-27, no. 3, pp. 279–283, 1979.

[B266] Wyss, J. C., and Sheeran, S. T., "A practical optical modulator and link for antennas," *Journal of Lightwave Technology*, vol. LT-3, no. 2, pp. 316–321, Apr. 1985.

[B267] Yamashita, Y., and Takahashi, T., "Use of the finite element method to determine epicardial for body surface potentials under a realistic torso model," *IEEE Transactions on Biomedical Engineering*, vol. BME-28, no. 9, pp. 611–621, Sept. 1984.

[B268] Yee, K. S., "Numerical solution of initial boundary value problems involving Maxwell's equations in isotropic media," *IEEE Transactions on Antennas and Propagation*, vol. AP-17, pp. 585–589, May 1966.

[B269] Zaffanella, L. E., Sullivan, T. P., and Visintainer, I., "Magnetic field characterization of electrical appliances as point sources through in situ measurements, "*IEEE Transactions on Power Delivery*, vol. 12, pp. 443–450, 1997.

[B270] Zivanovic, S. S., Yee, K. S., and Mei, K. K., "A subgridding method for the time-domain finite-difference method to solve Maxwell's equations," *IEEE Transactions on Microwave Theory and Techniques*, vol. MTT-39, pp. 471–479, 1991.